ARMY RESEARCH LABORATORY

Impact of NiB Coating on the Efficiency, Scuffing, and Wear of Gear Contacts

by Ahmet Kahraman

ARL-CR-713 **May 2013**

prepared by

GearLab – Gear and Power Transmission Research Laboratory
The Department of Mechanical and Aerospace Engineering
The Ohio State University
201 West 19th Ave.
Columbus, OH 43210

under contract

W911NF-10-2-0033

NOTICES

Disclaimers

The findings in this report are not to be construed as an official Department of the Army position unless so designated by other authorized documents.

Citation of manufacturer's or trade names does not constitute an official endorsement or approval of the use thereof.

Destroy this report when it is no longer needed. Do not return it to the originator.

Army Research Laboratory
Aberdeen Proving Ground, MD 21005-5066

ARL-CR-713 **May 2013**

Impact of NiB Coating on the Efficiency, Scuffing, and Wear of Gear Contacts

Ahmet Kahraman
The Ohio State University

prepared by

GearLab – Gear and Power Transmission Research Laboratory
The Department of Mechanical and Aerospace Engineering
The Ohio State University
201 West 19th Ave.
Columbus, OH 43210

under contract

W911NF-10-2-0033

REPORT DOCUMENTATION PAGE	Form Approved OMB No. 0704-0188

1. REPORT DATE *(DD-MM-YYYY)*	2. REPORT TYPE	3. DATES COVERED (From - To)
May 2013	Final	1 March 2010–31 March 2010

4. TITLE AND SUBTITLE
Impact of NiB Coating on the Efficiency, Scuffing, and Wear of Gear Contacts

5a. CONTRACT NUMBER
W911NF-10-2-0033

5b. GRANT NUMBER

5c. PROGRAM ELEMENT NUMBER

6. AUTHOR(S)
Ahmet Kahraman

5d. PROJECT NUMBER

5e. TASK NUMBER

5f. WORK UNIT NUMBER

7. PERFORMING ORGANIZATION NAME(S) AND ADDRESS(ES)
Gear Lab – Gear and Power Transmission Research Laboratory
The Department of Mechanical and Aerospace Engineering
The Ohio State University
201 West 19th Ave.
Columbus, OH 43210

8. PERFORMING ORGANIZATION REPORT NUMBER

9. SPONSORING/MONITORING AGENCY NAME(S) AND ADDRESS(ES)
U.S. Army Research Laboratory
ATTN: RDRL-VTP
Aberdeen Proving Ground, MD 21005-5066

10. SPONSOR/MONITOR'S ACRONYM(S)

11. SPONSOR/MONITOR'S REPORT NUMBER(S)
ARL-CR-713

12. DISTRIBUTION/AVAILABILITY STATEMENT
Approved for public release; distribution is unlimited.

13. SUPPLEMENTARY NOTES

14. ABSTRACT

The influence of various surface treatments on lubricated rolling-sliding contacts is investigated. The surfaces considered are ground, chemically polished, and highly polished, with root-mean-square roughness amplitudes of about 0.4, 0.1, and 0.02 μm, respectively. A chemically applied, low-friction nickel boron (NiB) surface coating is also investigated. These surface treatments are applied to two base materials: AISI 5120 alloy steel, representative of automotive gear steels, and AISI 9310 steel, representing the most common aerospace gear steel. A two-disk test methodology was developed using two types of oils: 80W90 as a typical ground vehicle oil and DOD-PRF-85734 as a typical aerospace gear oil. Traction (friction coefficient), wear, and scuffing experiments were performed to evaluate the performance of these surface treatments. Results of these two-disk experiments show that a reduction in surface roughness results in significant reductions in friction and wear while enhancing scuffing performance of contacts even under starved lubrication conditions. In addition, spur gear tests were performed with the same surface treatments and showed a reduction in mechanical power loss with smoother surfaces. Results of both the two-disk and spur gear experiments show that the NiB coating lacks the durability required for gear applications.

15. SUBJECT TERMS
surface engineering, tribology, traction, wear, scuffing, transmission efficiency

16. SECURITY CLASSIFICATION OF:			17. LIMITATION OF ABSTRACT	18. NUMBER OF PAGES	19a. NAME OF RESPONSIBLE PERSON
a. REPORT	b. ABSTRACT	c. THIS PAGE			Kelsen LaBerge
Unclassified	Unclassified	Unclassified	UU	92	19b. TELEPHONE NUMBER (*Include area code*) 216-443-2078

Standard Form 298 (Rev. 8/98)
Prescribed by ANSI Std. Z39.18

Contents

List of Figures

List of Tables

1. Introduction

1.1 Background and Motivation

One class of power losses occurring in drive trains is caused by friction in the lubricated contacts of such power train components as gears and bearings. Improvements in efficiency through reductions in such losses are achievable through advanced materials and coating technologies, which can simultaneously impact the power density of drive systems and engine cycles. As friction-induced load-dependent (mechanical) power losses take place at lubricated contact interfaces of such components, the surface roughness characteristics and the elastohydrodynamic lubrication (EHL) conditions of these contact interfaces become the focus of efforts to reduce such power losses. Numerous commercial engineered surface techniques have been advocated to reduce the amplitudes of machined contact surfaces and remove the directionality of the machining marks. Similarly, a number of surface coating technologies have been claimed to reduce mechanical power losses through their "antifriction" characteristics. Yet, there have been only a few studies that compare performance of such surface treatments while monitoring other durability consequences. The motivation of this study was to provide an experimental evaluation of a number of surface roughness reduction methods and a chemical deposition-type surface coating in terms of their friction, scuffing (including cases when the contacts are starved of lubricant), and wear performance in comparison with the baseline case of hard-ground surfaces. This experimental study employed a rolling contact (two-disk) test methodology for such evaluations as well as a spur gear setup for the resultant efficiency consequences.

In line with the intended applications of the U.S. Army, both ground vehicle and aerospace gear and bearing contact conditions were considered. A typical automotive gear steel (AISI 5120) and an axle lubricant (80W90) were used for the ground vehicle evaluations, and AISI 9310 steel and DOD-PRF-85734 were used for the aerospace applications evaluations. Measured traction (friction coefficient), wear, and scuffing performances of surface treatment under both automotive and aerospace conditions were compared to provide guidelines for their potential application to actual machine elements.

Based on the results of the two-disk experiments, these surface treatment methods will be applied selectively to actual spur gears and evaluated for their impact on spin and mechanical power losses of gears operating under speed, temperature, and torque conditions representative of actual operating conditions.

Potential applications of these evaluated technologies are ground vehicle and aviation power trains, ground vehicle diesel engines, electric generators, and ground vehicle and aviation turbine engines. This research and its objectives are of interest to the Army due to the potential for increases in propulsion system efficiency. Improvements in efficiency and/or fatigue

characteristics of gear components will benefit by increasing the reliability, availability, and, therefore, the safety of ground and air vehicles. Improvements will also impact the Army's logistical footprint through a reduction in the consumption of petroleum, oil, and lubricants as well as expendable parts. Therefore, the results of this research provide the potential for a reduction in hazardous materials, environmental emissions, and cost.

1.2 Literature Review

The impact of contact surface conditions on various aspects of gear and bearing contacts have been a topic of various studies. As-machined surfaces (shaved, shaped, broached, hard-ground, and honed) typically have roughness amplitudes that are comparable to the minimum lubricant film thickness, resulting in λ ratios (minimum film thickness to root-mean-square surface roughness amplitude) that are often very small ($\lambda < 1$). As demonstrated in a study by Li and Kahraman (*1*), through a mixed EHL model (*2*), contact conditions with $\lambda < 1$ results in breakdown of fluid film in the contact interface to cause metal-to-metal (asperity) contact of surfaces. This not only significantly reduces efficiency of components but also impacts their durability through scuffing, wear, pitting, and/or micropitting.

Two logical ways to increase λ ratio at a given contact operating condition are to (1) use a higher viscosity lubricant to increase film thickness and (2) reduce the roughness amplitudes of contact surfaces through various polishing techniques. Experimental literature contains a number of gear or roller test studies that attempted to quantify the impact of one or more of these methods on the performance of lubricated contacts.

In a study by Krantz and Kahraman (*3*), the effect of lubricant viscosity on gear wear rates and pitting lives was investigated by examining spur gear specimens tested with seven different lubricants. It was found that the higher viscosity lubricants result in longer pitting lives as well as reduced wear coefficients. Spur and helical gear efficiency studies by Xu et al. (*4*), Petry-Johnson et al. (*5*), Moorhead (*6*), Vaidyanathan (*7*), Li and Kahraman (*8*), Li et al. (*9*), and Britton et al. (*10*) all showed experimentally that an increase in oil viscosity through a high viscosity fluid or a reduction in operating temperature reduces the load-dependent (mechanical) power losses. This was confirmed by Talbot et al. (*11*) through planetary gear-set power-loss experiments as well. Some of these studies (*4*, *8*, *9*) also indicate that increased viscosity causes load-independent power losses (due to churning and gear-mesh pocketing) and, in the process, wipes out some or most of the reductions in mechanical losses. The windage power loss studies of Seetharaman and Kahraman (*12*), Seetharaman et al. (*13*), Talbot (*14*), and Hilty (*15*) point to such increases in spin losses with increased lubricant viscosity as well.

Increasing λ ratio through reductions in surface roughness by means of surface polishing has been investigated in various studies. There are a number of commercially marketed processes that can polish machined surfaces either chemically or mechanically, reducing by 4 to 20 times the roughness amplitudes of ground or shaved surfaces. Gear experiments (*4*, *5*, *8*, *14*) show sizable reductions in spur or planetary gear-mesh mechanical power losses of shaved or ground gears whose surfaces are chemically polished. For instance, Petry-Johnson et al. (*5*) report a 19% decrease in mechanical power loss of spur gear boxes when surface roughnesses for ground gears are reduced from 0.32 to 0.08 μm through chemical polishing. These studies also showed that the surface roughness changes do not influence spin losses at all.

Several other studies preferred to use simpler contact arrangements, such as a two-disk setup to study roughness effects. Diab et al. (*16*) used a two-disk machine to compare traction behavior of polished and ground surfaces within a narrow slide-to-roll ratio (ratio of sliding velocity to rolling velocity) range of ±0.2. Similar two-disk experiments (*17*) or ball-on-disk experiments (*4*, *18*) show that the friction coefficient of a contact interface can be reduced by reducing surface roughness.

A number of contact fatigue investigations studied the influence of surface roughness on gear durability. Among them, Bluestein (*19*) and Klein (*20*) performed shaved and chemically polished spur-gear pitting tests using FZG-type machines to show three to five times increases in pitting lives when surfaces are polished. Klein's data was later correlated to the pitting model of Li et al. (*21*), who showed the same improvements by smoothening the surfaces. In addition, Li (*22*) performed two disk-pitting tests on surface roughness effects that were correlated to a point-contact pitting model of Li and Kahraman (*23*). Gear fatigue tests by Krantz et al. (*24*) and several other studies (*25*–*27*) confirm the same effects of surface finish.

Several other studies involved temperature-induced failures such as scuffing due to heat generated at the contact interfaces. These studies looked into the impact of surface roughness as well as methods to reduce boundary friction coefficient at asperity contacts through oil additives that provide tribofilms or surface coatings. Popgoshev and Valori (*28*) studied the impact of materials and lubricant types on scuffing failures. Lee and Cheng (*29*) focused on correlating asperity contacts and the lubricant film thickness to resultant scuffing performance. Liou (*17*) used a heat balance model and two-disk experiments to search for a scuffing limit for an automotive gear steel-lubricant combination. In Alanou et al. (*30*), the effect of different surface treatments and coatings on scuffing was investigated. In these tests, ground, superfinished, and superfinished-plus coated surfaces were tested at a given constant sliding speed value, with the contact pressure increased incrementally up to 1.7 GPa, to determine the load at which scuffing occurs. These tests indicated that superfinished surfaces scuffed at higher loads. Results of this study were not conclusive, as flaking of the coatings in certain conditions was observed. A recent theoretical and experimental study by Li et al. (*31*) indicates the same effects on a ball-on-disk contact.

1.3 Thesis Objectives

It is clear from the literature review that there is not a comprehensive study on the various effects of engineered surface techniques on friction, wear, and scuffing performance of lubricated contacts under aerospace and automotive conditions. All of the studies on surface roughness effects compared a certain single-level of polished surfaces to as-machined surfaces. These studies fail to relate basic two-disk-type tests to actual gear experiments. Coatings considered for gear contact applications are typically thin film coatings applied through physical vapor deposition (PVD) techniques with some significant cost penalty. There is no study on chemically deposited coatings. This study aims to fill some of these gaps in the literature.

The specific technical objectives of this study were as follows:

- Quantify the improvements to friction of ground surfaces that can be achieved through application of surface polishing techniques and nickel boron (NiB) coating of sliding roller contacts and gears.
- Determine the ability of the NiB coating to retain critical dimensions of the roller and gear teeth while providing required wear resistance. Investigate the compatibility of the NiB coating with approved aerospace and ground lubricants.
- Investigate the surface wear consequences of polishing and NiB coating treatments considered.
- Assess the improvements to contact scuffing performance with the NiB coating and surface polishing under both normal and loss-of-lube conditions.

This study was limited to two gear steels, 9310 for aerospace applications and 5120 for automotive applications, paired with DOD-PRF-85734 and 80W90 oils, respectively. A two-disk setup and a four-square-type gear test setup were devised and gear and roller specimens with desired surface treatments fabricated and tested.

1.4 Thesis Outline

In section 2 of this report, the two-disk test methodology will be explained. Details of each test setup and procedures developed for the traction, wear, and scuffing tests will be provided. Test matrices defined for each type of test will be introduced. Section 3 presents all of the two-disk test results and discusses them in terms of the performance of each surface treatment. Section 4 describes a gear test machine, including specimens, instrumentation, and measurement procedures. In addition, a gear efficiency test matrix is defined and gear power loss results are presented and discussed. The last section summarizes the test results, draws the major conclusions, and recommends future work that can be done to further characterize performance of each surface finish technique.

2. Two-Disk Test Methodology

2.1 Two-Disk Test Machine

The two-disk test machine shown in figure 1 was used in this study to evaluate the friction coefficient, wear, and scuffing performance of roller specimens made from two different gear steels with four different engineered surfaces. The schematic of the test machine is shown in figure 2. This test machine allows a pair of disks to be pushed against each other and operate at given values of rolling and sliding speeds.

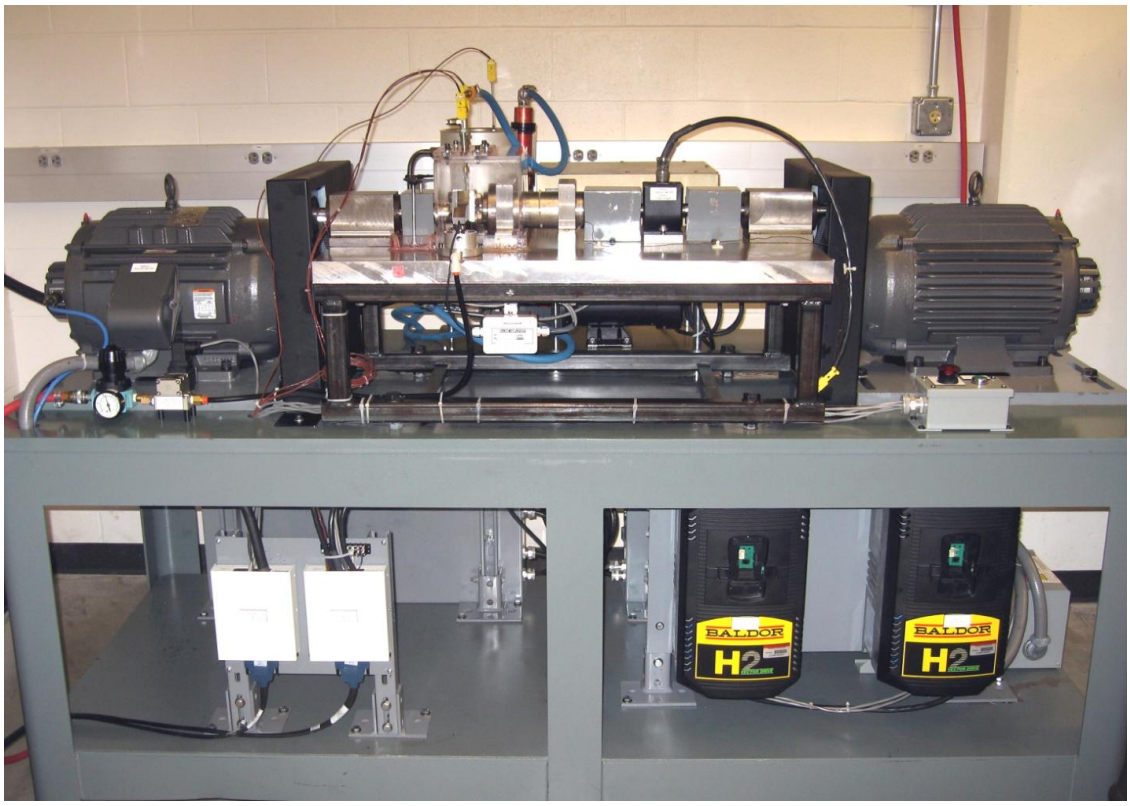

Figure 1. Twin-disk test machine used in this study.

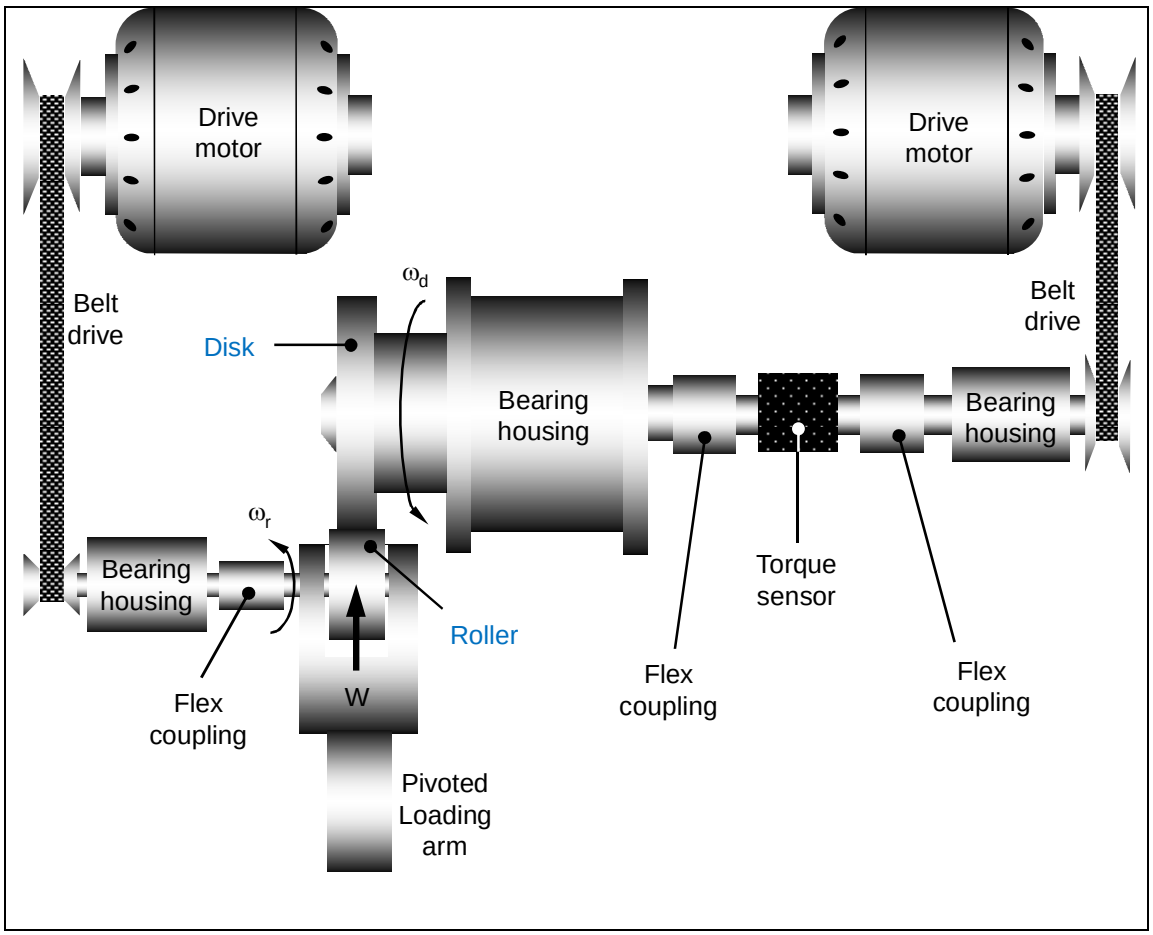

Figure 2. A top view schematic of two-disk test machine used in this study (*17*).

Desired speed conditions were achieved by independently controlling the rotational speeds of the *roller* (smaller of the two disk specimens) and the *disk* (larger of the two disk specimens). Both drive units, powering the roller and the disk, were 10-hp 3-phase alternating-current vector motors, connected to a 2:1-ratio timing belt, as illustrated schematically in figure 2. These drives were controlled by a LabVIEW script. This program was able to independently drive each motor to set roller and disk speeds, ω_1 and ω_2 (in rad/s), to achieve any rolling and sliding speeds at the roller contact interface.

The disk-side driveshaft was rigidly supported by a pair of rolling element bearings within their housing. The roller shaft was supported in the loading fixture by a pair of high-precision ball bearings on one side and one needle roller bearing on the other. Figure 3 shows a close-up view of this arrangement. The roller shaft was threaded on one side to receive a washer and locking nut to axially fix the position of the roller. In its nominal unloaded position, the roller was located at a very small distance from the disk with no contact. The loading lever shown in figure 3 pushed the roller and its shaft toward the disk to initiate contact, in the process offsetting the roller shaft axis from the roller-side drive shaft. To accommodate this offset while loading,

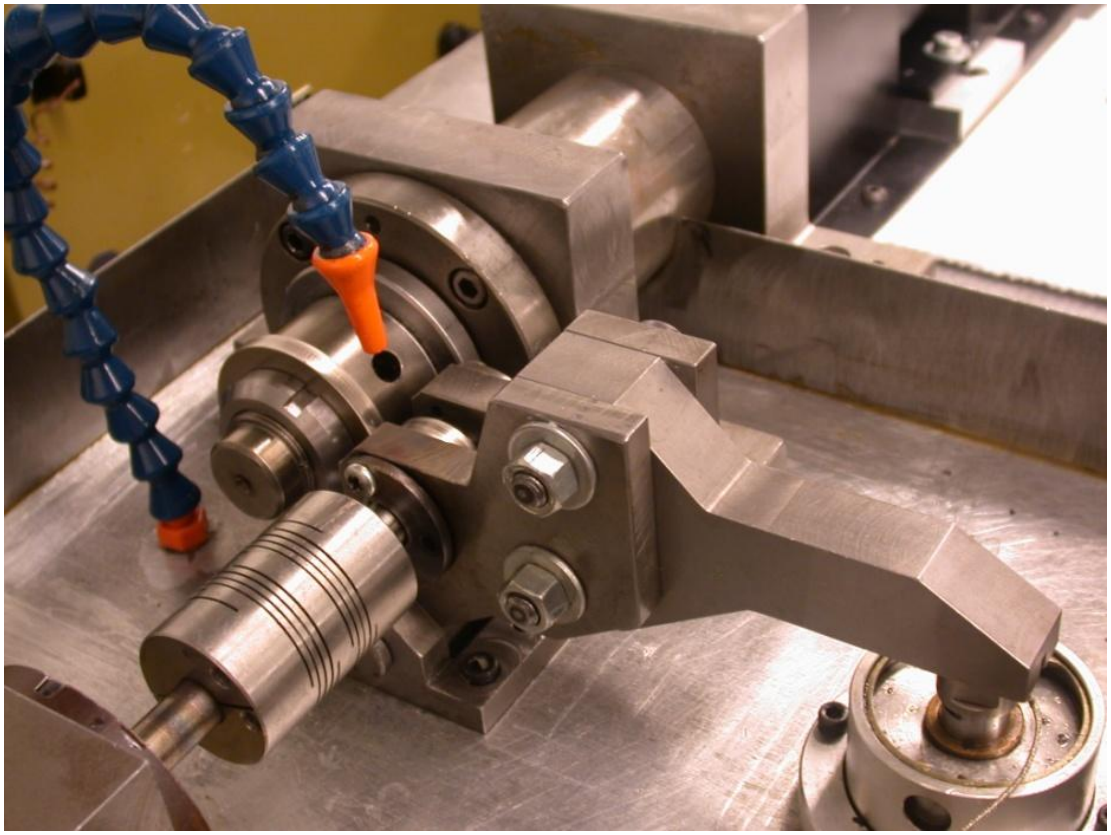

Figure 3. Closeup view of the test pair, roller and disk shafts, roller-side flexible coupling, and the loading arm mechanism.

a flex-coupling (helical spring type) was used to connect the roller shaft and the roller-side drive shaft, as shown in figure 3. The disk was shrunk-fit onto the shaft and a locking nut was tightened to prevent axial motion. This shaft was rigidly supported by four angular contact ball bearings as well as a needle thrust bearing.

A small low-flow-rate lubrication system was used with the tests. The oil was heated inside the reservoir and pumped through flexible hosing into the test area. The maximum obtainable temperature for the oil was 150 °C. Any constant flow-rate was possible within the flow-rate range of 0.4–3.3 lpm. Much lower flow-rates, <0.1 lpm, were also achieved by restricting certain sections of the hose and manipulating the nozzle.

The loading arm applied a normal force through a controlled proportional valve leading to a pneumatic cylinder. The pressure regulator provided the cylinder with a pressure with up to 550 kPa, corresponding to a normal load of 4450 N. This force was monitored by a button-head-type load cell with a threshold of 1112 N, which was inserted at the end of the loading arm in a small recess. A torque meter with a capacity of 3.5 Nm and ±0.5% of full-scale resolution was utilized between the disk shaft and its motor through two helical-style flexible couplings to measure torque within the system. The same LabVIEW program used for controls also monitored and recorded the torque throughout each test.

Two K-type thermocouples were used to measure the bulk surface temperature of the specimen. Mounted on the test box cover through a drilled-out bolt with an integrated spring, this arrangement allowed for the thermocouple tips to come into contact with the test specimen but not induce a measureable amount of downward force. A third thermocouple was placed inside the oil reservoir to measure supply temperature. The temperature measurements were also monitored and recorded in the LabVIEW program.

A safety cover was built to contain heat and add locations for thermocouple placement, as well as to contain oil spray and maintain safety. The cover was a sheetmetal frame with Lexan windows. This cover not only contained the test specimen but also the flexible coupling for the roller shaft. Separate safety covers were in place to shield other rotating components such as belts, sheaves, and couplings.

2.2 Test Specimens

The test specimens were comprised of two cylinders. The roller had an outside radius of r_1 = 15.875 mm with no lead crown and a face width of 7.6 mm. The disk, on the other hand, had a radius of r_2 = 28.575 mm and face width of 6.3 mm. The disk had a circular lead crown of radius r_{2c} = 75 mm to ensure an elliptical contact pattern with no edge-loading between the disks. Figures 4 and 5 show the engineering drawings of the roller and disk specimens, respectively. Figure 6a shows the variation of the half-track width *b* (half-width of the contact ellipse in the axial direction) and the half-width *a* in the circumferential direction of rolling and sliding as a function of the normal load F_n acting on the rollers. Similarly, figure 6b shows the variation of the maximum contact stress σ_{max} (*32*) as a function of F_n. This indicates that the desired contact stress levels can be obtained with this disk pair design with a reasonable contact size.

Two different gear steels were used: AISI 5120, representing a typical automotive gear steel, and AISI 9310, representing a common aerospace gear steel. During the final finishing of the outside surfaces, a special process developed earlier (*17*, *23*) was applied to induce grinding marks in axial direction to simulate the contact conditions of gears.

Once the specimens were evaluated for surface roughness, they were ranked by roughness values and sent out for further processing. A batch of ground specimens with roughnesses within $R_q \in [0.4, 0.7]$ μm were kept as the baseline ground sets (figure 7a). A batch of ground roller and disk specimens were processed using a proprietary commercial polishing process to achieve ultrasmooth contact surfaces with roughnesses of $R_q \approx 0.02$ μm, as illustrated in figure 7b. Similarly, a commonly used chemical polishing process was applied to a third batch of ground specimens to achieve smoother isotropic surfaces at $R_q \approx 0.1$ μm, as illustrated in figure 7c.

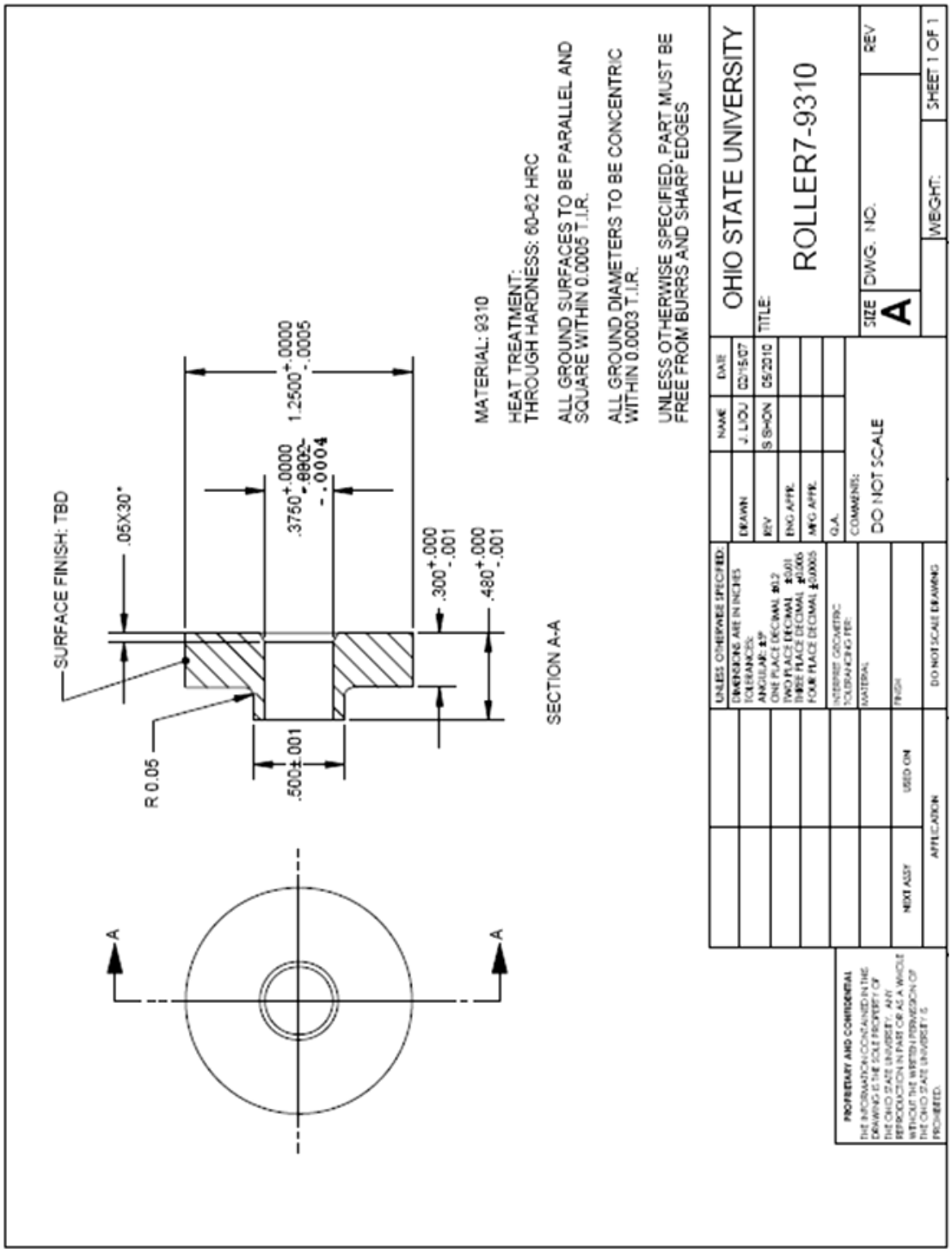

Figure 4. Engineering drawing of the roller specimens.

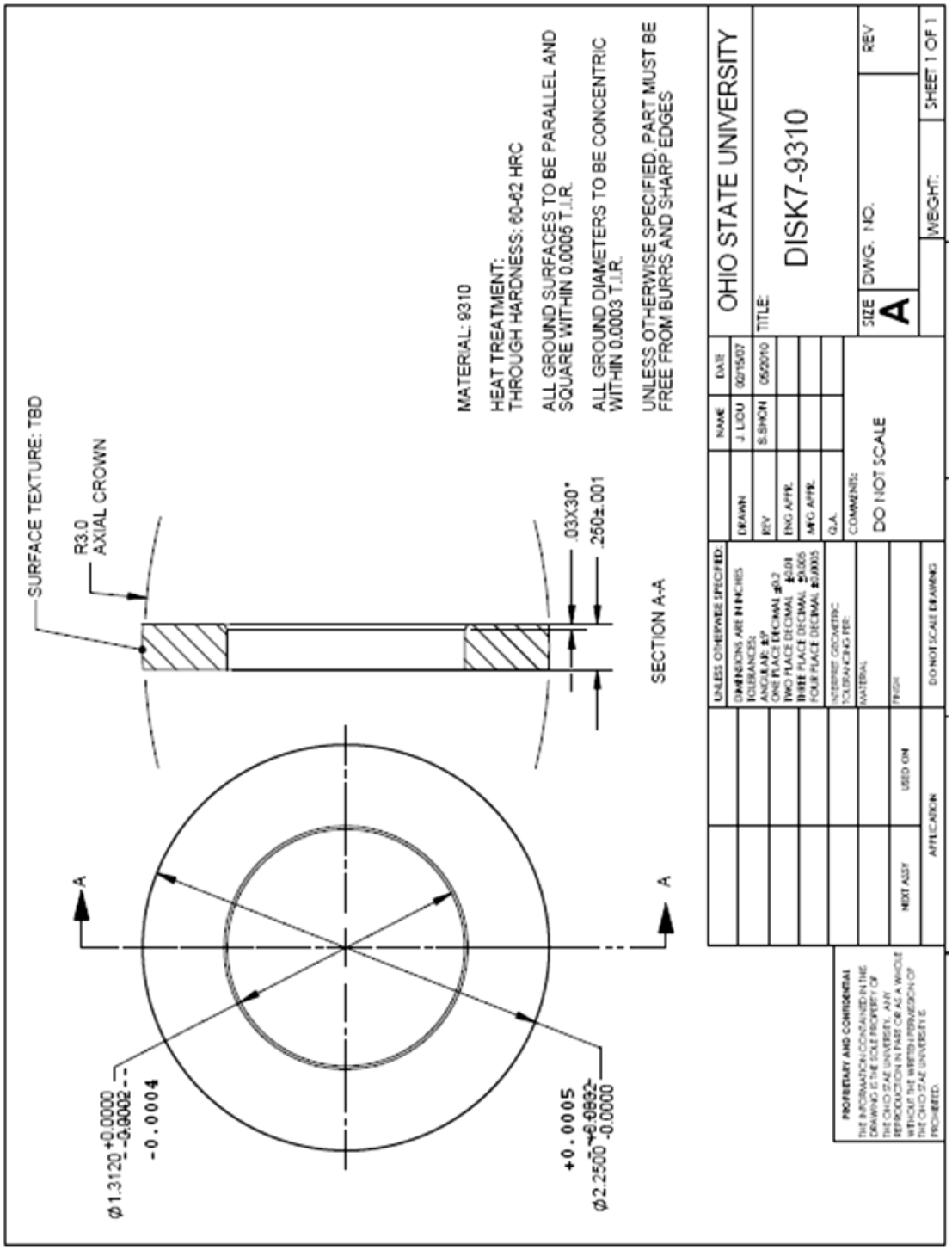

Figure 5. Engineering drawing of the disk specimens.

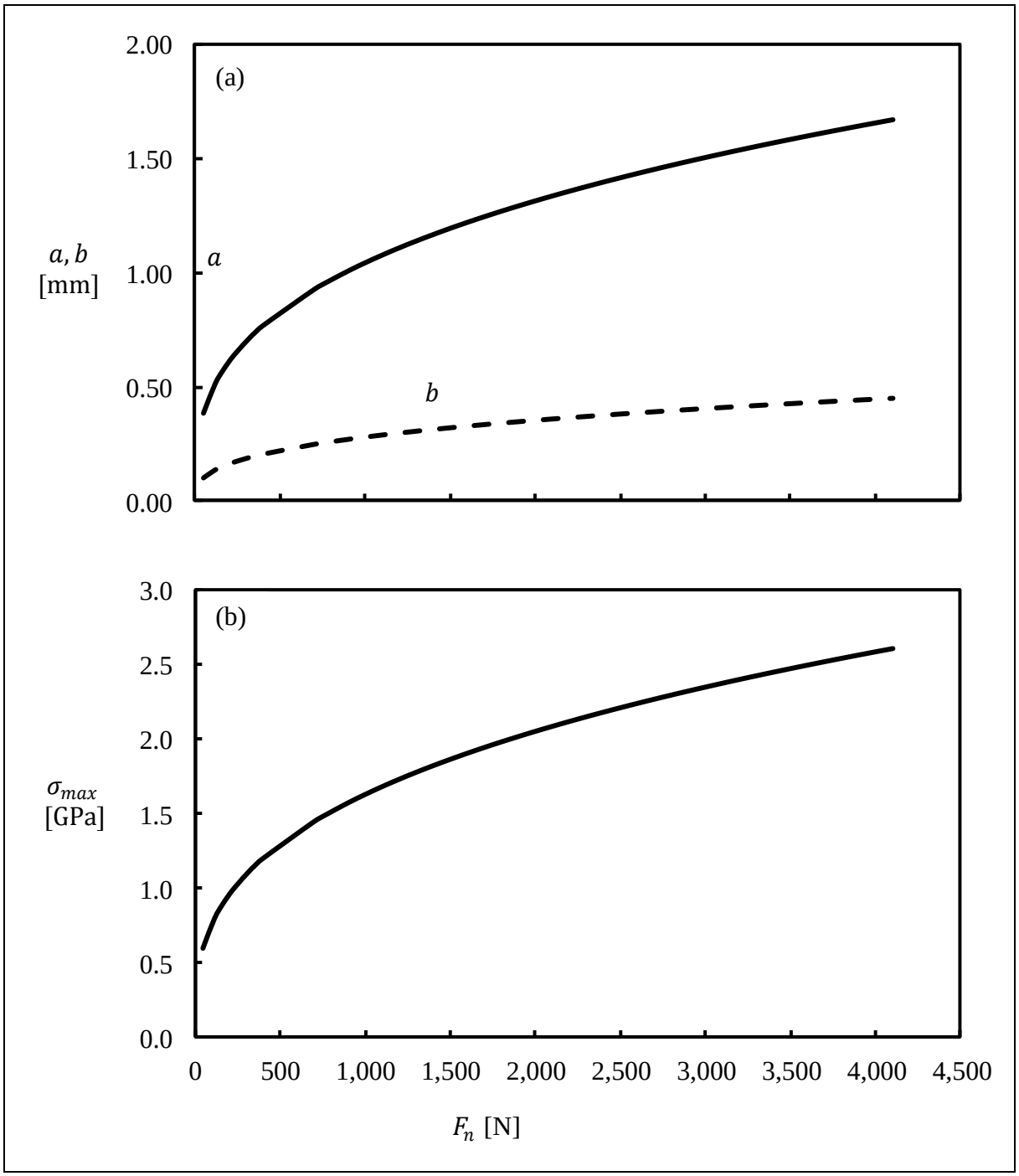

Figure 6. Variation of (a) half-lengths *a* and *b* of the contact ellipse and (b) maximum contact stress with the normal force.

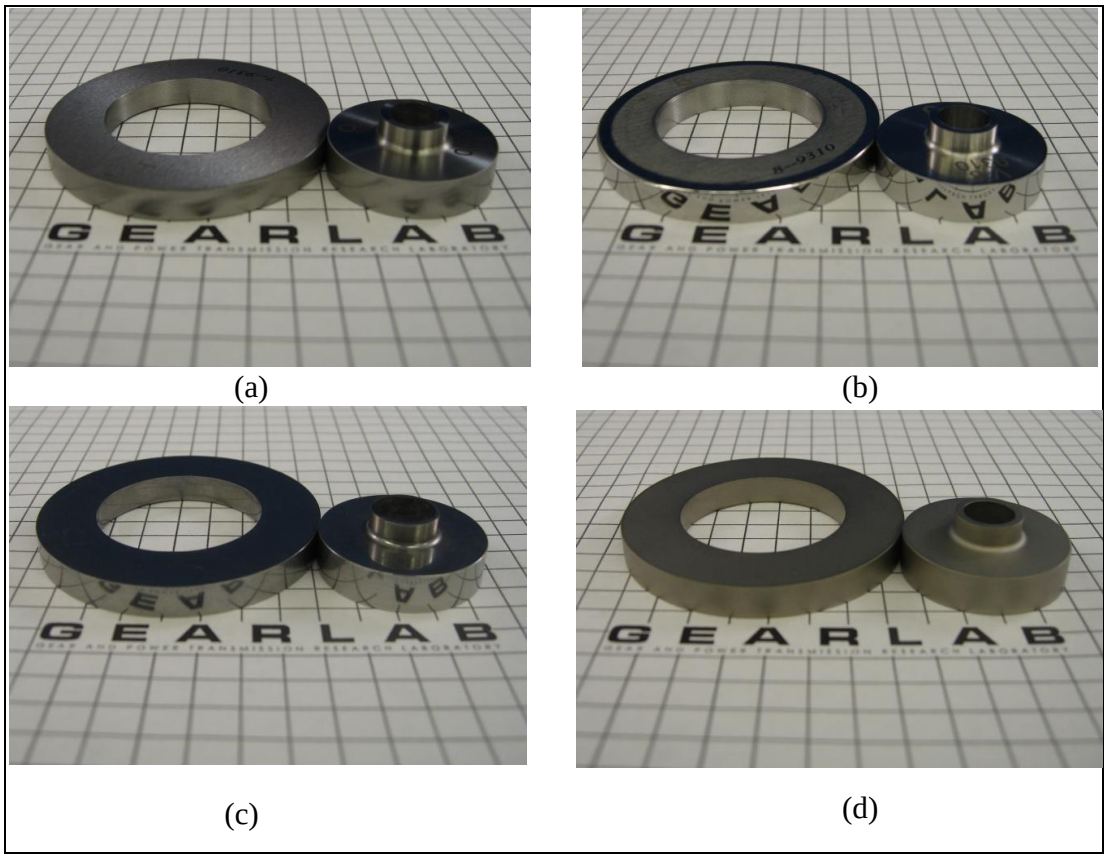

Figure 7. Test specimens used in this study: (a) ground (G), (b) highly polished (HP), (c) chemically polished (CP), and (d) NiB-coated.

One last batch of specimens was chemically polished and then coated with a commercial NiB coating, which was selected by the sponsor, the U.S. Army Research Laboratory, and dip-applied to all specimen external surfaces. It had thickness controllability within [0.25, 250] μm ([0.00001, 0.01] in). In this study, a recommended coating thickness of 25 μm (0.001 in) was used. The specimens used for this were intentionally undersized by the coating thickness to allow for direct accommodation into the test machine with no hardware changes. This particular coating had a hardness of 63 to 65 Rockwell hardness C scale (HRC) if not heat-treated after its application and up to 74 HRC if heat-treated. Due to concern that the case-hardened substrate could be tempered and lose much of its hardness during the heat treatment of the coating, the coated specimens were not put through further heat treatment. Figure 7d shows a pair of rollers that are NiB-coated.

Figure 8 shows measured initial surface profile traces (in the direction of rolling) of representative rollers from each of these four surface variations. In figure 8a, the axially G roller has a roughness of R_q = 0.43 μm, the HP roller in figure 8b has R_q = 0.02 μm, and the CP roller trace in figure 8c has R_q = 0.13 μm. Meanwhile, although it was applied to the CP (relatively smooth) specimens, NiB-coated specimens were found to be rather rough. The measured trace in figure 8d for a coated roller was R_q = 0.81 μm.

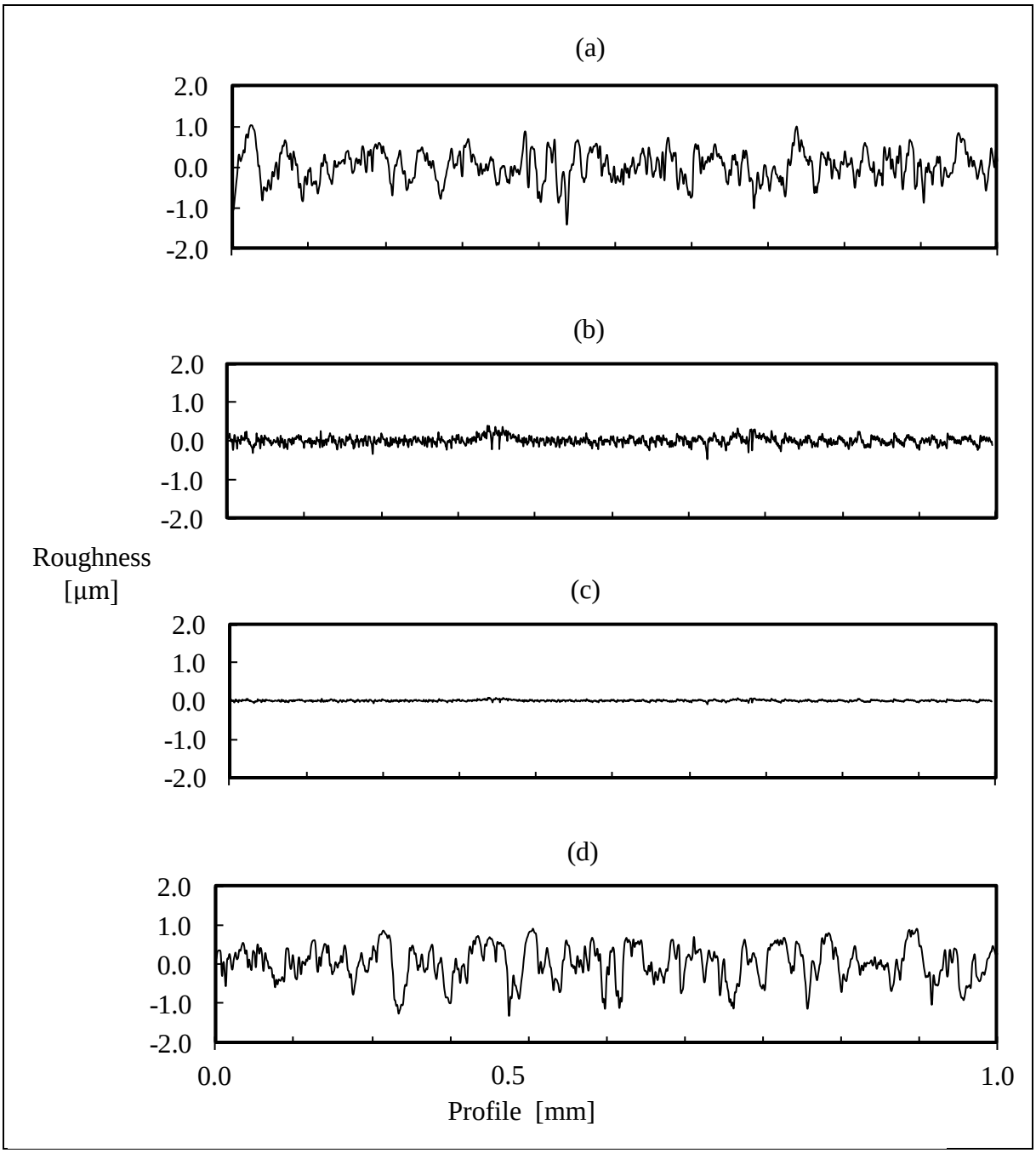

Figure 8. Example measured roughness profiles for (a) G, (b) CP, (c) HP, and (d) NiB-coated rollers.

Lubrication types were selected to properly coincide with the steel gear applications. The AISI 9310 specimens were tested using DOD-PRF-85734 lubricant to represent aerospace application. For this study, the commercial blend Aeroshell 555 was selected. The AISI 5120 specimens were tested with 80W90 oil that is commonly used in the commercial truck differentials of various military ground vehicles, such as armored tanks. The viscosity of the DOD-PRF-85734 at 100 °C is typically 5.25 mm^2/s, while the viscosity of the 80W90 at the same condition is 14.2 mm^2/s.

2.3 Test Procedures

Each of the three tests that comprised this study—traction, wear, and scuffing— was set up in the same manner. First, the disk was heated using an induction heater to approximately 150 °C to increase its bore diameter to fit onto the disk shaft. The specimens were designed to have a slight interference to prevent any relative motion between the disk and shaft. A locknut was then tightened to secure the disk axially. Next, the roller was placed between the forks of the loading fixture and the two precision ball bearings were placed into the applicable diameters within the lower fork. The roller shaft was then manually pushed through the upper fork of the loading fixture until interference with the inner diameter of the roller occurred. A small arbor press was used to apply axial force onto the roller shaft to insert it through the remaining thickness of the roller and then through the ball bearings. A lock washer and nut were threaded onto the end of the shaft to secure the inner race of the bearings. Finally, on each side of the forks, there was a retaining component that secured the positions of the outer races of the bearings axially.

This roller assembly was then moved to the testing platform and the load cell was inserted into the end of the loading fixture. A cylindrical pin, below the contacting surfaces of the disk and roller at the base of the loading assembly, was inserted to form the pivot point. The roller shaft was then connected to the drive shaft through a flexible coupling. By tightening this coupling down, no further axial motion was allowable. Great care was taken to ensure the same contact region throughout each test.

2.3.1 Traction Tests

The traction tests were performed first in the study, the goal of which was to characterize traction (friction coefficient) values for each surface finish and oil variation. The rotational speeds of the roller (ω_1) and disk (ω_2) were both linearly varied at the same time interval to achieve a constant rolling (entraining) speed value,

$$u_r = \frac{1}{2}(u_1 + u_2), \tag{1}$$

where $u_1 = r_1\omega_1$ and $u_2 = r_2\omega_2$, while in the process varying the sliding velocity

$$u_s = u_1 - u_2 \tag{2}$$

linearly from a user-defined negative limit to a positive one. As a result, the corresponding dimensionless slide-to-roll ratio, which is defined as

$$R = \frac{u_s}{u_r} = \frac{2(u_1 - u_2)}{u_1 + u_2}, \tag{3}$$

was varied within the range $R \in [-1.0, 1.0]$. Within the limits of the test machine, this range was accomplished for three rolling speed values of u_r = 5, 10, and 15 m/s.

Prior to actual tests, several trial tests were performed to determine the optimal ramp-up and ramp-down rates for the traction tests. Prior tests done on an earlier version of the same test machine (*17*) did not have the capability to implement programmed speed profiles and, therefore, were reported to be impacted by the changes taking places to the contact surface roughnesses throughout a traction test. Consequently, optimizing (minimizing) the length of test with sufficient data points and without any tangible changes to surface roughness profiles was critical. A number of trial runs were performed, as specified in table 1. The corresponding R_q values at the end of each of these trial traction tests are compared in figure 9. A 5-min test was adapted for the rest of the traction tests as a sufficiently long test with a secondary impact on the surface roughnesses.

Table 1. Preliminary tests performed to define a traction test duration with minimum surface roughness changes.

Test	**Duration (min)**	**Change in *R***
Run In	10	–1 (constant)
Test 1	2	–1 to +1
Test 2	2	+1 to –1
Test 3	5	–1 to 1
Test 4	5	+1 to –1

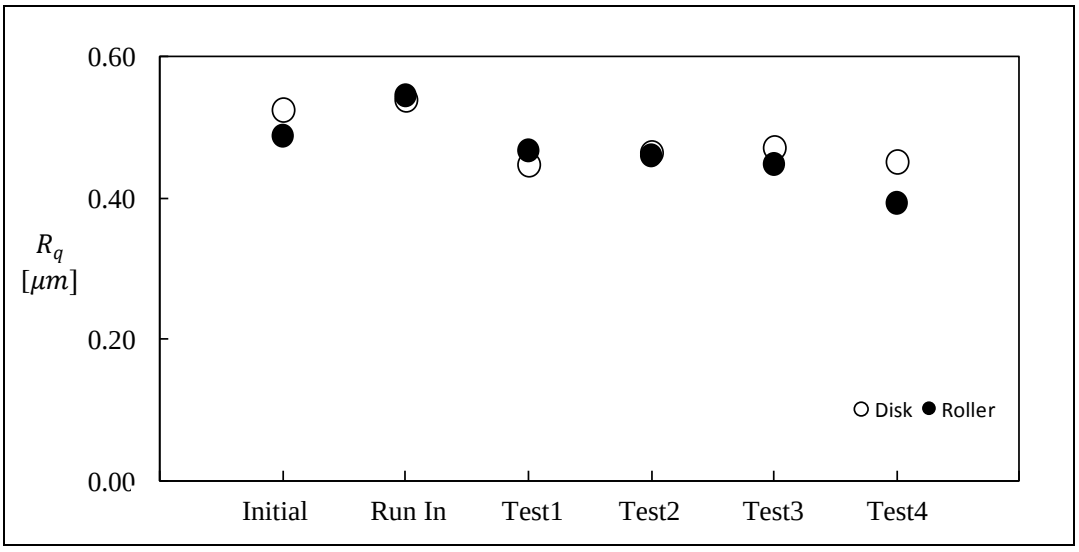

Figure 9. Measured R_q values of roller and disk specimens throughout the preliminary study according to table 1.

Each traction test was performed at a user-defined constant normal load (F_n) value. The torque provided to the disk by its drive, which is equal the total traction torque T_t experienced by the disk-side driveline, was measured by the torque sensor shown in figure 2. Considering that T_t consists of the contact friction torque T_c and the disk-side drive shaft bearing friction torque T_b,

$$T_t = T_c + T_b, \tag{4}$$

determining contact traction required determining and removing T_b from the measured T_t signal. First, T_b was measured by simply running an unloaded traction test ($F_n = 0$ such that $T_c = 0$ to yield $T_t \approx T_b$). Next, the traction test was repeated at the desired F_n value and $T_c = T_t - T_b$ was determined from these two tests. The friction coefficient of the contact was then computed as

$$\mu = \frac{T_c}{r_2 F_n}. \tag{5}$$

Figure 10 illustrates this procedure used to remove bearing traction. In figure 10a, a raw T_t measurement at a given F_n is shown. As both T_b and T_c constitute this T_t signal, the traction data is not skew-symmetric about the origin of the graph at = 0. In figure 10b, the corresponding T_b measurement (at $F_n = 0$) within the same *R* range (representing the effect of the variation of ω_2) is shown. Here, T_b is observed to increase linearly with increasing *R* (or with increasing ω_2). Finally, figure 10c represents the roller contact traction curve that is obtained by using figure 10a and 10b according to equation 4.

According to figure 6b, the test machine with the specified roller geometries was capable of a maximum contact stress of up to 2.6 GPa. A maximum contact stress value of 2.0 GPa and an intermediate value of 1.2 GPa were selected as the load conditions in traction tests.

The lubrication system was turned on initially at a flow rate of 1 lpm to heat the specimens to the set test temperature value. The test specimens were rotated slowly under no load during this heating period. Once the specimens reached the desired initial surface temperatures, the traction tests previously described were performed at a test flow rate of 0.5 lpm.

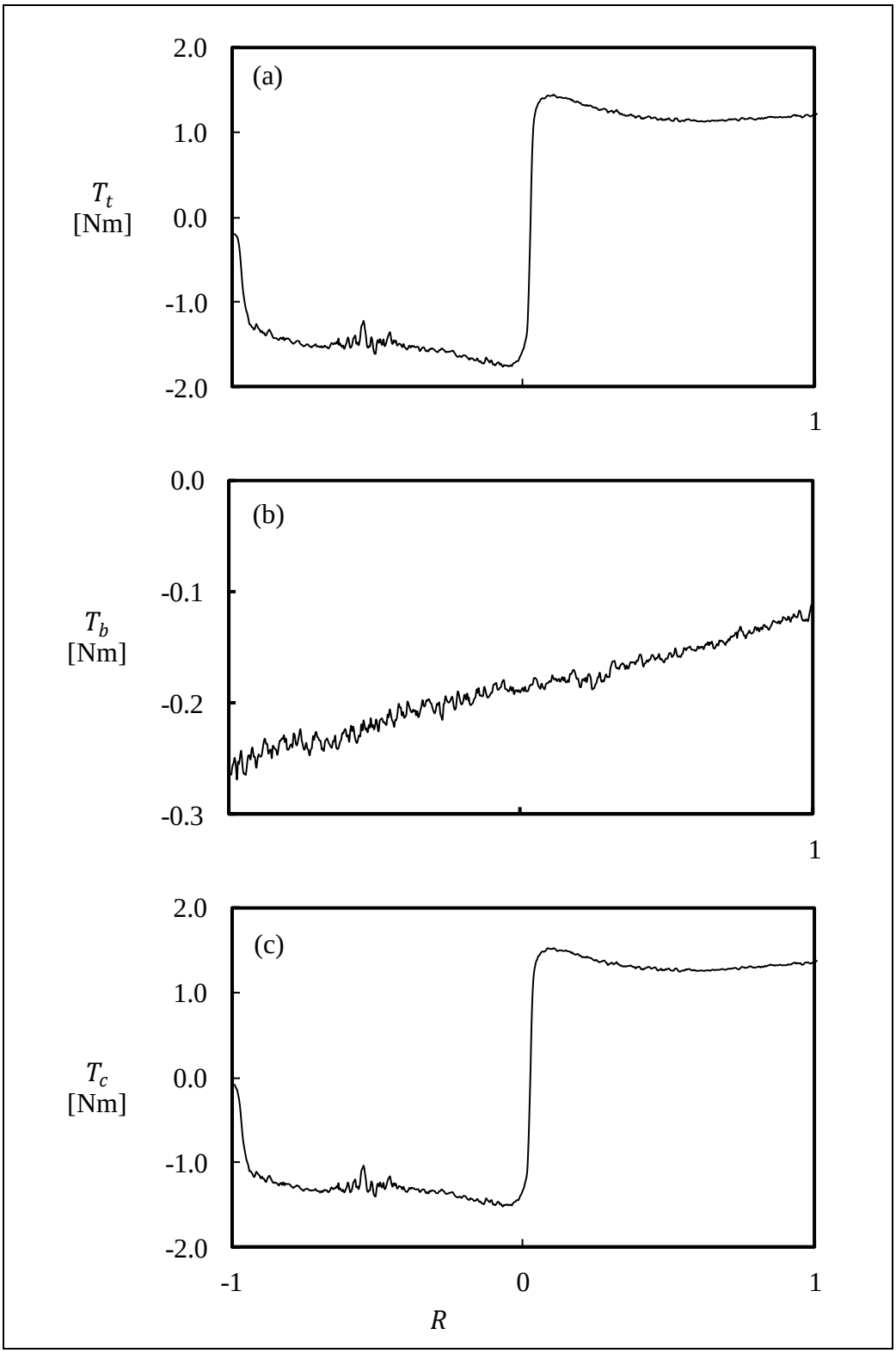

Figure 10. An example set of measured (a) T_t, (b) T_b, and (c) the resultant T_c calculated from (a) and (b).

2.3.2 Wear Tests

The wear test procedure was defined with multiple interim inspections. A maximum test duration of 30 million roller cycles was considered. This corresponded to 70 h of testing at u_r = 15 m/s and R = –1.0. This high-speed high-sliding condition was found to be suitable for inducing wear within the total loading cycles defined. The largest load increment corresponding to a maximum contact stress of 2 GPa was utilized by the same reasoning. The interval for interim inspections was set initially at 10 million cycles, while in certain tests this was reduced to every 2 million cycles to more accurately document the wear rate. A suspension criterion of maximum wear depth of 25 μm across the profile of either the disk or roller was adapted. Any wear accumulation beyond this value within the first 30 million roller cycles was not allowed. The lubrication flow rate was set and maintained at 0.5 lpm for the duration of the wear tests. Oil inlet temperature was maintained at 90 °C.

2.3.3 Scuffing Tests

The scuffing tests were performed under two different conditions: fully lubricated and starved. Both types of tests were carried out the same way, with only lubrication conditions being different. Fully lubricated tests had an oil flow rate of 0.5 lpm, while the flow rate for the starved condition was limited to 0.01 lpm. To achieve such a low flow rate, the pump motor was turned to its lowest setting and the nozzle was restricted to create a small periodic drip.

Before testing began, the specimens were brought to a constant surface temperature under the same procedure as the traction tests. Again the tests were performed at u_r = 15 m/s and R = –1.0 to create a challenging contact environment. The normal load F_n was increased in steps, as shown in figure 11, after every 5 min by a certain amount to achieve a 0.1 GPa increase in the maximum contact stress up to 2.4 GPa. Figure 11 plots these stress levels on the same graph. No reliable automated means was available to stop the test when surfaces scuffed. Instead, the operator manually stopped the machine when a sudden increase in the measured traction torque value was observed. An example traction torque measurement from a scuffing test shown in figure 12 illustrates such a spike at the onset of scuffing.

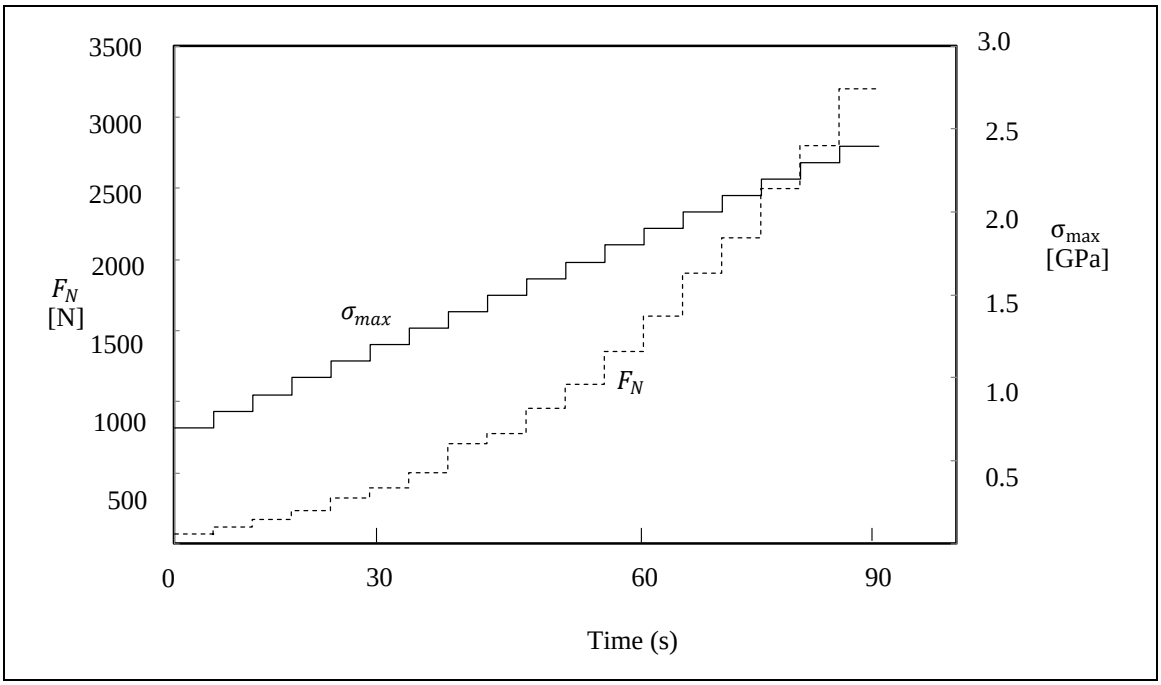

Figure 11. Loading schedule used in scuffing tests.

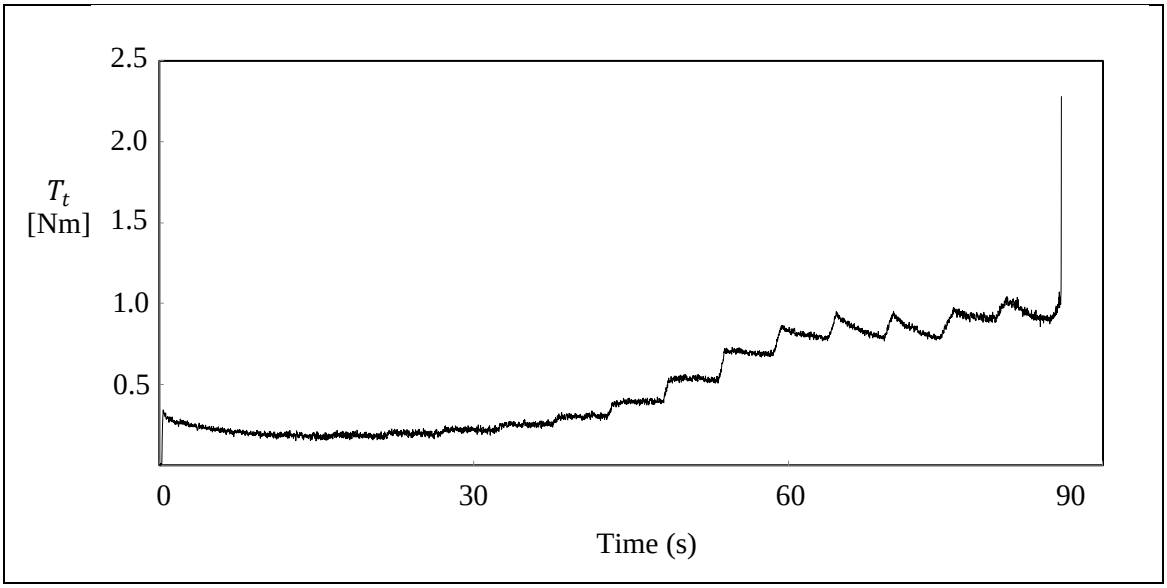

Figure 12. An example T_t measurement during a scuffing test exhibiting a spike due to onset of scuffing failure.

2.4 Inspection Procedures

Upon receipt of the specimen, the profile direction of the disk and roller were measured on a gear coordinate measurement machine (CMM) (Gleason M&M 255) to ensure the proper curvature (for the roller) and straightness (for the disk). Figure 13 shows a disk (a) and a roller (b) being measured on the gear CMM. Additionally, the surface roughness along the profile direction was measured using a surface profiler (Taylor-Hobson Form Talysurf-i60). Figure 14 shows a disk being measured for its roughness in the rolling (circumferential) direction. Three measurements were conducted to create an average roughness value of the part, and care was taken to ensure that the measurements were conducted in the middle of the specimen, as this is the location of contact.

Measurements of the disk and roller were taken before and after the traction tests. During the wear tests, at each inspection interval, the disk and roller were again measured with both machines. The scuffing test specimens were measured only before the test began, as surfaces were extremely rough after most scuffing tests.

(a)

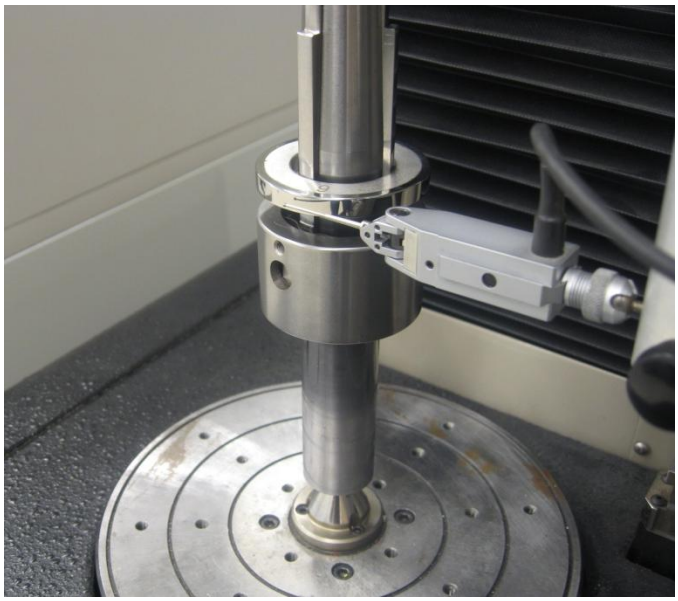

(b)

Figure 13. A disk (a) and roller specimen (b) being measured on the gear CMM.

(a)

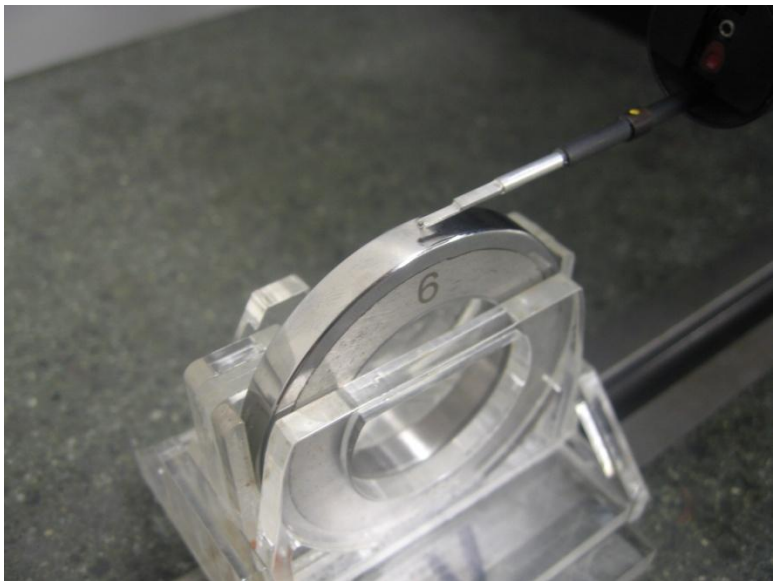

(b)

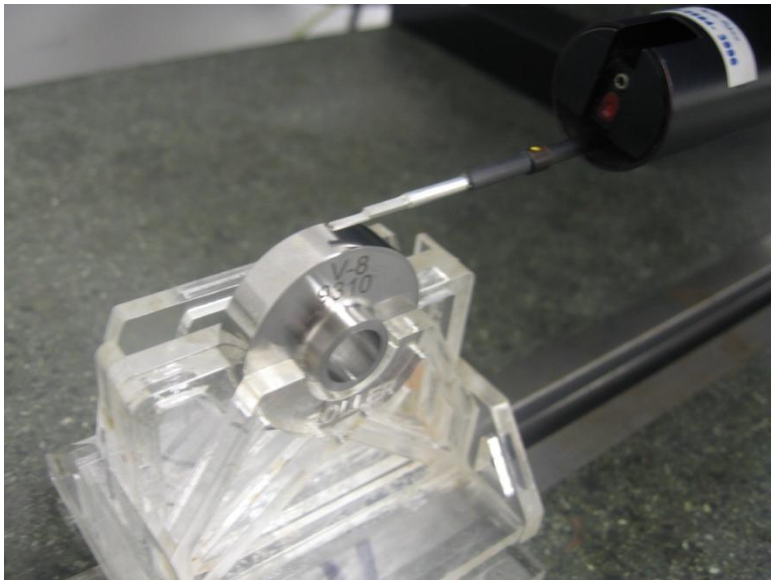

Figure 14. A disk (a) and roller specimen (b) being measured on the surface roughness profiler.

2.4.1 Surface Roughness Settings

The inspection of each surface utilized different cutoff values and evaluation lengths due to the relative roughness amplitudes of the different surface finishes. A smooth surface requires less evaluation length than a rougher surface, as the resolution needs to be greater with the smoother surface and both horizontal and vertical are linked in the evaluation. A 2-µm tip probe was utilized on the inspection machine. Table 2 specifies the settings used to determine roughness values of the specimens in this study.

Table 2. Surface roughness inspection parameters utilized on the roughness inspection machine.

Surface Finish	Cutoff (mm)	Evaluation Length (mm)
Ground	0.8	4.0
NiB-coated	0.8	4.0
Chemically polished	0.25	1.25
Highly polished	0.08	0.4

3. Two-Disk Test Results

3.1 Introduction

In this section, the conduct of the tests described in section 2 is detailed according to test matrices defined for each test. The following three sections, respectively, present the test conditions and measurement results for traction, wear, and scuffing tests. Other relevant information such as repeatability studies and surface bulk temperatures are also presented wherever applicable.

3.2 Traction Tests

One method of evaluating the performance of an engineered surface is by comparing the traction performance with a baseline ground surface. The friction coefficient µ dictates the mechanical power losses at gear and bearing contacts to define efficiency of these components. The tests performed in this section were intended to provide a comparison of µ for these surface variations under tightly controlled conditions.

Traction tests were categorized by oil type. Hard-ground, chemically polished, and NiB-coated specimens were tested with 80W90 oil, as these surface treatments would be suitable for ground vehicle transmission applications. Tests with HP specimens were excluded from this group of tests for ground vehicle applications because of the cost of the process. All the specimens in this

group were made out of 5120 gear steel. Meanwhile, a second group of 9310 specimens having G, CP, and HP surfaces was tested using a DOD-PRF-85734 oil to represent the aerospace requirement.

Table 3 presents the traction test matrix. Each surface type was tested with each lubricant at two maximum contact pressure values of $\sigma_{\max} = 1.2$ and 2.0 GPa and at three rolling speed values of $u_r = 5$, 10, and 15 m/s each with a slide-to-roll ratio range of $R \in [-1.0, 1.0]$. These values were selected based upon various operating loads and speeds that the ground vehicle might encounter and where the aerospace application might apply. Accordingly, the test matrix given in table 3 consisted of 36 individual traction tests. All of these tests were performed at an oil inlet temperature of 90 °C. Table 4 lists the minimum film thickness (h_{min}) values (calculated by using the Hamrock-Dowson formula) and the corresponding lambda ratio ($\lambda = h_{\min}/R_q$, where R_q is the combined root-mean-square (RMS) surface roughness of the contact surfaces) values for each of the tests specified in table 3.

Table 3. Traction test matrix.

Material	**Lubricant**	**Surface Treatment**	u_r **(m/s)**	$\sigma_{\max}$ **(GPa)**
9310	DOD-PRF-85734	Ground	5, 10, 15	1.2, 2.0
		Chemically polished	5, 10, 15	1.2, 2.0
		Highly polished	5, 10, 15	1.2, 2.0
5120	80W90	Ground	5, 10, 15	1.2, 2.0
		Chemically polished	5, 10, 15	1.2, 2.0
		NiB-coated	5, 10, 15	1.2, 2.0

Table 4. Computed minimum film thickness and lambda ratio values for tests with (a) MIL-PRF-23699 oil and (b) 80W90 oil.

Lubricant	Surface Treatment	u_r (m/s)	σ_{max} (GPa)	h_{min} (μm)	λ
(a)					
DOD-PRF-85734	G	5	1.2	0.11	0.27
		10	1.2	0.18	0.44
		15	1.2	0.23	0.58
		5	2.0	0.10	0.25
		10	2.0	0.16	0.39
		15	2.0	0.21	0.52
DOD-PRF-85734	CP	5	1.2	0.11	1.09
		10	1.2	0.18	1.75
		15	1.2	0.23	2.30
		5	2.0	0.10	0.99
		10	2.0	0.16	1.58
		15	2.0	0.21	2.08
DOD-PRF-85734	HP	5	1.2	0.11	5.45
		10	1.2	0.18	8.73
		15	1.2	0.23	11.51
		5	2.0	0.10	4.92
		10	2.0	0.16	7.90
		15	2.0	0.21	10.40
(b)					
80W90	G	5	1.2	0.19	0.24
		10	1.2	0.31	0.38
		15	1.2	0.41	0.51
		5	2.0	0.17	0.21
		10	2.0	0.27	0.34
		15	2.0	0.36	0.45
80W90	CP	5	1.2	0.19	0.24
		10	1.2	0.31	0.38
		15	1.2	0.41	0.51
		5	2.0	0.17	0.21
		10	2.0	0.27	0.34
		15	2.0	0.36	0.45
80W90	NiB	5	1.2	0.19	0.24
		10	1.2	0.31	0.38
		15	1.2	0.41	0.51
		5	2.0	0.17	0.21
		10	2.0	0.27	0.34
		15	2.0	0.36	0.45

To complement tests with certain material and lubricant at each u_r value, unloaded tests were also performed to measure bearing power losses alone. The procedure outlined in section 2 and illustrated in figure 10 was then applied to obtain T_c according to equations 4 and 5. Therefore, bearing losses have been removed from the data presented in this section.

Once testing of all material treatments and lubricants was completed, a repeatability study of the machine was conducted. The HP specimens were retested at all speeds and loading conditions. As illustrated in figure 15, the results from repeatability tests were very close to each other, indicating that the results presented in this section can be viewed in confidence.

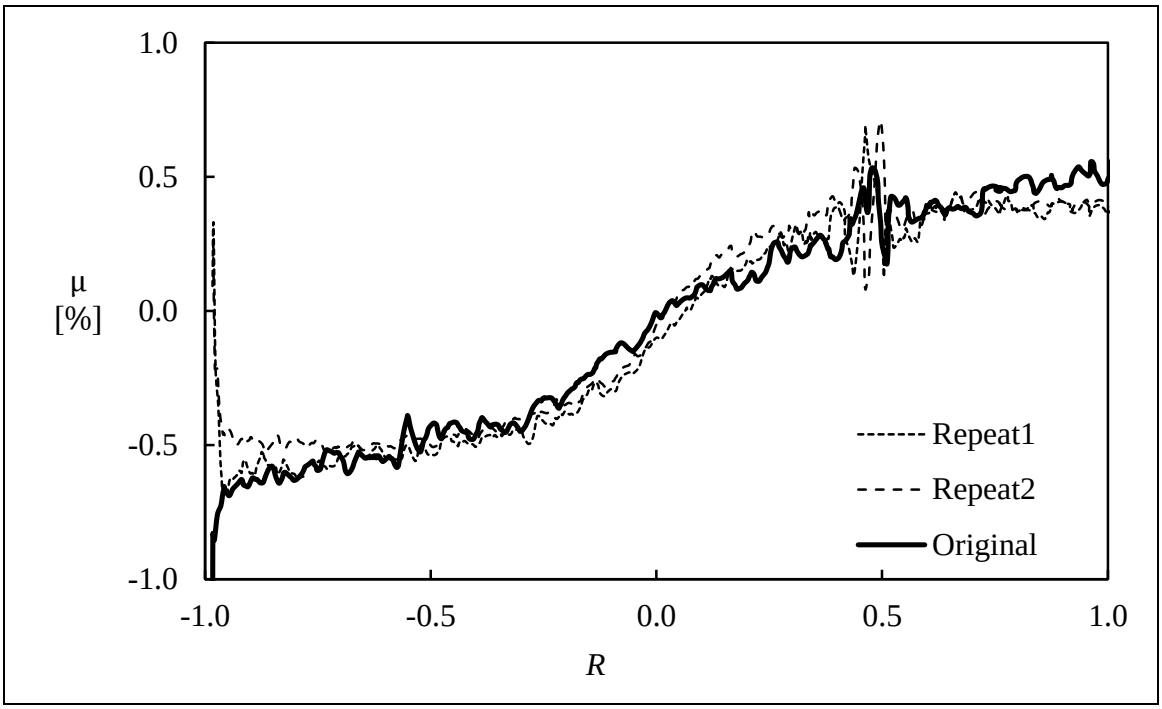

Figure 15. Traction repeatability tests performed on HP specimens, where σ_{max} = 1.2 GPa and u_r = 5 m/s.

3.2.1 Measured Friction Coefficient Curves

In figure 16, measured traction curves for G, CP, and HP steel 9310 specimens are compared at (a) $\sigma_{max} = 1.2$ GPa and $u_r = 5$, (b) 10 m/s, and (c) 15 m/s with DOD-PRF-85734 lubricant. Meanwhile, the corresponding results for $\sigma_{max} = 2.0$ GPa are shown in figure 17. It is observed from these figures that the HP surfaces with the lowest R_q value resulted in the lowest μ values regardless of u_r and σ_{max}, followed by CP and then G. For instance, in figure 17a for $u_r = 5$ m/s and $\sigma_{max} = 2.0$ GPa, $\mu = 2.64\%$, 2.10%, and 1.57% at $R = 0.5$ for the G, CP, and HP surfaces, respectively. The corresponding λ values in table 4a are 0.25, 0.99, and 4.92, confirming that higher λ values correspond to lower μ values. Lower values of λ represent smaller oil film thicknesses compared with roughness heights, such that asperity contacts increase and, in the process, increase μ significantly.

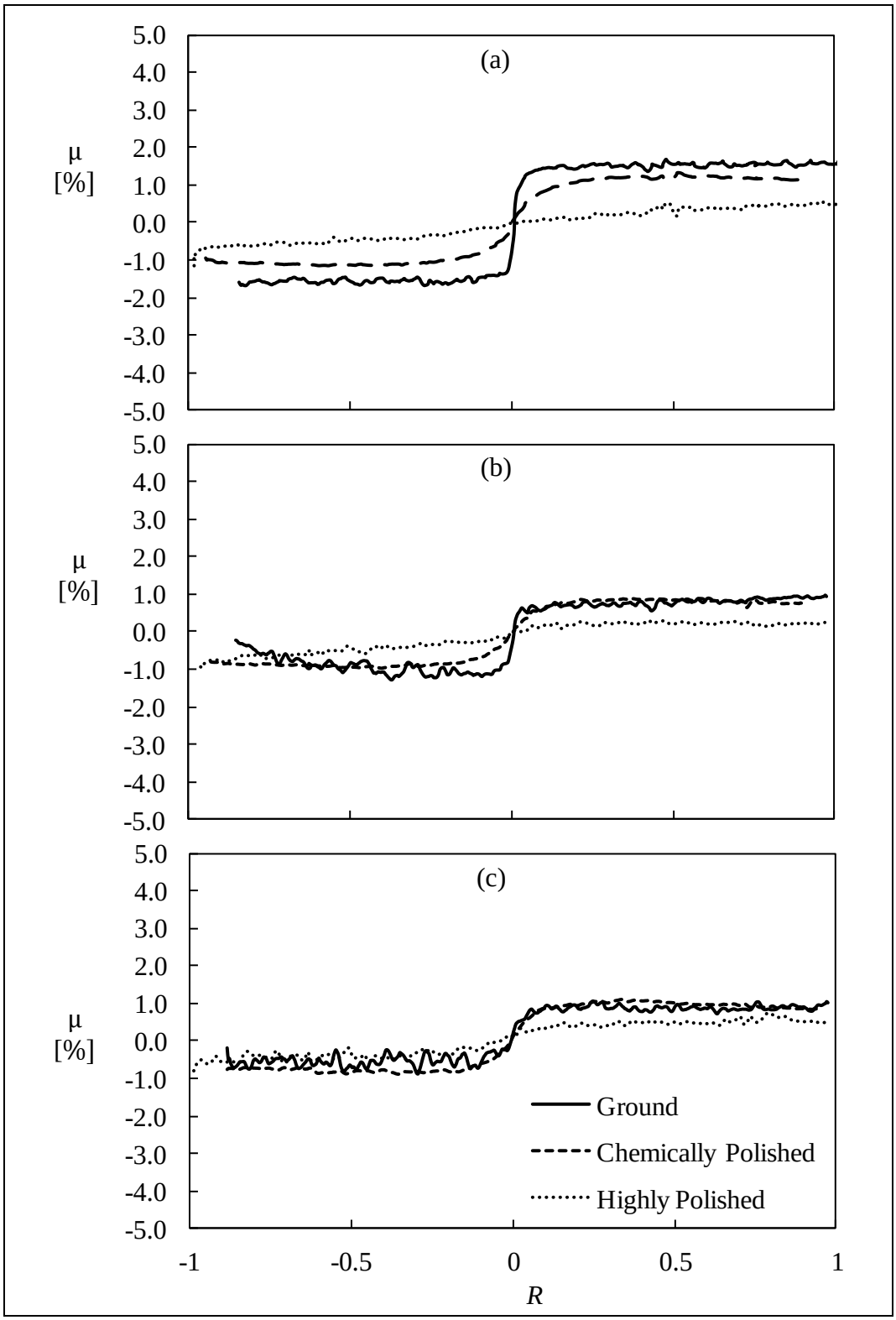

Figure 16. Comparison of the measured μ values of G, CP, and HP surfaces for σ_c = 1.2 GPa and u_r values of (a) 5, (b) 10, and (c) 15 m/s. Oil is DOD-PRF-85734.

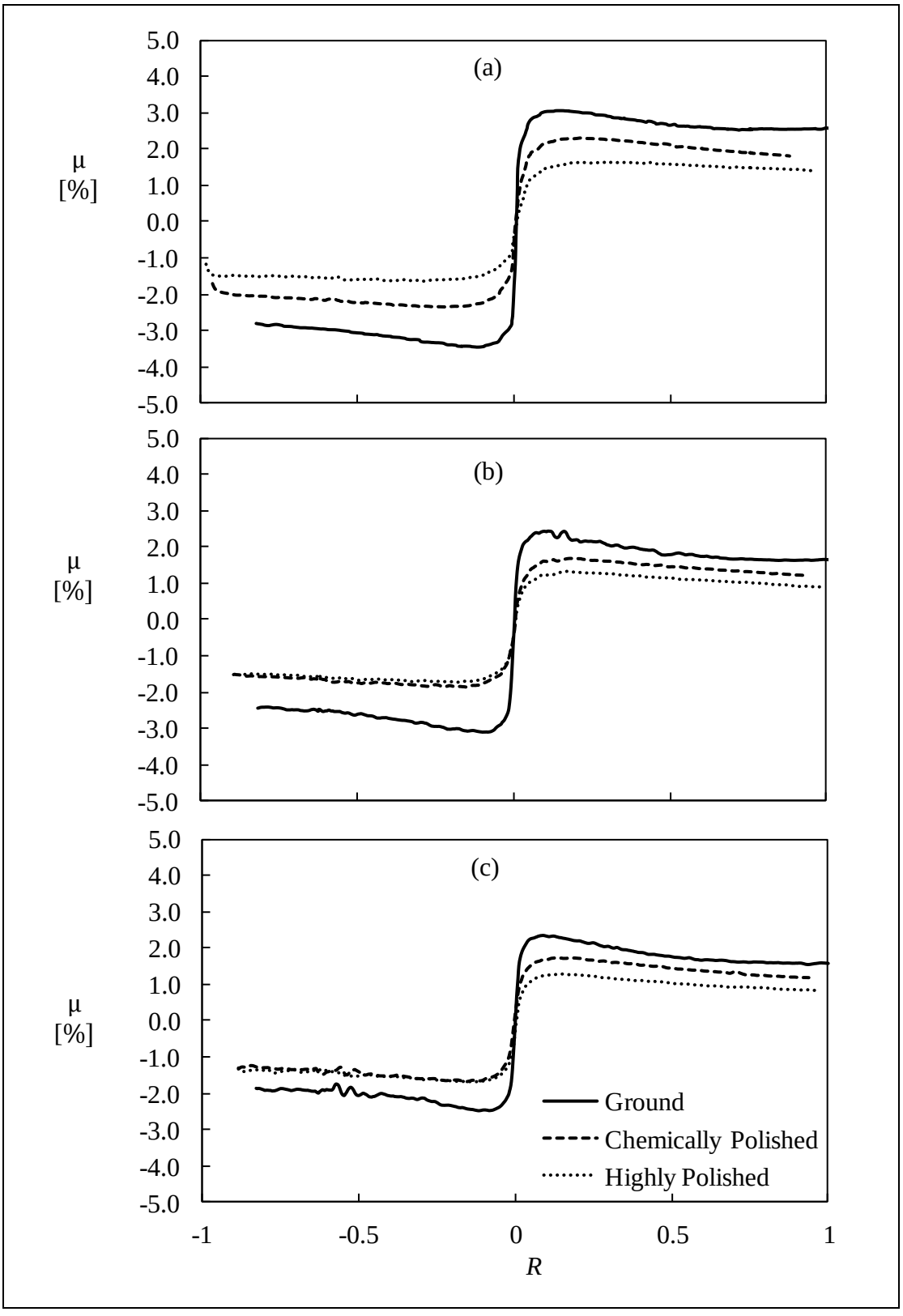

Figure 17. Comparison of the measured μ values of G, CP, and HP surfaces for σ_c = 2.0 GPa and u_r values of (a) 5, (b) 10, and (c) 15 m/s. Oil is DOD-PRF-85734.

It is also observed from figures 16 and 17 that μ decreases with increased rolling speed u_r. For instance, in figure 16 ($\sigma_{max} = 1.2$ GPa), G specimens registered $\mu = 1.57\%$, 0.85%, and 0.81% at *R* = 0.5 for $u_r = 5$, 10, and 15 m/s , respectively. Similarly, in figure 17 ($\sigma_{max} = 2.0$ GPa,), the specimens registered $\mu = 2.64\%$, 1.77%, and 1.74% for $u_r = 5$, 10, and 15 m/s, respectively, again at R = 0.5. This is due to the fact that EHL film thickness increases with u_r, resulting in a larger λ and fewer asperity contacts. The change in μ with u_r is significantly less for smoother (larger λ) surfaces, supporting this reasoning further.

A comparison of respective curves in figures 16 and 17 provide information about the influence of σ_{max} (or normal load) on μ. At $u_r = 15$ m/s and *R* = 0.5, G surfaces had $\mu = 0.81\%$ for $\sigma_{max} = 1.2$ GPa and $\mu = 1.74\%$ for $\sigma_{max} = 2.0$ GPa. A larger normal load results in reduced film thickness to increase μ.

In figure 16, for $\sigma_{max} = 1.2$ GPa, ripples are observed in measured traction curves throughout the test data. This was a direct result of vibrations that occurred in the loading mechanism of the test machine under lighter loads. Such adverse dynamic effects were less important under higher load values, as evident in figure 17, where the traction curves are much smoother.

The measured traction curves of the G, CP, and NiB-coated specimens run with 80W90 lubricant are shown in figures 18 and 19 for $\sigma_{max} = 1.2$ and 2.0 GPa, respectively. Again, the smoother surface CP specimens have the lowest friction coefficient compared to the G and NiB-coated specimens. For example, at $u_r = 5$ m/s and $\sigma_{max} = 2.0$ GPa, $\mu = 3.40\%$, 2.34%, and 3.70% at *R* = 0.5 for the G, CP, and NiB-coated surfaces, respectively. With the respective surface roughnesses of $R_q = 0.4$, 0.1, and 0.8 μm (corresponding to λ = 0.43, 1.71, and 0.21), these results indicate that the value of μ is largely dictated by the roughness amplitudes, while NiB coating did not have any special "antifriction" influence.

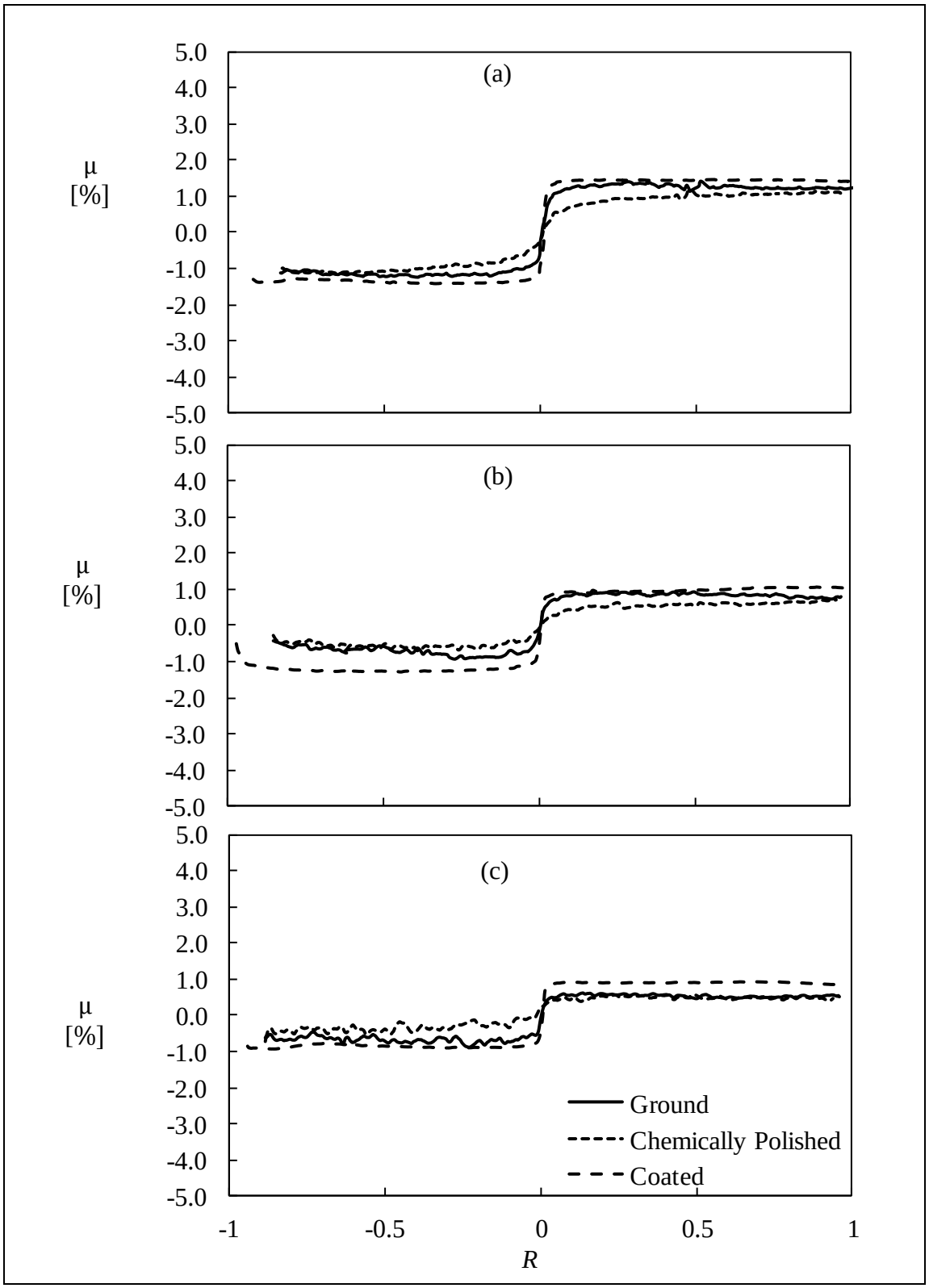

Figure 18. Comparison of the measured μ values of G, CP, and NiB-coated surfaces for σ_c = 1.2 GPa and u_r values of (a) 5, (b) 10, and (c) 15 m/s. Oil is 80W90.

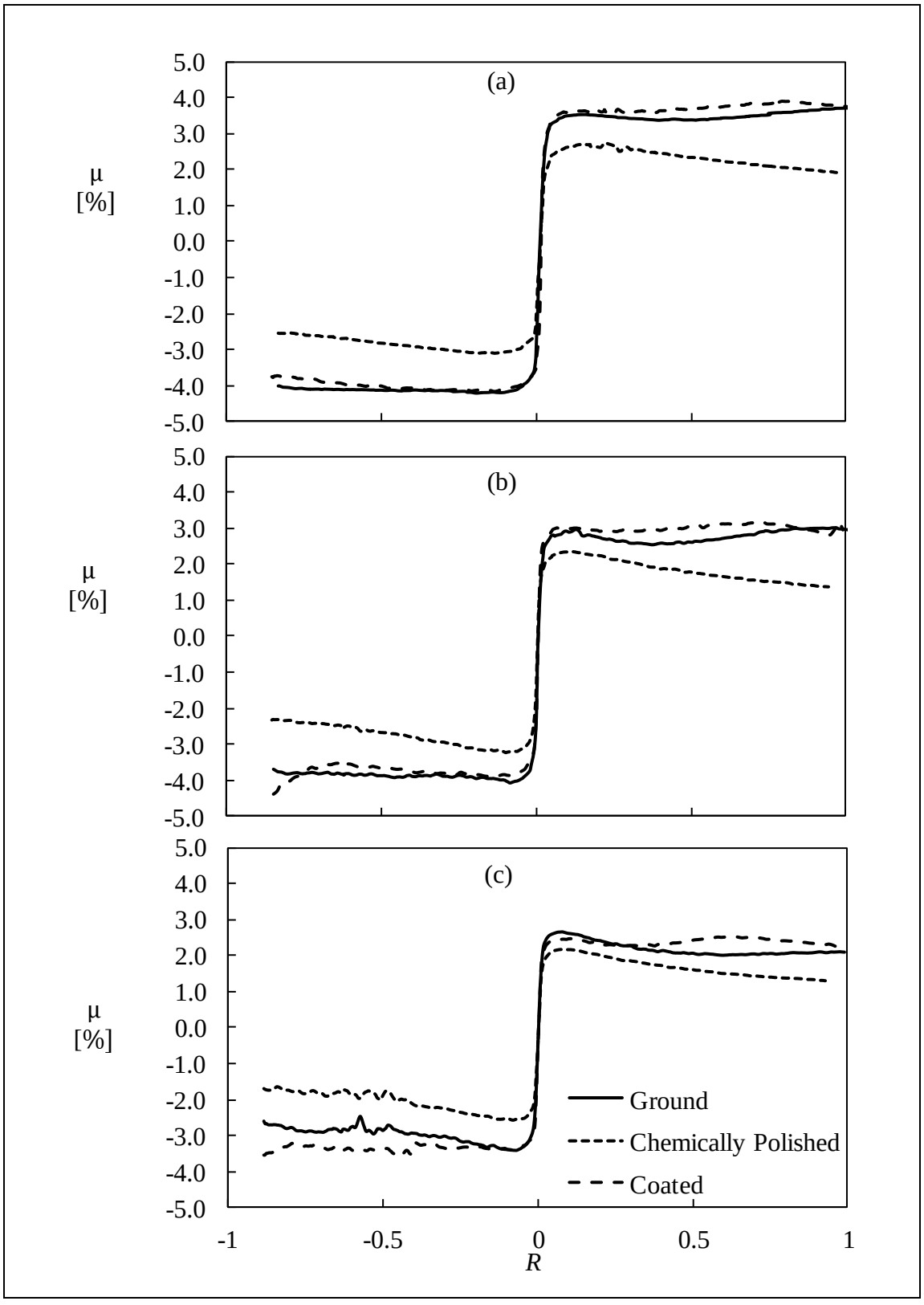

Figure 19. Comparison of the measured μ values of G, CP, and NiB-coated surfaces for σ_c = 2.0 GPa and u_r values of (a) 5, (b) 10, and (c) 15 m/s. Oil is 80W90.

3.3 Wear Tests

All of the wear tests, regardless of oil, were run under the same operating conditions of $\sigma_{max} = 2.0$ GPa, $u_r = 15$ m/s, and $R = 1.0$. Each wear test was performed with interim inspections after each 10 million roller cycles. The disks and rollers were measured for wear at each interim inspection. Any test reaching a maximum wear depth limit of 25 μm or 30 million cycles was suspended. A 30-million-cycle test took about four days to complete. Due to availability of specimens, one wear test was performed for each surface treatment except for HP surfaces, which were tested twice for repeatability purposes. The NiB-coated specimens were also tested twice to better document the wear accumulation within the first 10 million cycles of testing.

3.3.1 Wear Test Results

The CP and HP specimens all completed the 30-million-cycle wear tests limit with little to no measureable wear. Figure 20 shows the final wear profiles for CP rollers after 30-million-cycle tests with DOD-PRF-85734 and 80W90 oils, respectively. Meanwhile, figure 21b shows the same for an HP roller after a 30-million-cycle test with DOD-PRF-85734 oil. It is observed from these measured axial profiles that there is no sign of wear, as the profiles are identical to initial profiles. This is again primarily due to full-film EHL conditions afforded by the smoother surfaces at these speed and load conditions. Due to limited availability, no G pairs were tested for wear.

The NiB-coated specimens, however, were observed to go through a rapid wear progression starting from the initial stages of the tests. After the first 10-million-cycle inspection of the first NiB-coated wear test, it was observed that the entire 25-μm-thick layer of NiB coating wore off, exposing the steel substrate. A second test with interim inspections at 2, 4, 5, and 10 million cycles was performed to better document the accumulation of wear. Figure 21 displays measured axial roller profiles at these interim inspections to show the wear progression of NiB-coated specimens. Starting with an initial roller profile defining a perfect cylinder in figure 21a, about 7-μm maximum wear depth is observed after 2 million roller cycles (figure 21b), which is doubled after another 2 million loading cycles (figure 21c). Finally, in figure 21e at 10 million roller cycles, a 25-μm wear depth is evident. The worn profile consists of a flat range in the middle with a uniform 25-μm depth and steep steps in both sides. Figure 22a compares the roller wear profile at 10 million cycles to the initial profile, and it is clear that the coating layer in the middle (1.5–6.5 mm along the axial directions) wore off while the steel substrate did not. This indicates that NiB coating is not sufficiently wear-resistant to withstand the contact conditions of a typical gear interface. Similarly, figure 22b shows the same for the coated disk: about 13-μm maximum wear depth at 10 million cycles. Considering that the ratio of the diameter of the roller to the diameter of the disk is 0.56, a point on the roller surface goes through more loading cycles for every loading cycle of a point on the disk. The ratio of the wear depth of the roller to that of the disk corresponds exactly to this ratio. Figure 23 shows digital images of final roller

and disk surfaces at 10 million cycles. Steel substrate is clearly exposed in the middle of the contact zone in these images. Figure 24 shows further magnified images of the roller at 10 million cycles. By comparing the shape of the remaining coating around the removed portions of coating, it can be concluded that the coating flaked off. This jagged appearance, rather than smooth distinct lines, supports this conclusion.

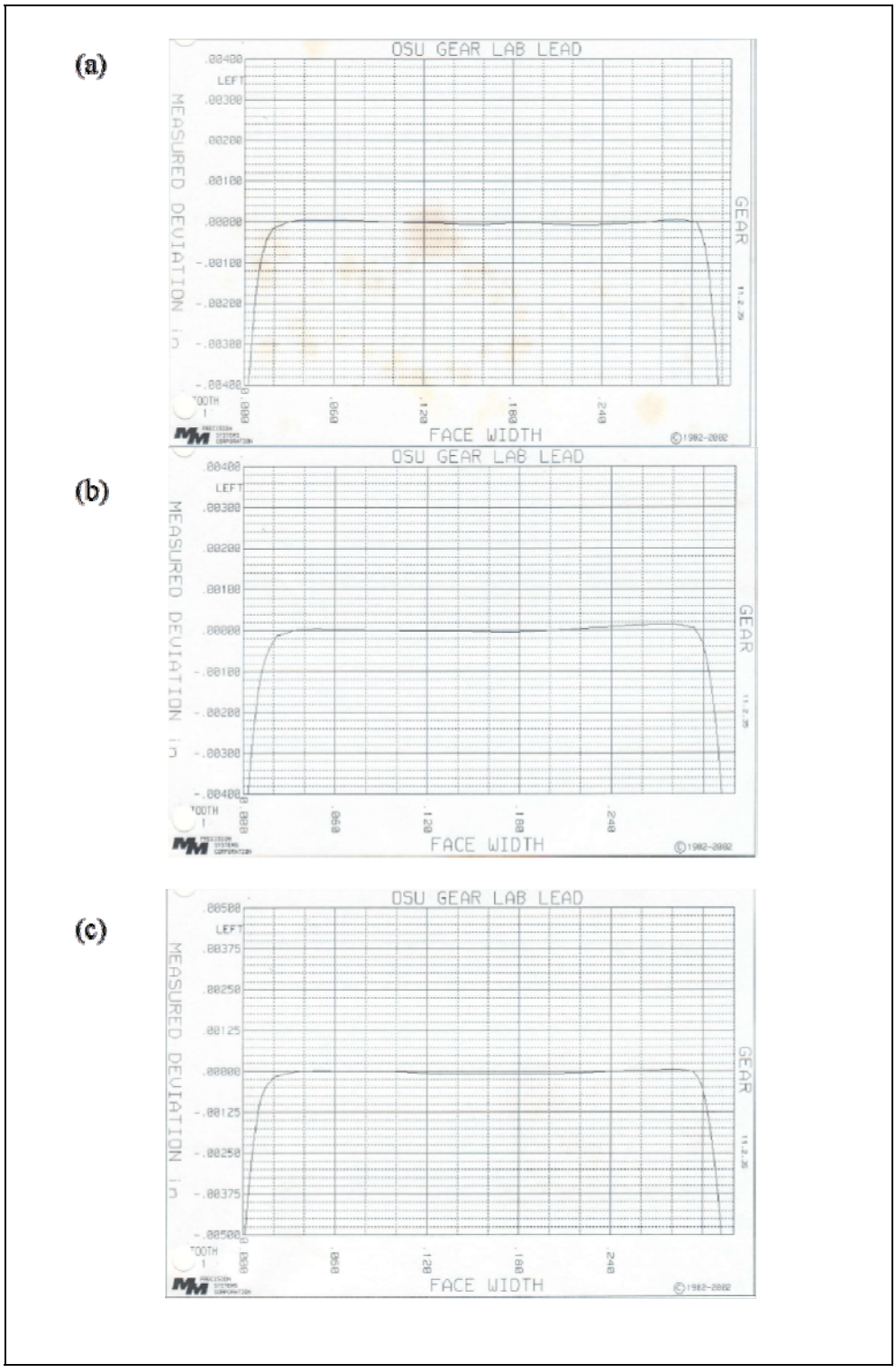

Figure 20. Measured roller axial profile traces after 30-million-cycle wear test: (a) CP specimens with DOD-PRF-85734, (b) HP specimens with DOD-PRF-85734, and (c) CP specimens with 80W90.

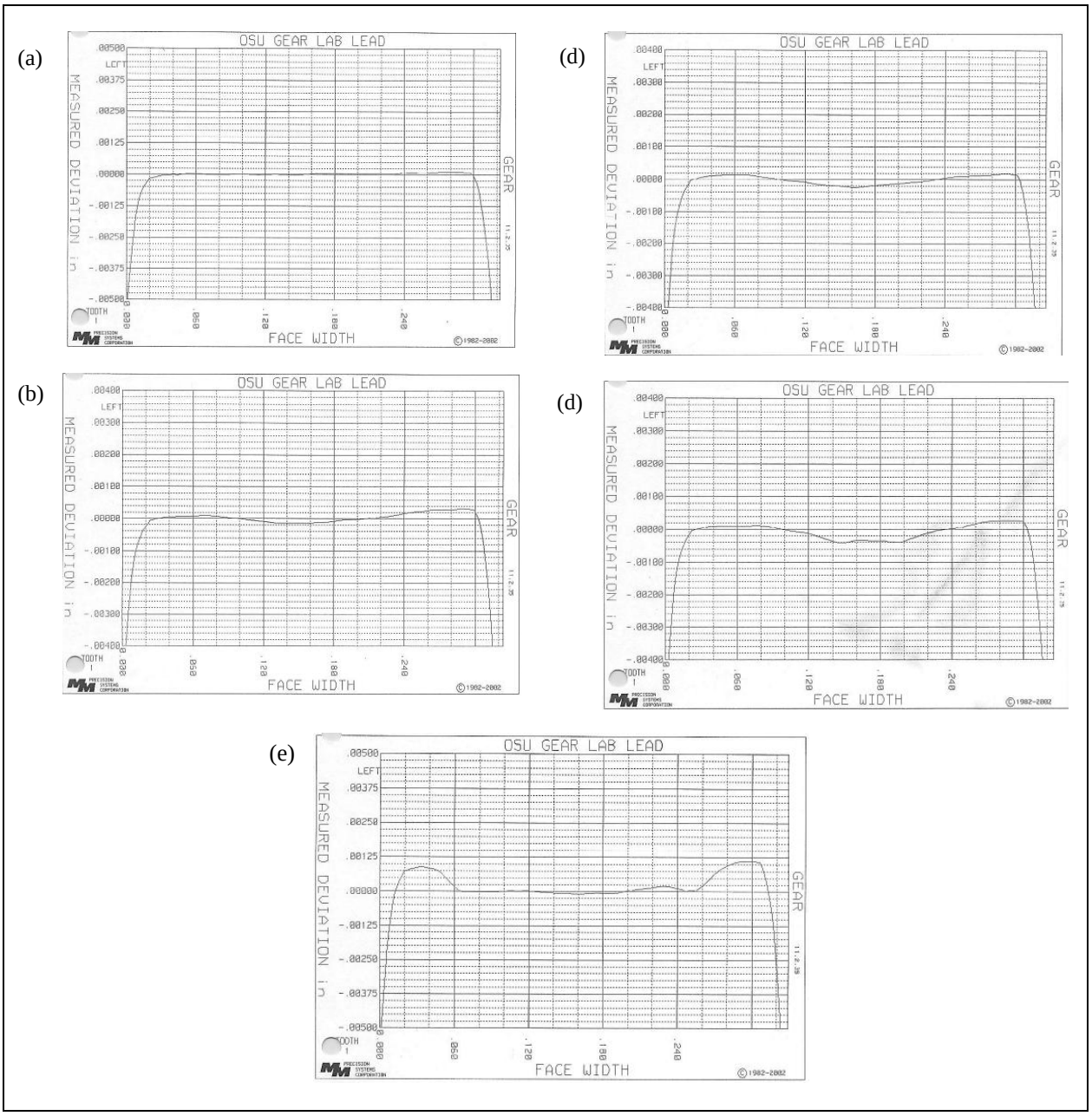

Figure 21. Measured roller axial profile traces form a wear test with NiB-coated specimens and 80W90 oil at (a) initial surface, (b) 2, (c) 4, (d) 5, and (e) 10 million cycles.

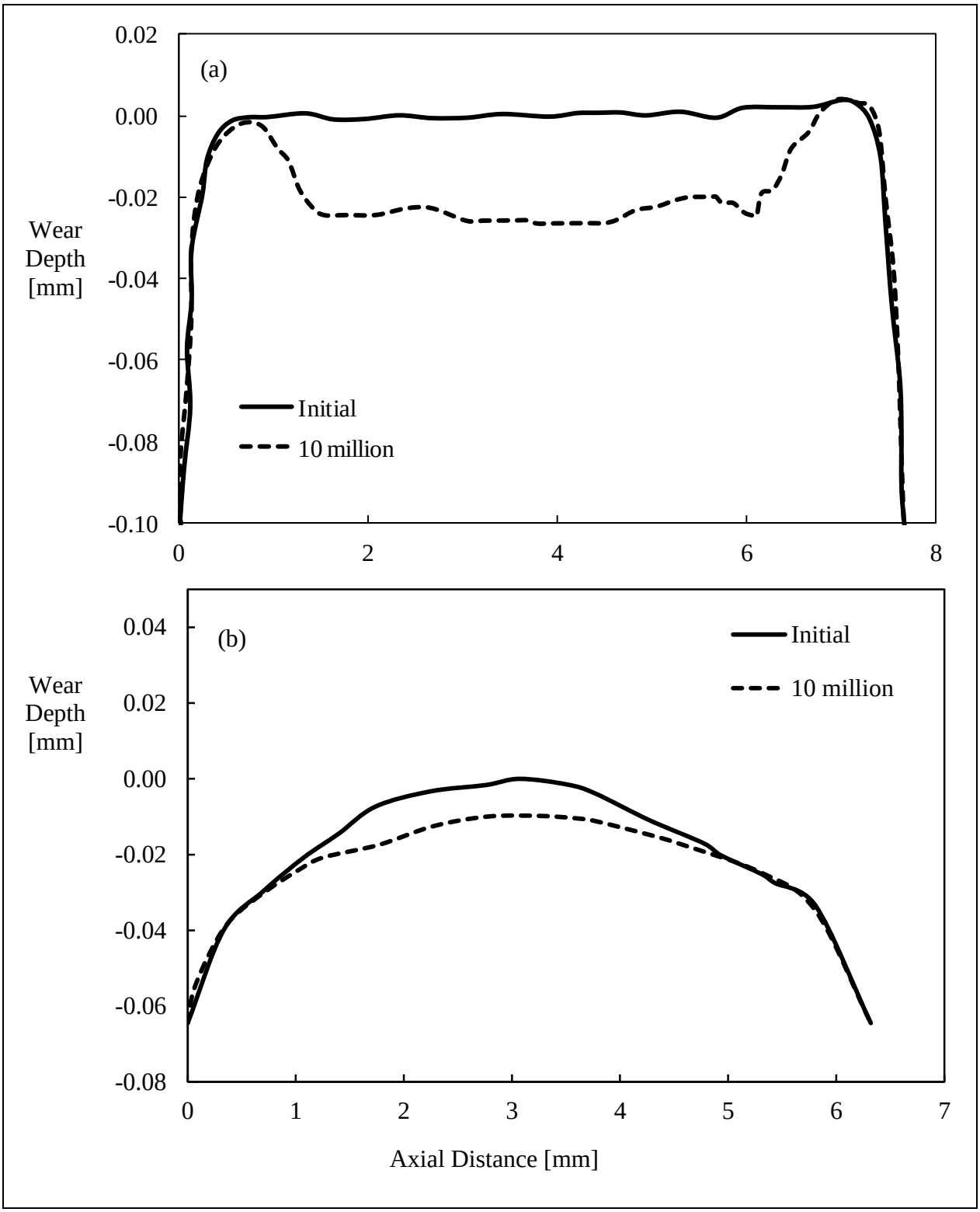

Figure 22. Comparison of initial and 10-million-cycle axial profiles of NiB-coated (a) roller and (b) disk specimens.

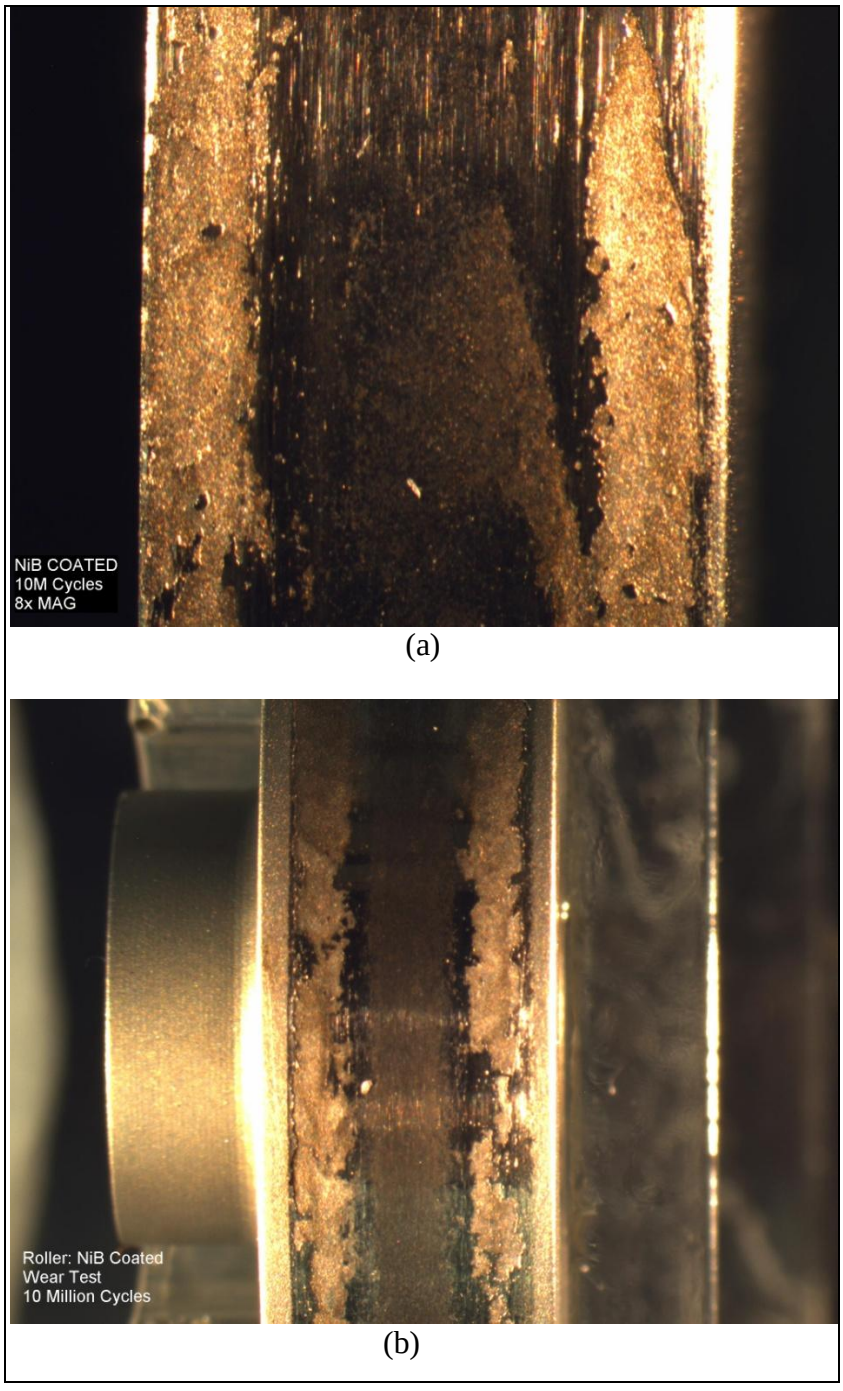

Figure 23. Digital images of NiB-coated (a) disk and (b) roller specimens after 10 million roller wear cycles.

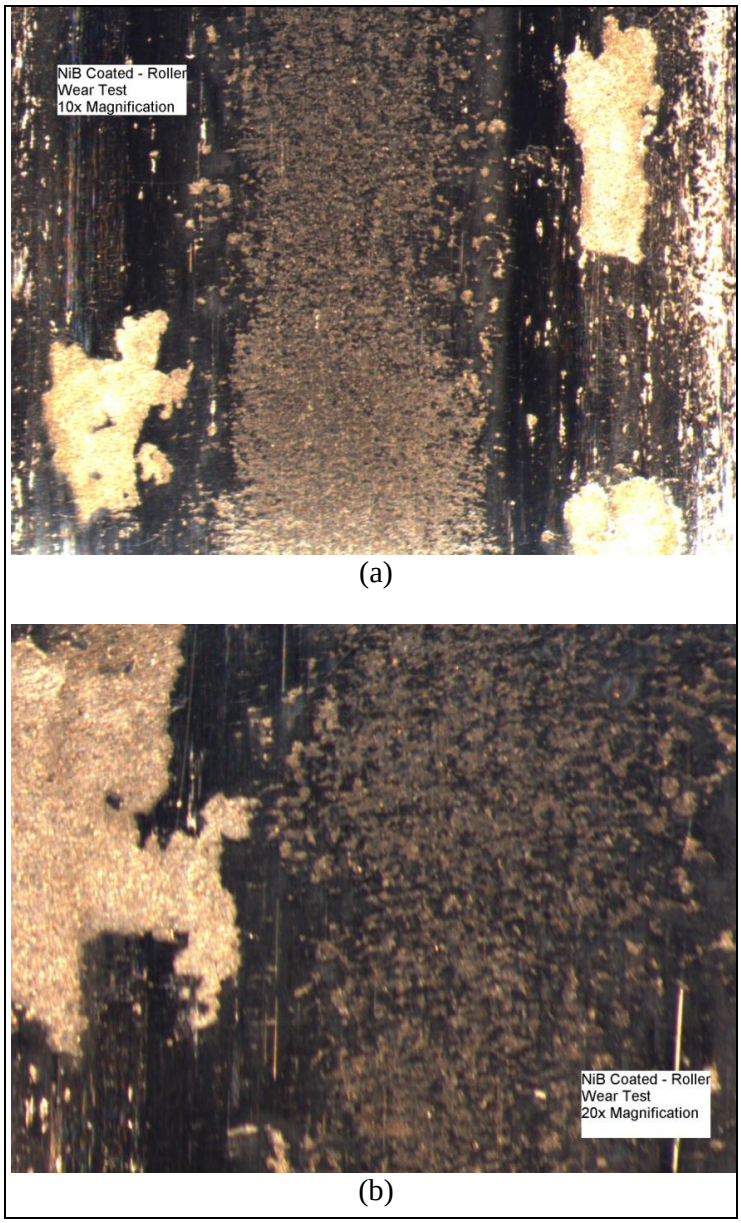

Figure 24. Digital images of NiB-coated roller after 10 million roller wear cycles at (a) 10 and (b) 20 times magnification.

3.4 Scuffing Tests

Test matrix used for scuffing investigation is shown in table 5. It consists of a total of 12 tests, 6 under full lubrication conditions (oil flow rate of 0.5 lpm) and 6 starved oil conditions (flow rate under 0.1 lpm). Specimens made of both materials (9310 and 5120) and all types of surface treatments (G, CP, and HP with DOD-PRF-85734 and 9310; and 5120 with 80W90) are included in this test matrix. All of the tests were performed at $u_r = 15$ m/s and $R = -1$. Due to limited availability of specimens, one pair was tested for each test condition.

Table 5. Scuffing test matrix and summary of test results.

Material	Surface Treatment	Lubricant	Lubrication Condition	Stress at Scuffing (GPa)	Roller Temp. at Scuffing (°C)	Disk Temp. at Scuffing (°C)
9310	Ground	DOD-PRF-85734	Full	2.2	228	155
	Ground		Starved	1.6	153	100
	Chemically polished		Full	No scuff	139	139
	Chemically polished		Starved	No scuff	180	143
	Highly polished		Full	No scuff	147	135
	Highly polished		Starved	No scuff	163	156
5120	Ground	80W90	Full	2.1	318	207
	Ground		Starved	1.9	201	171
	NiB-coated		Full	2.3	299	205
	NiB-coated		Starved	1.6	177	150
	Chemically polished		Full	1.9	150	153
	Chemically polished		Starved	1.8	170	152

3.4.1 Scuffing Test Results

The results of the scuffing tests are summarized in table 5. Of the six DOD-PRF-85734 tests with 9310 specimens, only the two with G surfaces scuffed, while the CP and HP surfaces reached the maximum contact pressure of 2.2 GPa without any scuffing for both full and starved lubrication conditions. Under full lubrication conditions, G 9310 specimens with DOD-PRF-85734 reached 2.3 GPa when they scuffed, while the same type of specimens under starved lubrication conditions scuffed at only 1.6 GPa. Figure 25 shows the roller-surface bulk-temperature time histories for all six DOD-PRF-85734-9310 tests. Figure 26 shows the measured traction-torque time histories for the same six tests. Figure 25 indicates that the maximum roller bulk temperature (at scuffing) of the G specimens under full lubrication conditions is 228 °C, while it is only 153 °C for the corresponding starved condition. The traction-torque values (at scuffing) for these full and starved lubrication tests are found, from figure 26, to be 0.95 and 0.73 Nm, respectively. This indicates that the instantaneous temperature spikes (flash temperatures) are much higher in the starved case, so the maximum instantaneous temperature value (bulk temperature plus flash temperature) reaches the scuffing limit of the DOD-PRF-85734-9310 pairing. Digital images of the scuffed G roller and disk surface for the full lubrication and starved lubrication conditions are shown in figures 26a and 27a, respectively.

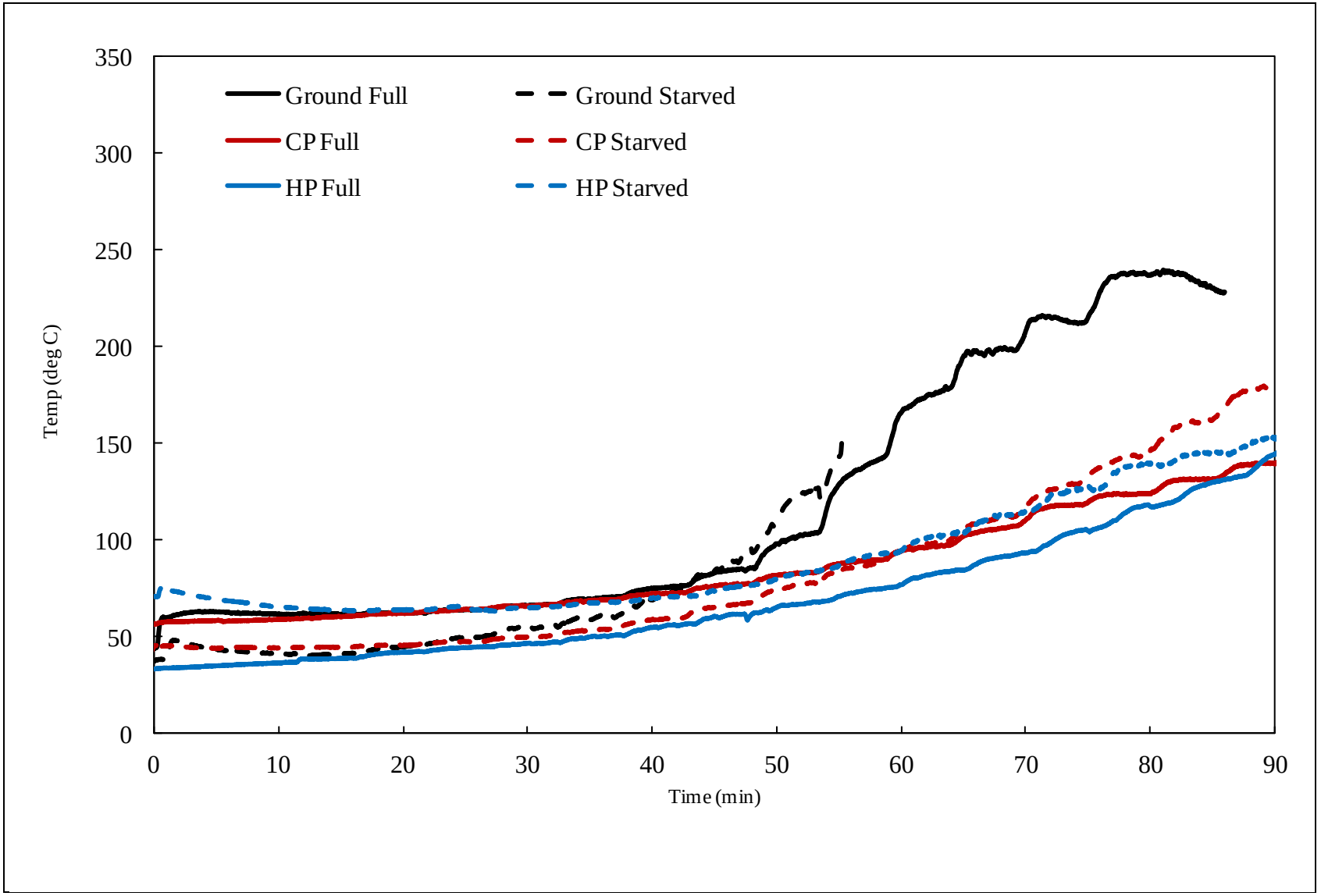

Figure 25. Measured surface bulk temperature of rollers during the scuffing test of 9310 specimens with G, HP, and CP surfaces under full and starved DOD-PRF-85734 lubrication conditions.

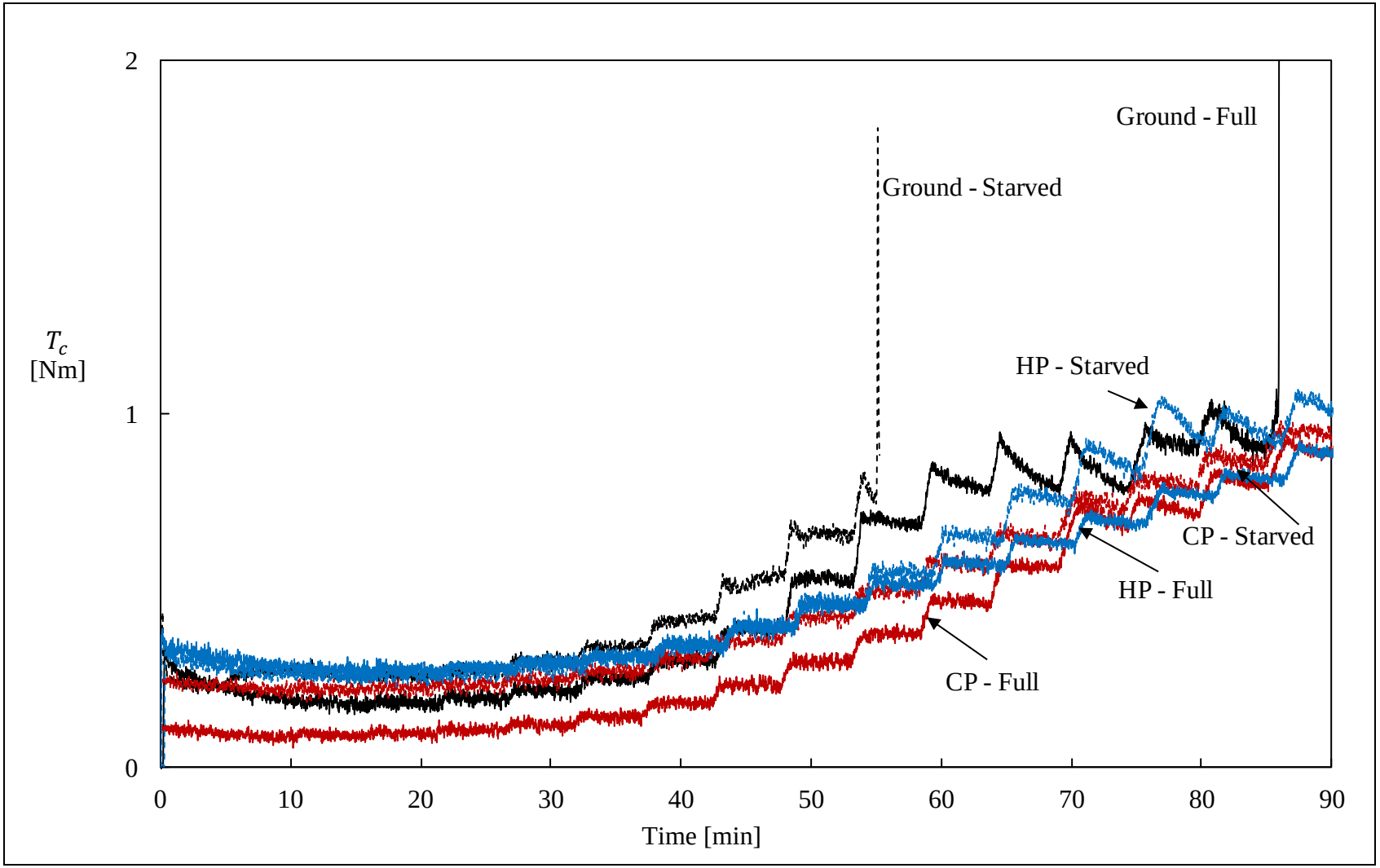

Figure 26. Measured traction-torques during the scuffing test of 9310 specimens with G, HP, and CP surfaces under full and starved DOD-PRF-85734 lubrication conditions.

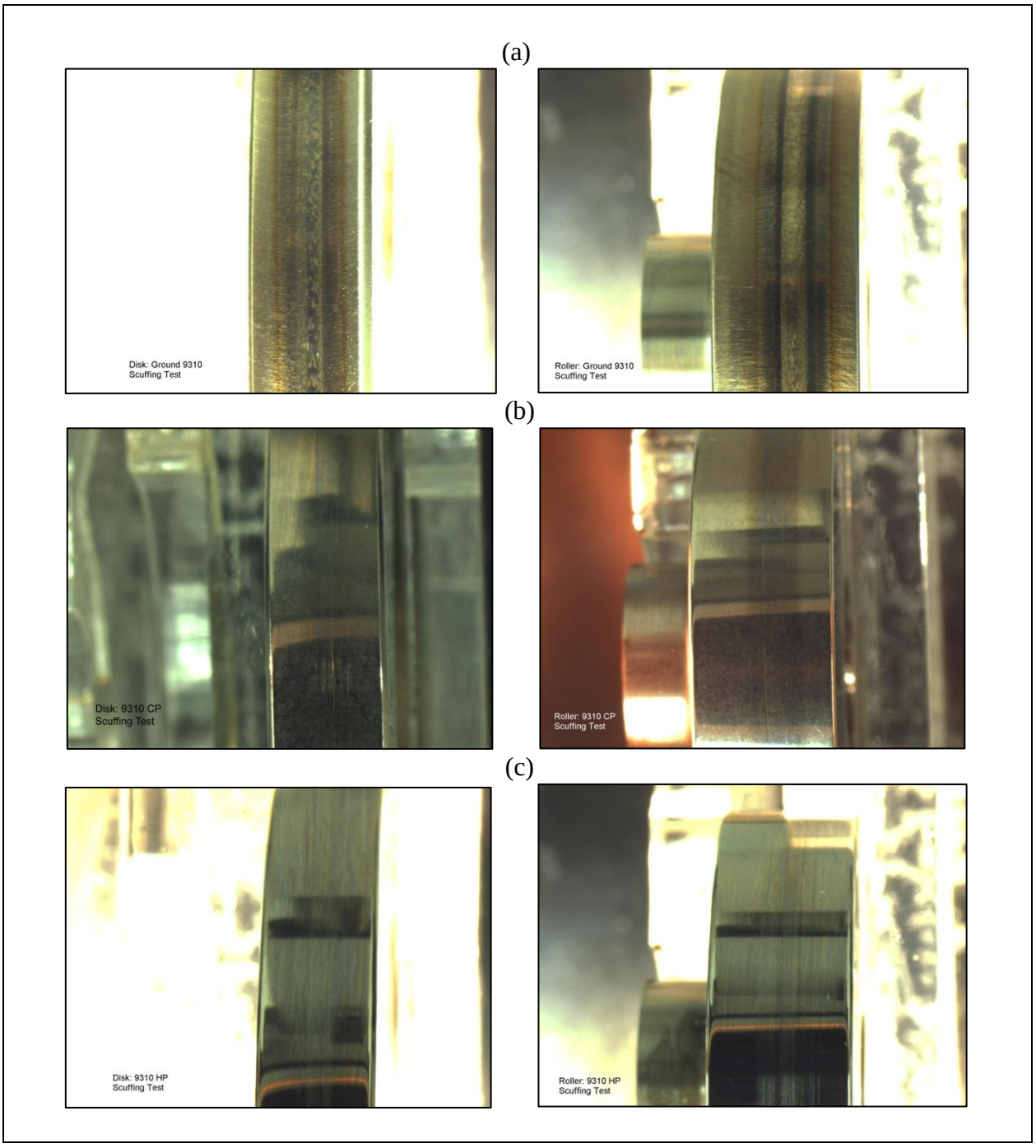

Figure 27. Digital images of scuffing tests with DOD-PRF-85734 oil under full lubrication conditions: (a) G, (b) CP, and (c) HP specimens.

As listed in table 5, CP and HP 9310 specimens tested with DOD-PRF-85734 oil did not produce any scuffing, regardless of the mode of lubrication (full or starved). In figure 24, bulk roller surface temperatures at the end of the CP and HP tests were below 180 °C and 147 °C, respectively. In addition, traction-torque values were low compared with the G specimens, as shown in figure 26. As a result, the heat generation did not cause maximum temperatures beyond the scuffing limit of this material-oil pair to cause scuffing. Figures 27b, 27c, 28b, and 28c provide digital images of the CP and HP rollers and disks at the end of the tests, each showing no signs of scuffing.

Meanwhile, all of the automotive steel 5120 specimens operating with 80W90 oil scuffed before reaching the maximum test contact pressure limit, as summarized in table 5. This suggests that the 5120-80W90 combination has a much lower scuffing limit than the 9310-DOD-PRF-85734 combination. Figure 29 shows the measured roller bulk temperatures for these six tests, while figure 30 plots the corresponding traction-torque time histories. The images of the scuffed roller and disk specimens are shown figures 30 and 31 for the full lubrication and starved lubrication cases, respectively. Note that bulk temperatures were much higher compared with the 9310-DOD-PRF-85734 tests. For instance, a ground roller reached 263 ºC to go with a final traction-torque (before scuffing) of 1.48 Nm. Note also that at the onset of scuffing, the bulk temperatures of G and NiB-coated specimens were higher for full lubrication conditions than for starved. For instance, scuffing temperature and contact pressure values for G specimens with full lubrication were 263 °C and 2.1 GPa, while they were 201 °C and 1.9 GPa for the starved lubrication. This indicates that the flash temperatures for the starved cases are higher than for the full lubrication cases. It is also clear from these results that NiB coating does not provide any advantages in terms of high-temperature behavior of the contact.

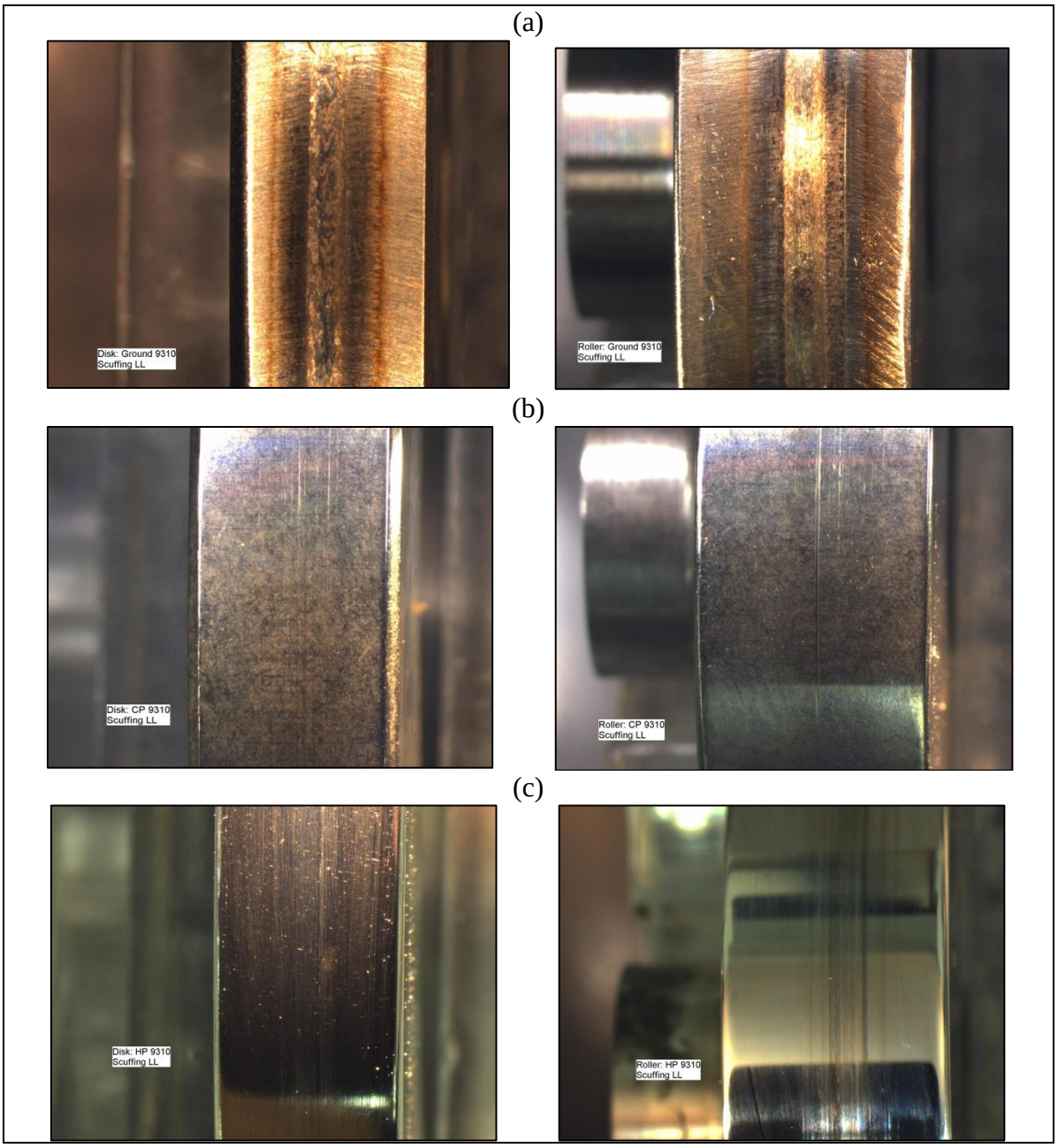

Figure 28. Digital images of scuffing tests with DOD-PRF-85734 oil under starved lubrication conditions: (a) G, (b) CP, and (c) HP specimens.

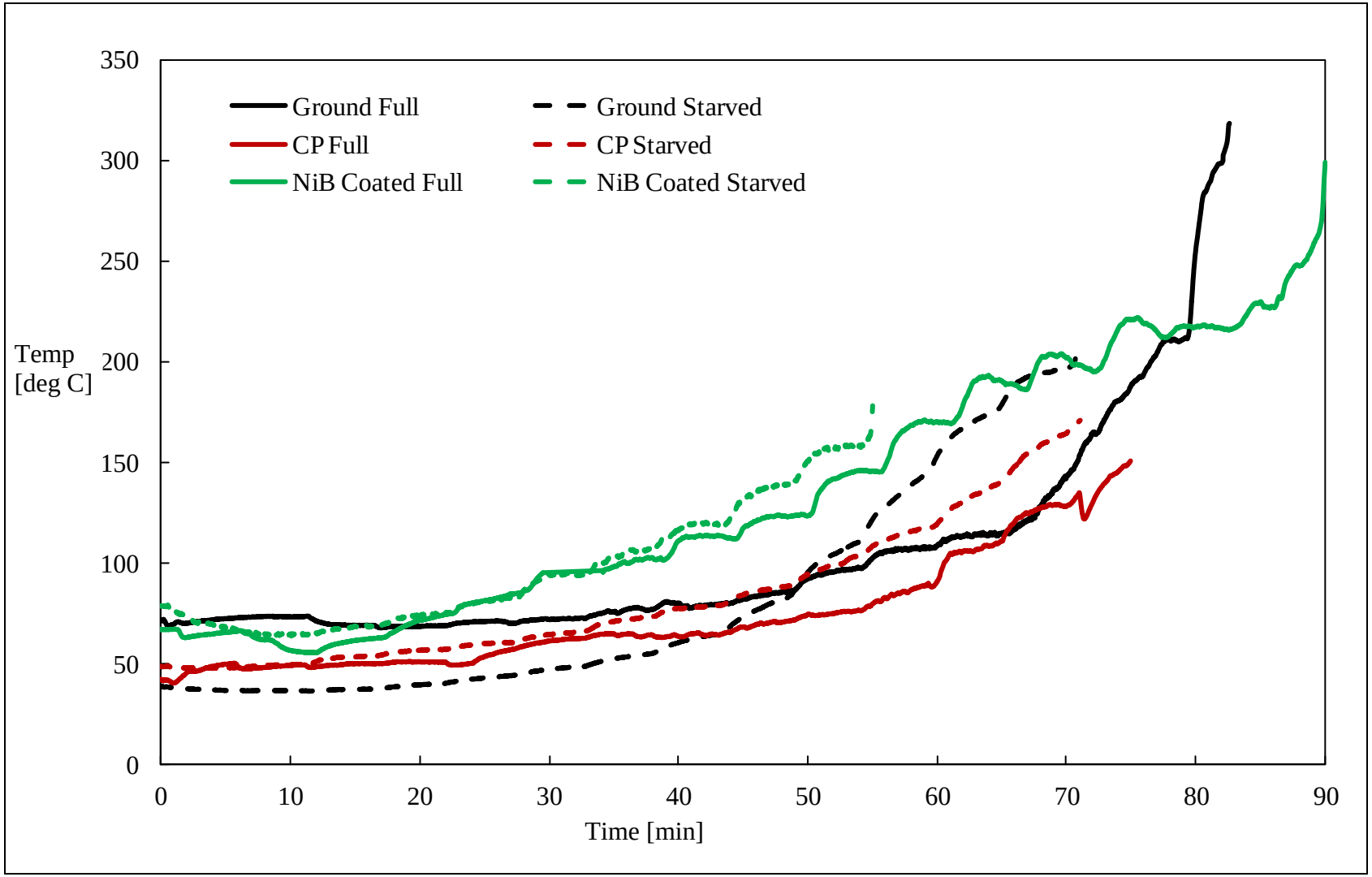

Figure 29. Measured surface bulk temperature of rollers during the scuffing test of steel 5120 specimens with G, CP, and NiB-coated surfaces under full and starved 80W90 lubrication conditions.

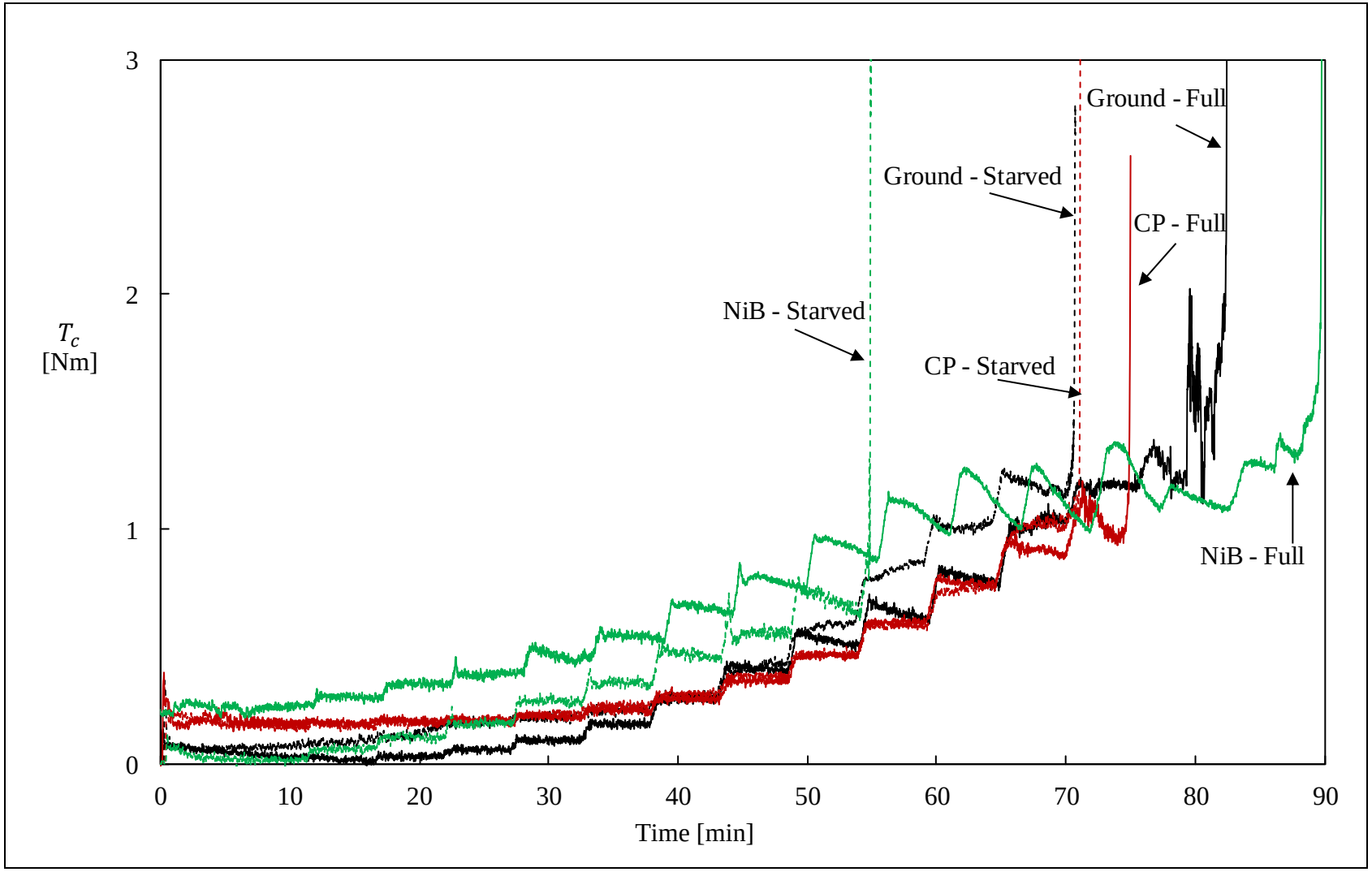

Figure 30. Measured traction torques during the scuffing test of steel 5120 specimens with G, CP, and NiB-coated surfaces under full and starved 80W90 lubrication conditions.

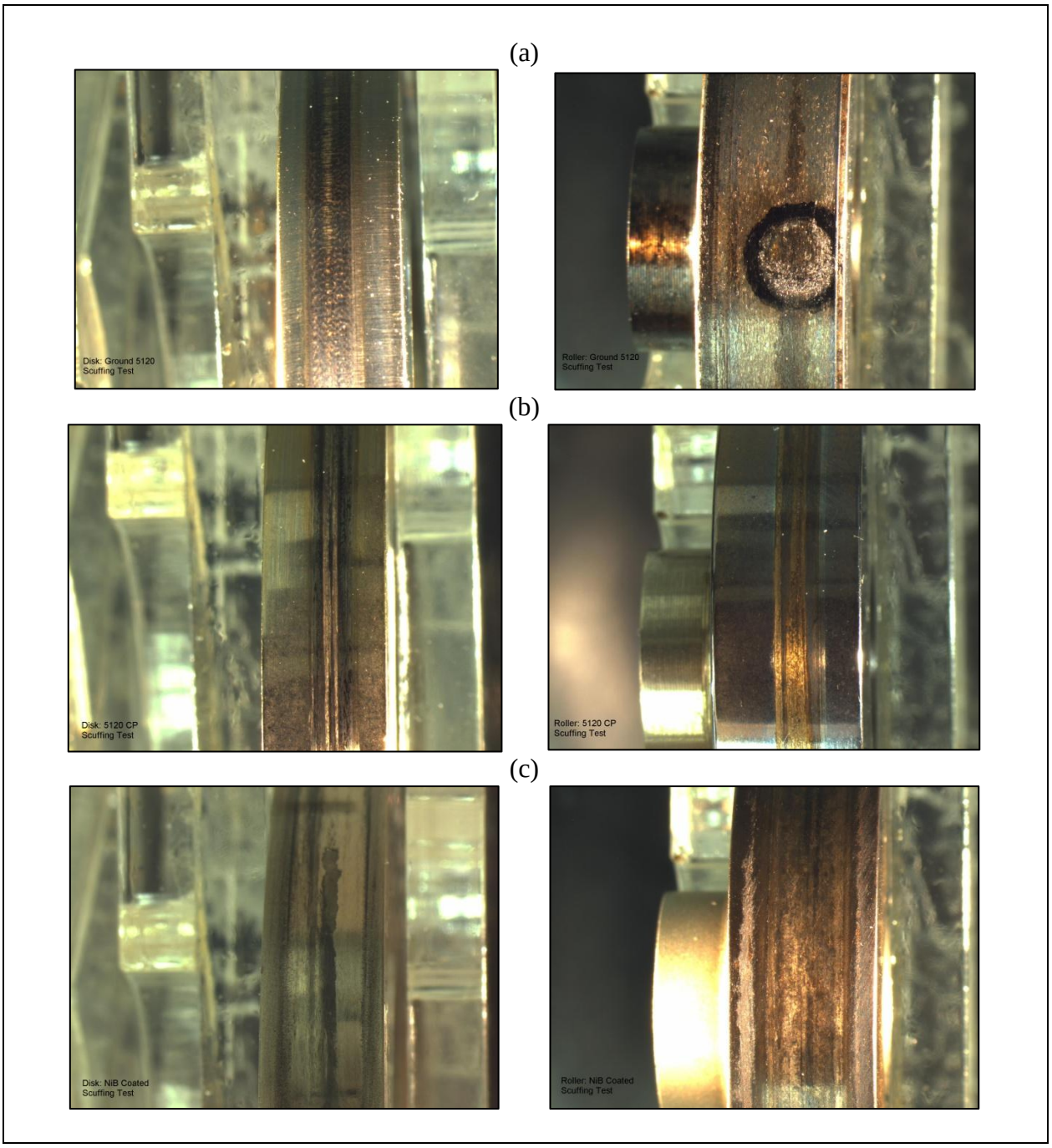

Figure 31. Digital images of scuffing tests of 80W90 oil under full lubrication conditions: (a) G, (b) CP, and (c) NiB-coated specimens.

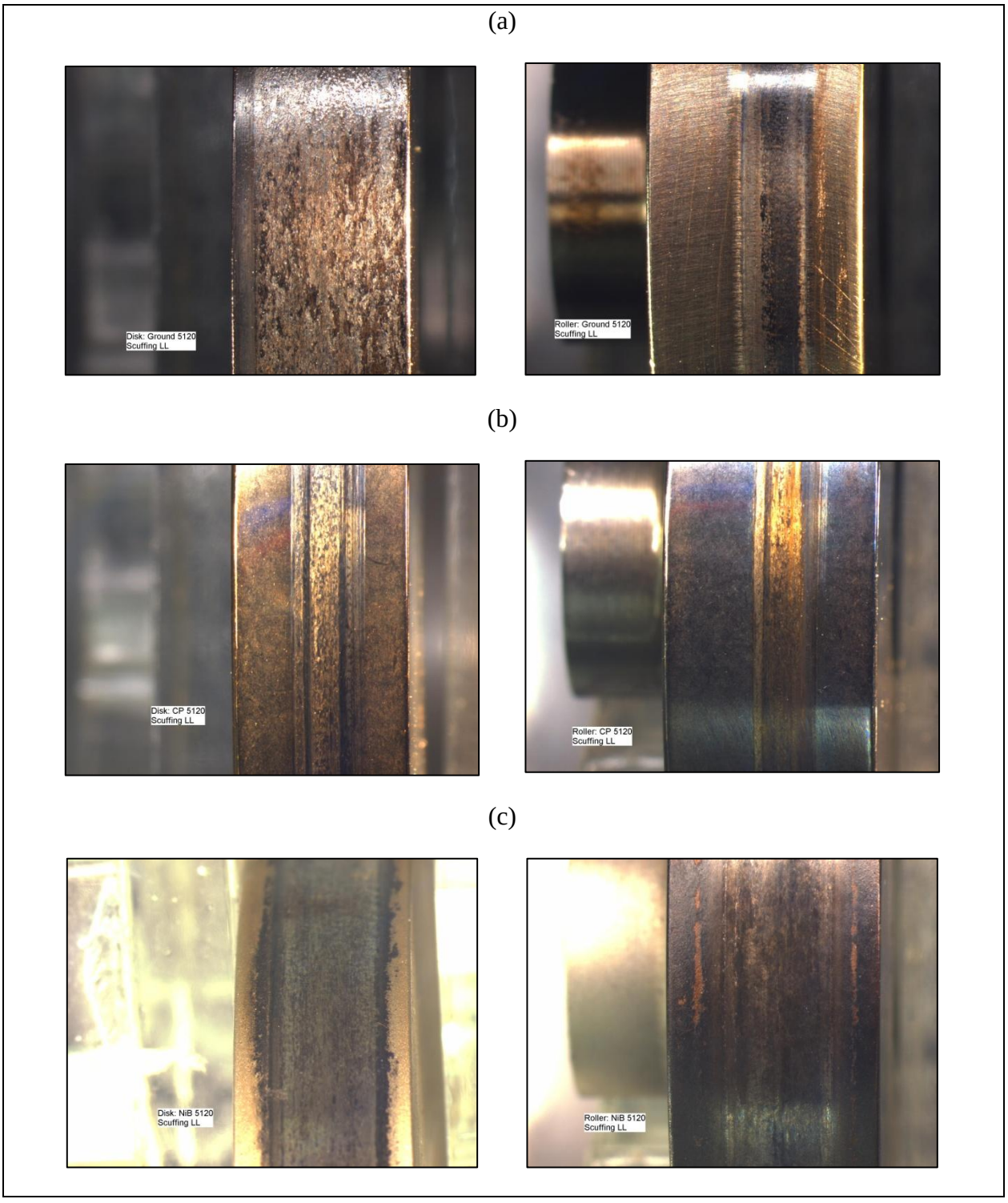

Figure 32. Digital images of scuffing tests with 80W90 oil under starved lubrication conditions: (a) G, (b) CP, and (c) NiB-coated specimens.

4. Evaluation of Gear Efficiency Performance of Surface Treatments

4.1 Introduction

In section 3, various engineered surface treatments, namely hard-G, CP, HP, and NiB-coated, were evaluated for their friction, wear, and scuffing performance by using a two-disk test methodology. It was shown that smoother surfaces result in lower friction coefficients regardless of speed, sliding ratio, lubricant type, or gear material type. This section aims to quantify the mechanical (load-dependent, friction-induced) efficiency consequences of the same surface treatments. A high-speed gear efficiency test machine was adapted, plus sets of spur gear specimens with desired surface characteristics were procured and tested to measure resultant power losses. The test setup and the test procedures are described first, followed by the gear test specimens, and the test matrix. At the end, the power loss results for gears having different surface treatments are compared to quantify their impact on gear efficiency.

4.2 Gear Efficiency Test Methodology

4.2.1 Test Setup

The gear efficiency test machine shown in figure 33 was used in this study. This setup was used in earlier spur (*4–6, 13, 33*) and helical (*7*) gear efficiency studies. Only the essential details of the test setup will be provided here, as complete details of the test machine and related instrumentation can be found in those earlier studies.

Figure 33. Gear efficiency test machine used in this study (*7*).

The test machine is comprised of two identical gearboxes, a reaction side box, and a test side box. Figure 34 shows the top cross-sectional view of the test machine with its main components labeled. Each gear is held in place between two bearings, a deep-groove ball bearing at the outer side of the housing (SKF Model 6206), and a four-point angular contact ball bearing (SKF Model QJ 206 MA) on the inner side of the housing. The respective gears from each gearbox are connected to each other through flexible shafts, creating a closed power circulation loop. A split coupling mounted on one of the connecting shafts is used to apply torque on this loop. One flange of the split coupling is fixed (held stationary with a pin); the bolts of the coupling are loosened; and a certain amount of torque is applied to the free flange of the coupling via a calibrated torque arm and dead weights. Tightening the coupling bolts and removing the torque arm and the pin allows this constant torque to be circulated in loop. Any torque loss due to load-independent and load-dependent power losses must be provided by the high-speed spindle that is connected to one of the shafts of the reaction gearbox, as shown in figure 34. A precision torque meter placed in the spindle reaction gear shaft interface measures the torque provided to (i.e., torque lost by) the loop to determine the combined power losses of the test and reaction gearboxes. As these gear boxes are identical in all aspects, half of this measured torque loss is attributed to each gear box.

The torque sensor used in this setup (Lebow TMS9000) was rated at a maximum torque of 50 Nm with an accuracy of 0.05% of the maximum torque rating. As shown in figure 35, gears were lubricated by oil jet into the mesh. Two thermocouples monitored the inlet and return oil temperatures. These data were then collected and processed through a National Instruments-based system with LabView.

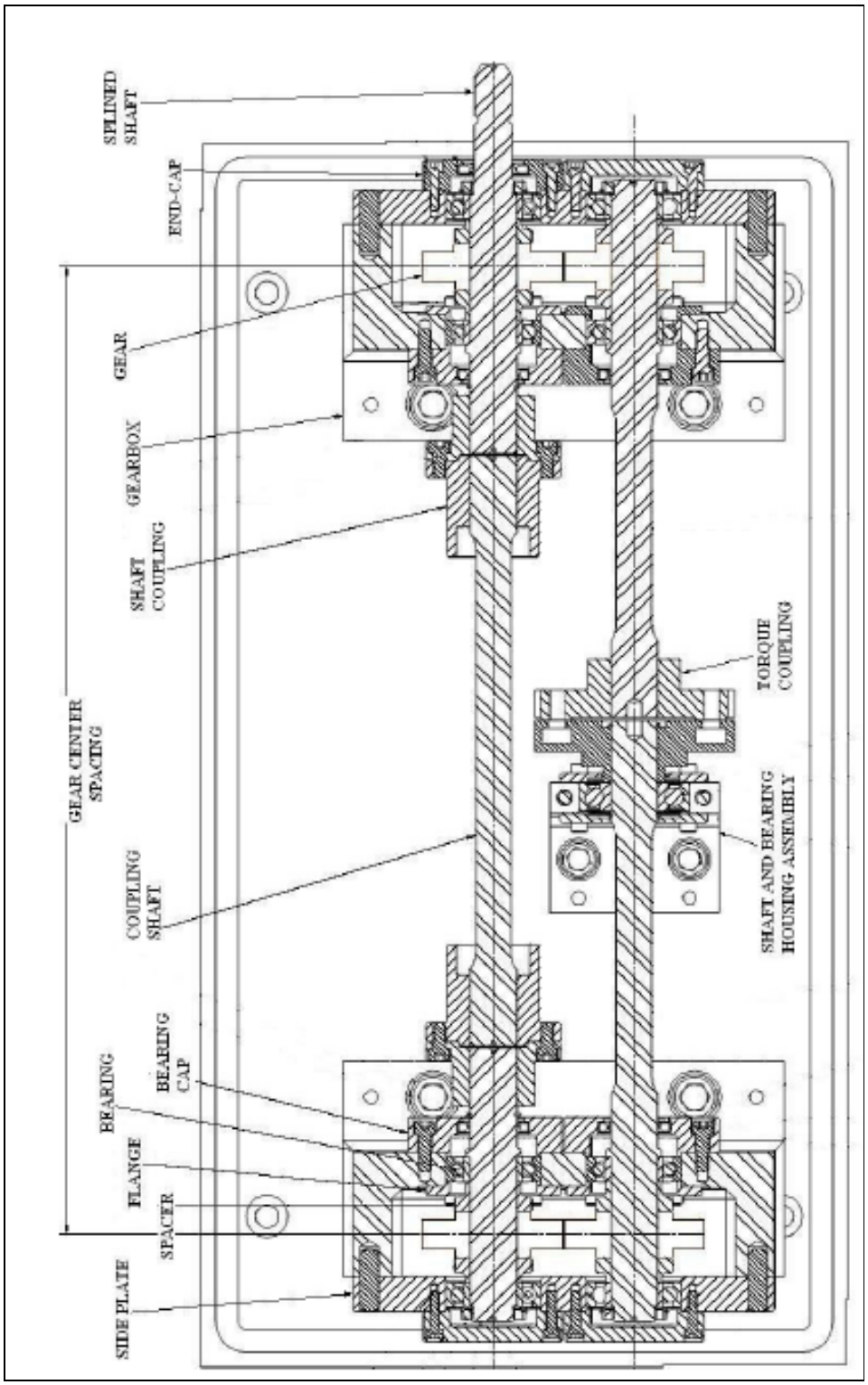

Figure 34. Top view cross-section of the gear efficiency test machine with its main components labeled (*7*).

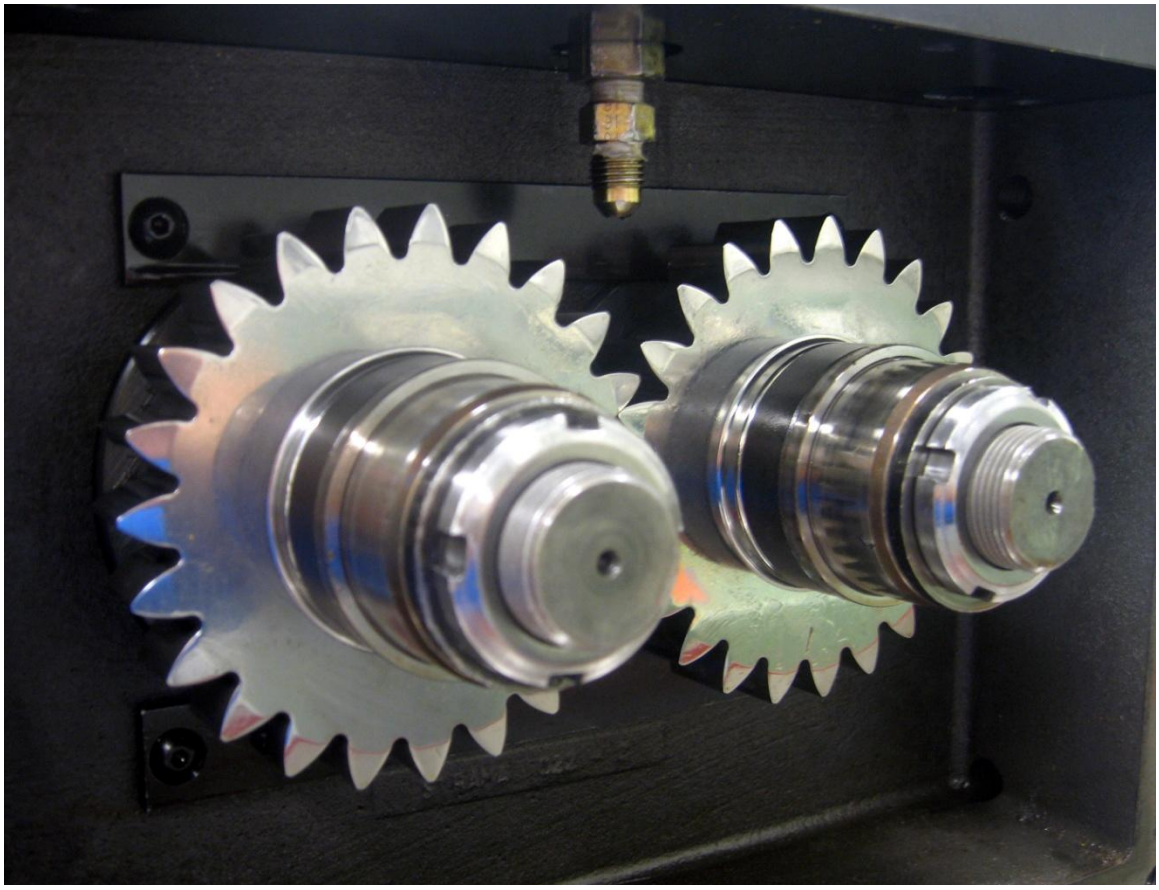

Figure 35. A close-up view of the test gearbox with the side cover removed to expose the test gear pair and nozzle.

4.2.2 Test Specimens and Test Matrix

All test gear pairs used in this study were unity-ratio pairs formed by two 23-tooth spur gears operated at a center distance of 91.5 mm. The same gear design was used by the earlier studies on spur gear efficiency (*5*, *6*, *13*, *33*). Table 6 lists basic design parameters of the test gear pairs. The gear surfaces were processed to have the same surface finishes as the roller and disk specimens tested in section 3. One G gear pair, two CP pairs (one pair for the test side and one pair for the reaction side), one HP pair, and two pairs of NiB-coated gears were run. Figure 36 shows one gear from each set of gears.

Table 6. Gear design parameters of the unity-ratio test gear pair used in the efficiency study.

Parameter	Value
Module (mm)	3.95
Pressure angle (°)	25.00
Face width (mm)	19.48
Center distance (mm)	91.50
Pitch diameter (mm)	90.85
Outside diameter (mm)	100.25

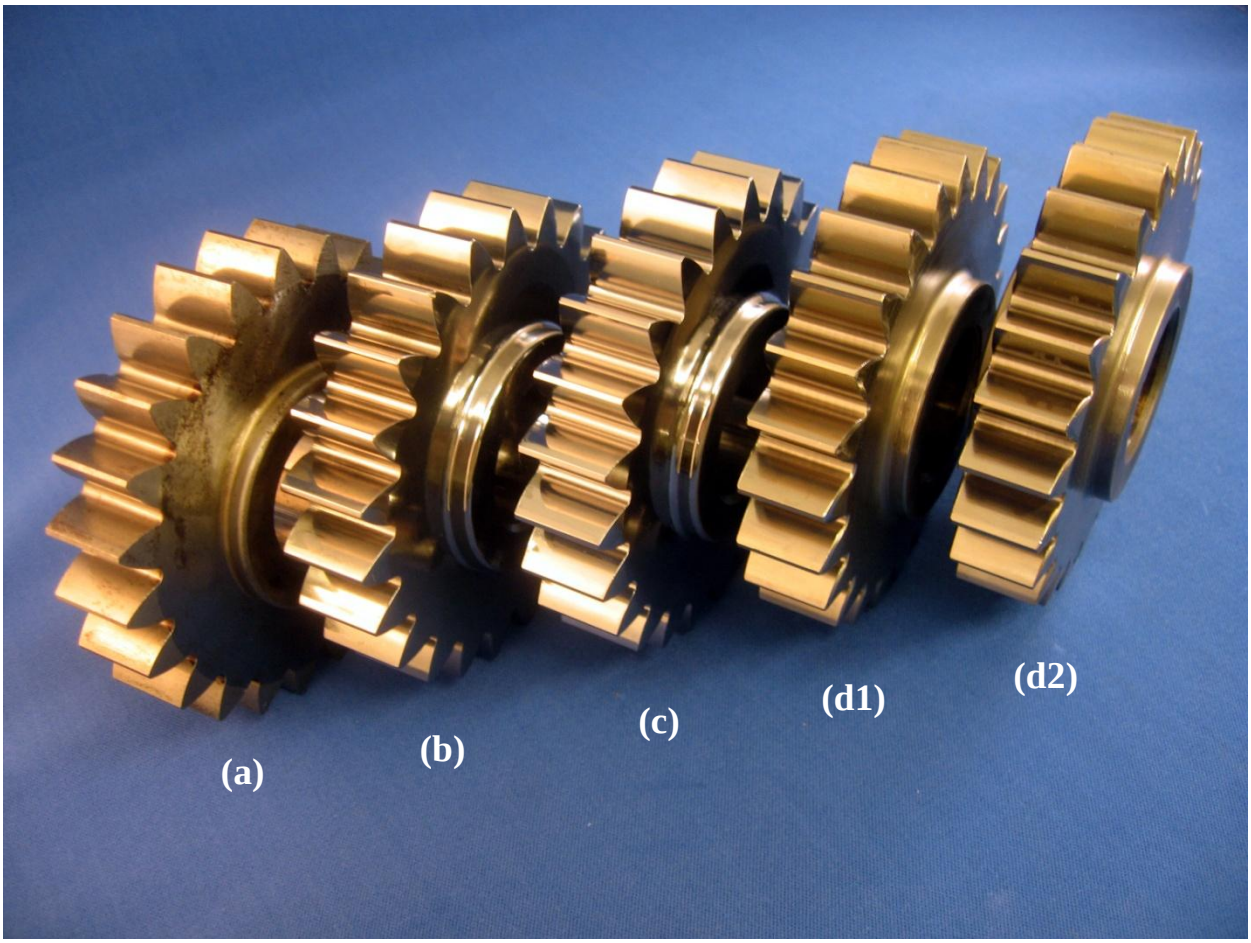

Figure 36. Examples of 23 tooth test gears used in this study: (a) G, (b) CP, (c) HP, and (d1, d2) NiB-coated gears.

Originally, the NiB-coated gears had to be cut undersized to accommodate the thickness of the coating for the gear to fit on the machine. These gears were, then, designed to be smaller in certain dimensions, so the dimensions listed in table 6 are obtained after a 25-μm (0.001-in) NiB coating is applied. Based on the results of the coated roller tests (figure 22), which showed significant wear of the coating layer that was not heat treated after coating, one pair of NiB-coated gears was heat treated after coating to create a much harder coating, as per manufacturer's specifications and recommendations. Conversely, the concern was whether this extra step would actually temper (soften) the substrate material. Thus, the other NiB-coated pair did not undergo this additional heat treatment process so that the performance of these two variations could be compared. Also noted in section 3, the NiB coating on relatively smooth (CP to $R_q \approx 0.1$ μm) rollers and disks resulted in much rougher coated surfaces at $R_q \approx 0.8$ μm. As such, measured friction coefficients for NiB-coated rollers were as high as those for the G rollers, as shown in figure 19. In an attempt to remedy this, both NiB-coated pairs were highly polished after the coating was applied. Table 7 lists roughness (R_q) values of the brand new gear surfaces, all measured in the profile (sliding and rolling) direction before testing. Note that the NiB-coated gears have roughness values similar to that of the CP gears.

Table 7. Measured surface roughness values for of test gears before testing.

Parameter	Value
Ground	0.49
Chemically polished	0.12
Highly polished	0.02
NiB-coated (heat-treated)	0.16
NiB-coated (not heat-treated)	0.15

Table 8 shows the test matrix that was executed in this study. It consists of five groups of tests (nos. 1–5), one for each surface variation. Three speed values ($\Omega = 2000$, 4000, and 6000 rpm, corresponding to $\omega = 2\pi\Omega/60 = 209.5$, 418.9, and 628.3 rad/s), and four transmitted gear torque values (T_c = 0, 143, 306, and 459 Nm) were included in this test matrix for each surface treatment. The speed values selected are more representative of ground vehicle transmission conditions, while the maximum contact stresses (0.9, 1.3, and 1.6 GPa) corresponding to these three torque values are typical to aerospace and automotive applications. Also included in table 8 are sets of tests at zero torque $(T_C = 0)$. These tests were included in the test matrix to determine spin (load-independent) power loss of the test gear box so that mechanical (load-dependent) losses can be isolated at any given torque value.

Table 8. Test matrix used in the gear efficiency study.

Test No. *i*	Surface Treatment
1	Chemically polished
2	Ground
3	Highly polished
4	NiB coated (heat-treated)
5	NiB coated (not heat-treated)

A pair of CP gears was used within the reaction gearbox for all tests listed in table 8. The power losses corresponding to the reaction gearbox were determined from the test that used CP gears for both of the test and reaction gearboxes as the half of the power measured for this test. For all other tests with gears having other surface treatments within the test gearbox, the test gearbox torque loss was determined by subtracting the reaction gearbox torque (from the test with CP gears in both gearboxes) from the measured total torque.

4.2.3 Test and Inspection Procedures

Before actual efficiency tests were performed for a test gear pair, a 1-h-long run-in test at 95 Nm (0.8 GPa) and 3000 rpm was completed. After this run-in test, gears were removed from the test gearbox to visually inspect them for signs of damage. The gearbox was then reassembled and the testing commenced.

All of the gear efficiency tests were performed using 80W90 lubricant at an inlet temperature of 100 °C (±2 °C). The oil supply pressures and flow rates for both gearboxes, as well as the supply to mesh and bearings, were tightly controlled throughout the entire tests.

Each test at a given speed and torque ran for 10 min. This duration was determined in earlier studies with the same machine and gears to be sufficient to establish steady-state torque loss values (*5–7, 13, 33*). During postprocessing, the average value of the 10-min segment of each torque time history was used as the torque loss of that test.

Test gears were inspected before efficiency tests to qualify them. Index, pitch, spacing, tooth, and tooth thickness errors, as well as the lead and involute traces, were measured for each gear set using a gear CMM, as shown in figure 37. This is the same CMM utilized in the roller and disk testing. A sample inspection report is presented in appendix A. In addition, tooth surface roughness measurements were performed, as illustrated in figure 38, along the midplane of the tooth in the profile direction. The R_q values tabulated in table 7 were obtained in this manner.

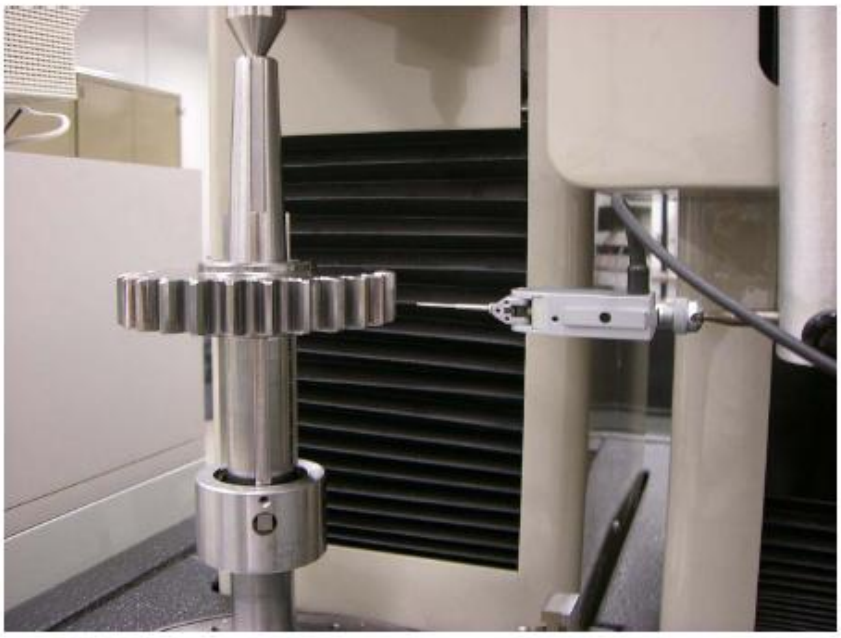

Figure 37. Measurement of a test gear's profiles on a gear CMM (*6*).

Figure 38. Measurement of a test gear on a surface roughness profiler (*6*).

4.2.4 Calculation of Components of Power Loss

The total torque loss from test no. *i* (average value of the torque measured during the 10-min test) in table 8 is considered to be the sum of the torque losses of the test and reaction gearboxes: $T_i(T_c,\omega) = T_{ti}(T_c,\omega) + T_{ri}(T_c,\omega)$. Reaction gearbox torque loss T_{ri} is determined from test no. 1 in table 8 as $T_{ri}(T_c,\omega) = T_{r1}(T_c,\omega) = \frac{1}{2}T_1(T_c,\omega)$. With the test gearbox torque loss $T_{ti}(T_c,\omega)$ defined, total power loss of the test gearbox (including four bearings and the spur gear pair) is found to be

$$P_i(T_c,\omega) = \omega T_{ti}(T_c,\omega). \tag{6}$$

Total test gearbox power loss is the sum of the spin (load-independent) and mechanical (load-dependent) power losses:

$$P_i(T_c,\omega) = P_{mi}(T_c,\omega) + P_{si}(\omega). \tag{7}$$

Since $P_{si}(\omega) = P_i(0,\omega)$, mechanical power loss for test no. *i* at a given torque and speed is found to be

$$P_{mi}(T_c,\omega) = P_i(T_c,\omega) - P_i(0,\omega). \tag{8}$$

Note that $P_{mi}(T_c,\omega)$ and $P_{si}(\omega)$ both contain respective losses associated with four bearings and a gear pair. In the case of $P_{si}(\omega)$, viscous losses of four bearings and the churning and pocketing losses of the gear pair form the spin loss. Similarly, mechanical losses of four

bearings and the mechanical gear mesh loss are combined to form $P_{mi}(T_c, \omega)$. Since the only difference between the five tests listed in table 8 is the surface texture of the gears, it can be safely assumed that only the gear mesh mechanical losses are altered from test to test. Any differences in $P_{mi}(T_c, \omega)$ among these tests must be solely due to the surface changes, while bearing losses (mechanical and viscous) and $P_{si}(\omega)$ should not be influenced by the surface roughness changes. With this, the bearing losses were not separated from the gearbox losses to isolate gear mesh-related losses. This is deemed to be acceptable as long as only the impact of surface treatment is concerned.

4.3 Gear Efficiency Test Results

The gear efficiency test matrix defined in table 8 consisted of five tests, each at three speeds and four torque conditions, during which 60 data points were collected. Following the run-in test for each test no. *i*, spin tests at $T_c = 0$ were performed to determine spin losses $P_{si}(\omega)$. Then, in the order of increasing T_c, the other loaded tests were performed.

Efficiency test fidelity is dependent on the validity of the assumption that gears, test setup, lubrication conditions, and instrumentation undergo no tangible changes during the efficiency tests. Gears, especially, must maintain their surface characteristics. This assumption was true only for the G, CP, and HP gear specimens; the NiB-coated specimens exhibited significant physical changes at the completion of their efficiency tests. Specifically, the NiB coating applied to surfaces could not endure a two-hour efficiency test. Figures 39a and 39b show images of NiB-coated gear teeth after the efficiency tests, indicating that the coating layer was worn out (or peeled off) during the tests. Heat treatment of the NiB coating did not prevent degradation. The post-test CMM inspections of an NiB-coated gear is shown in figure 40. The profile points where coating is removed are seen to be about 20 to 25 μm below the points where the coating layer is still intact. This corresponds exactly to the prescribed thickness of the NiB coating. From figures 39 and 40, it can be concluded that the NiB coating applied to gears was not durable enough for power loss results to be viewed confidently. The data presented later in this section must be interpreted in light of this situation.

Figure 41 compares the spin power loss $P_S(\omega)$ values of all five surface roughness variations. The surface roughness amplitudes were stated earlier to have no mechanism to influence $P_S(\omega)$. Figure 41 confirms this, as all five variations resulted in very similar $P_S(\omega)$ values. This also serves, to a certain extent, as an indication of the repeatability of the test setup. Overall, $P_S = 0.131$, 0.291, and 0.625 kW at $\Omega = 2000$, 4000, and 6000 rpm, respectively, with $P_S(\omega)$ changing in an exponential manner with Ω (or ω), confirming earlier spin loss data and predictions. Assuming the coated surfaces were able to maintain their integrity during this first stage of unloaded tests, the curves for the NiB-coated gears can also be considered legitimate.

(a)

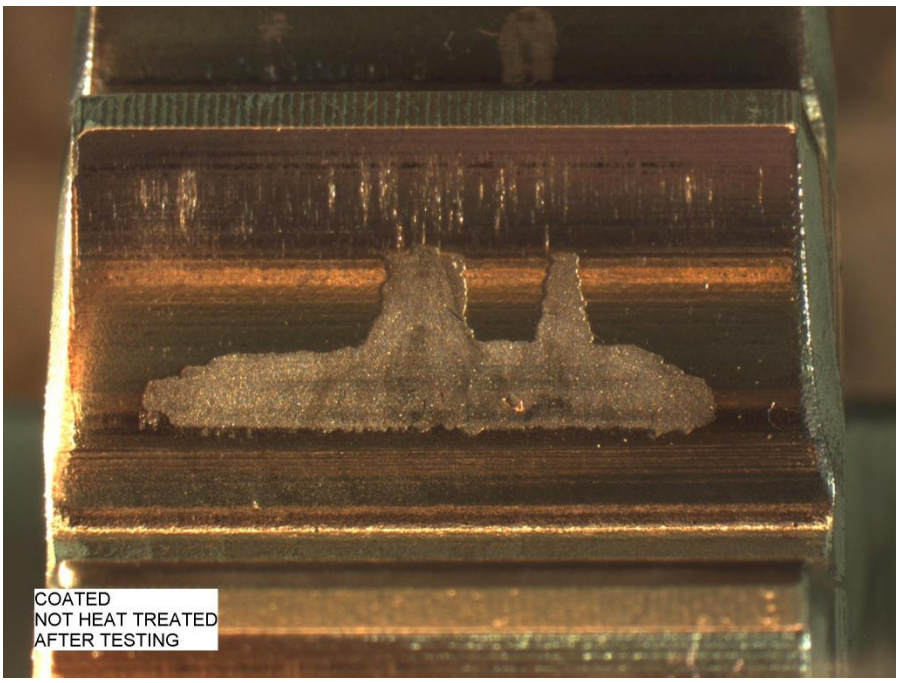

(b)

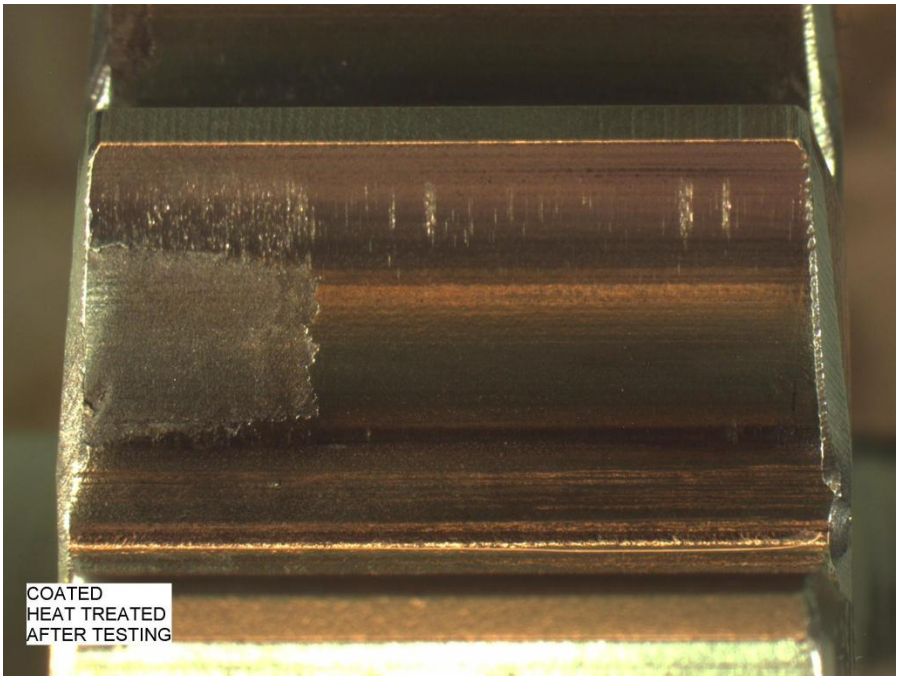

Figure 39. NiB-coated test gear teeth after completion of efficiency tests: (a) NiB-coated gear (not heat treated) and (b) NiB-coated gear (heat treated).

(a)

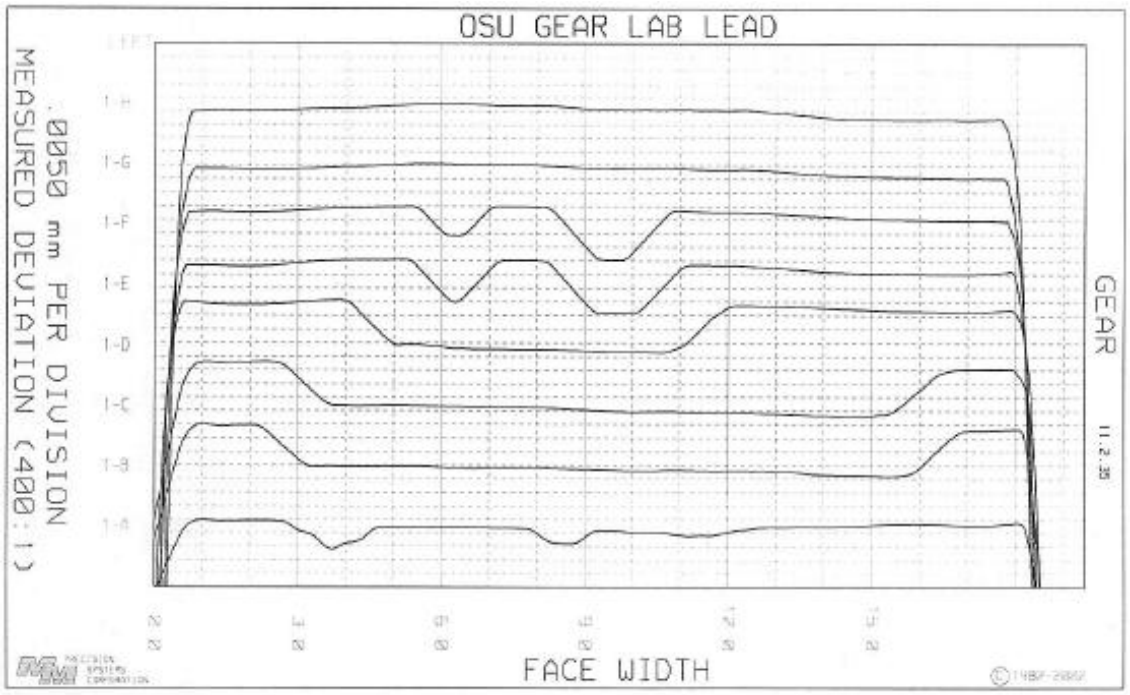

(b)

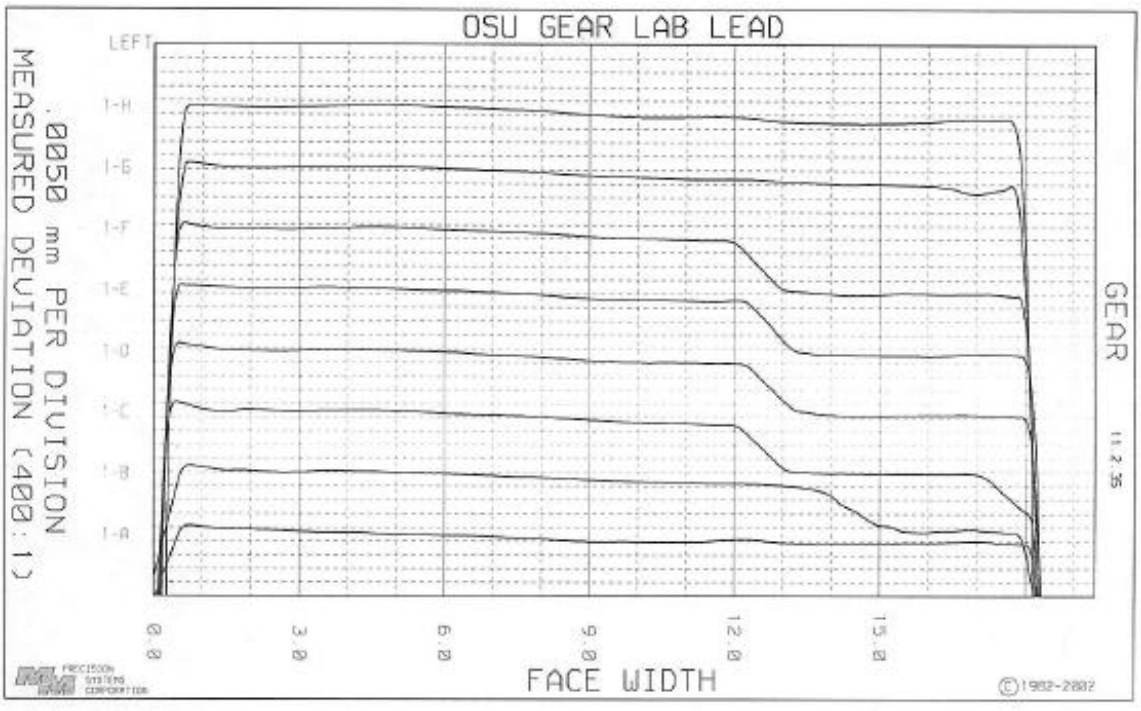

Figure 40. CMM lead traces of NiB-coated teeth after completion of efficiency test: (a) NiB-coated gear (not heat treated) and (b) NiB-coated gear (heat treated).

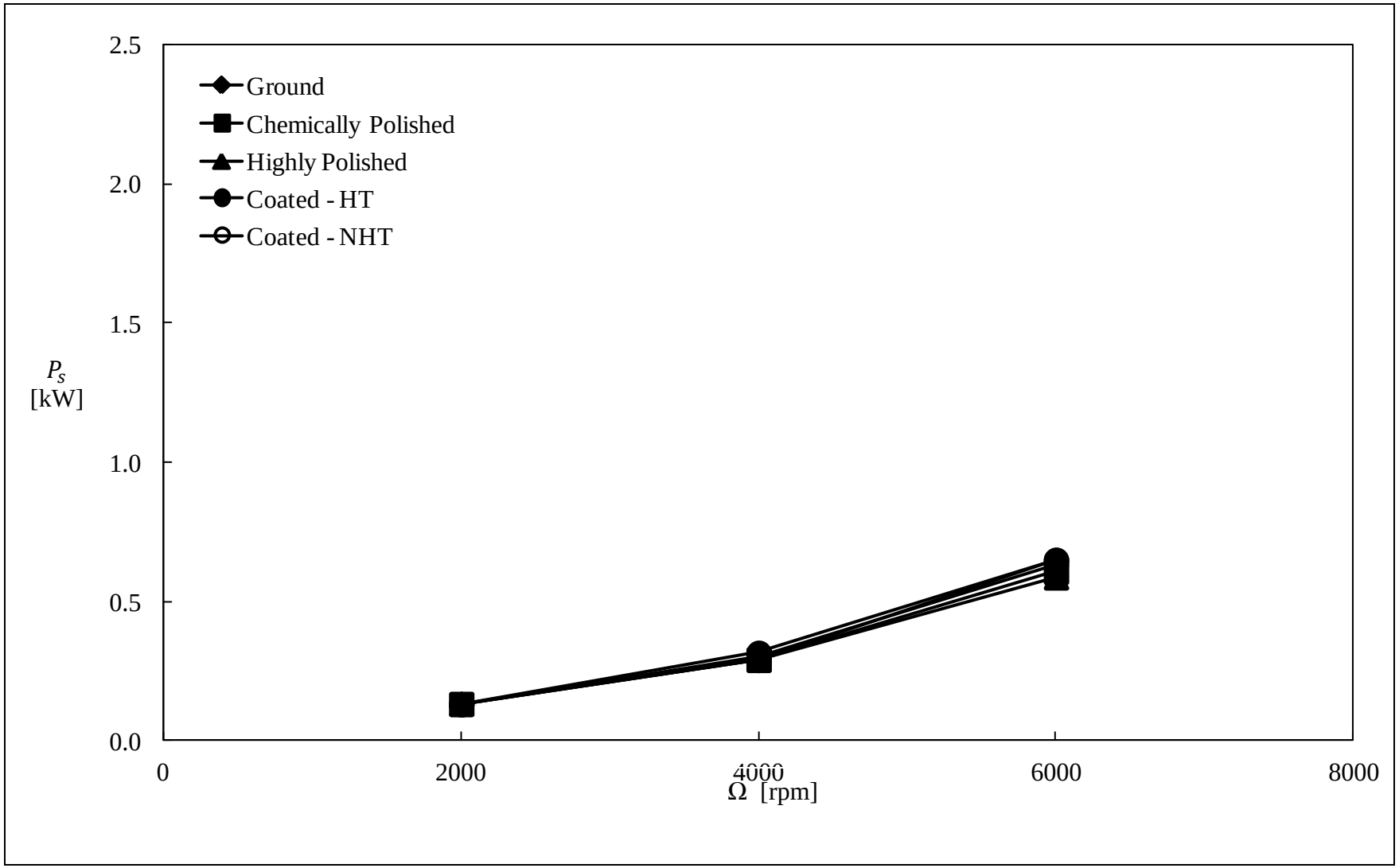

Figure 41. Comparison of measured spin power losses of gear pairs having different surface treatments.

Figures 42–44 compare $P_m(T_c, \omega)$ values for the five different surface treatments at $T_c = 143$, 306, and 459 Nm, respectively. The main observation from these three figures is that P_m increases with increased surface roughness amplitudes. Consistently, regardless of the value of T_c, HP gears resulted in the lowest P_m values, followed by CP and G gears. For instance, in figure 44 at $T_c = 459$ Nm, $\Omega = 4000$ rpm, $P_m = 0.595, 1.223$, and 1.510 kW for HP, CP, and G surfaces, respectively. This represents a 19% reduction in power losses for CP surfaces and a 61% reduction for HP surfaces, both compared to the G surfaces. The underlying physical reason for this improvement with reduced surface roughness amplitude is the reduction in instantaneous μ values (and reduction in asperity contacts) in gear contacts due to increased λ ratio. Similar results were observed in section 3 in terms of the influence of the R_q value on measured μ.

Data in figures 42–44 are presented in a different way in figures 45–47 to illustrate the variation of P_m with T_c at $\Omega = 2000, 4000$, and 6000 rpm, respectively. In figure 46, for $\Omega = 4000$ rpm, for instance, P_m values of G gears are 0.380, 0.998, and 1.510 kW for $T_c = 143, 306$, and 459 Nm, respectively, while they are only 0.241, 0.342, and 0.595 kW for HP gears.

The NiB-coated gears are seen in figures 42–47 to have power loss values comparable to those for G surfaces despite the fact that their initial roughness amplitudes were much lower. However, the degradation of these coated specimens, as documented in figures 39 and 40, can be attributed to this poor efficiency performance.

With figure 41 confirming that spin losses are not influenced by surface roughness conditions, and the rest of the results providing the data for the influence on the mechanical losses, a judgment can be made as to whether smoothening surfaces merits consideration. For instance, the ground surfaces at 143 Nm and 6000 rpm had $P_m = 0.505$ kW with the corresponding $P_s = 0.633$ kW, resulting in a total power loss ($P_t = P_m + P_s$) of 1.138 kW. In other words, about 44% of the total power loss of a gear pair operating at this high-speed low-load condition is mechanical losses. At this operating condition, highly polishing the surfaces reduces the total power to 0.978 kW, which is only a 14% reduction (a savings of 0.160 kW) over the total power loss of the G gears. Meanwhile, at the 459-Nm and 2000-rpm (high-torque and low-speed) condition, $P_t = 0.958$ kW ($P_m = 0.827$ kW and $P_s = 0.131$ kW) for the ground gears. The corresponding loss for highly polished gears is $P_t = 0.481$ kW ($P_m = 0.349$ kW and $P_s = 0.132$ kW), which represents a 50% reduction (or 0.477 kW) in power loss compared with the G gears. This indicates that power loss improvements through surface roughness improvements are most significant at high-torque and low-speed applications, where mechanical losses dominate the total loss.

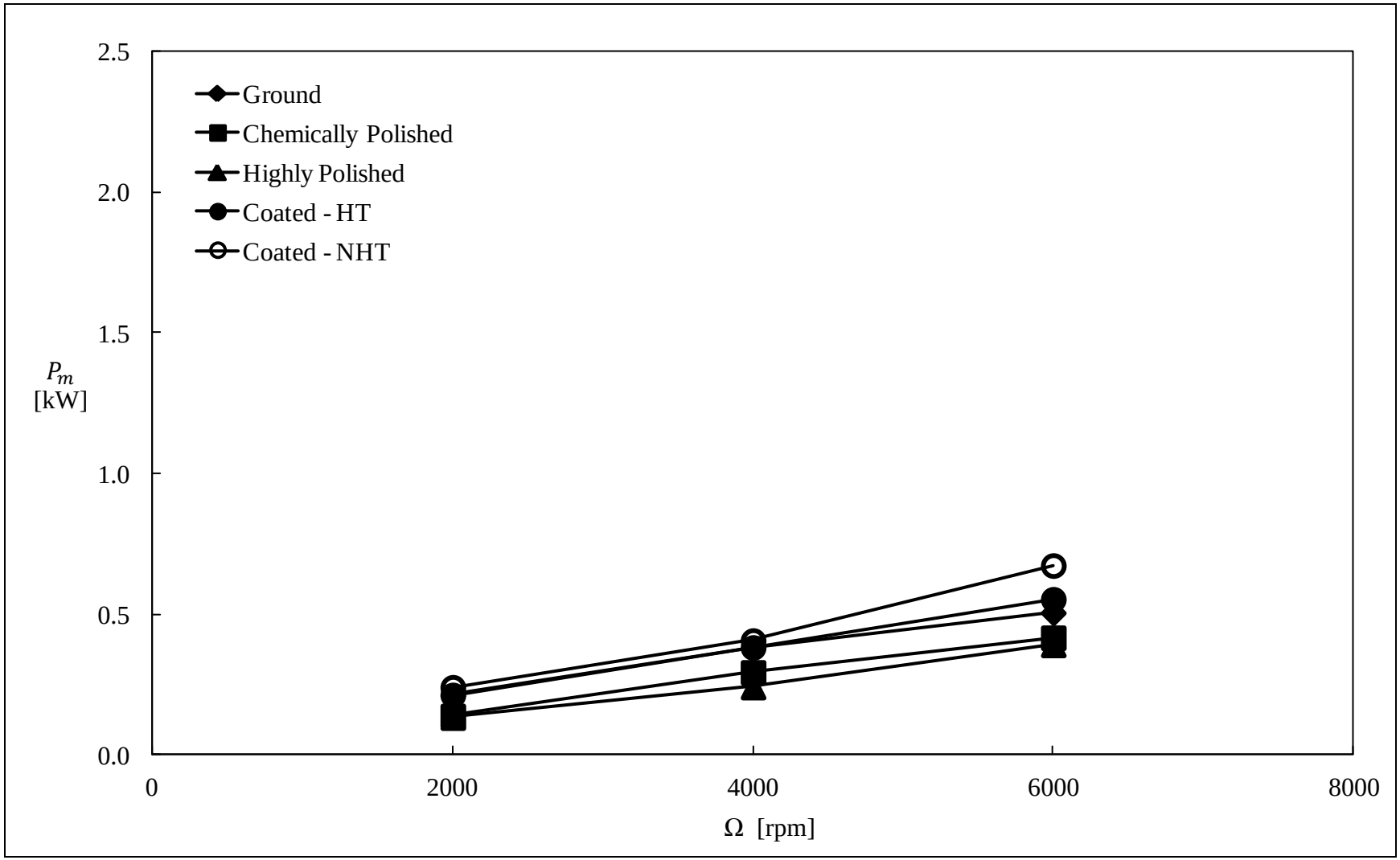

Figure 42. Comparison of measured mechanical power losses of gear pairs having different surface treatments at T_c = 143 Nm.

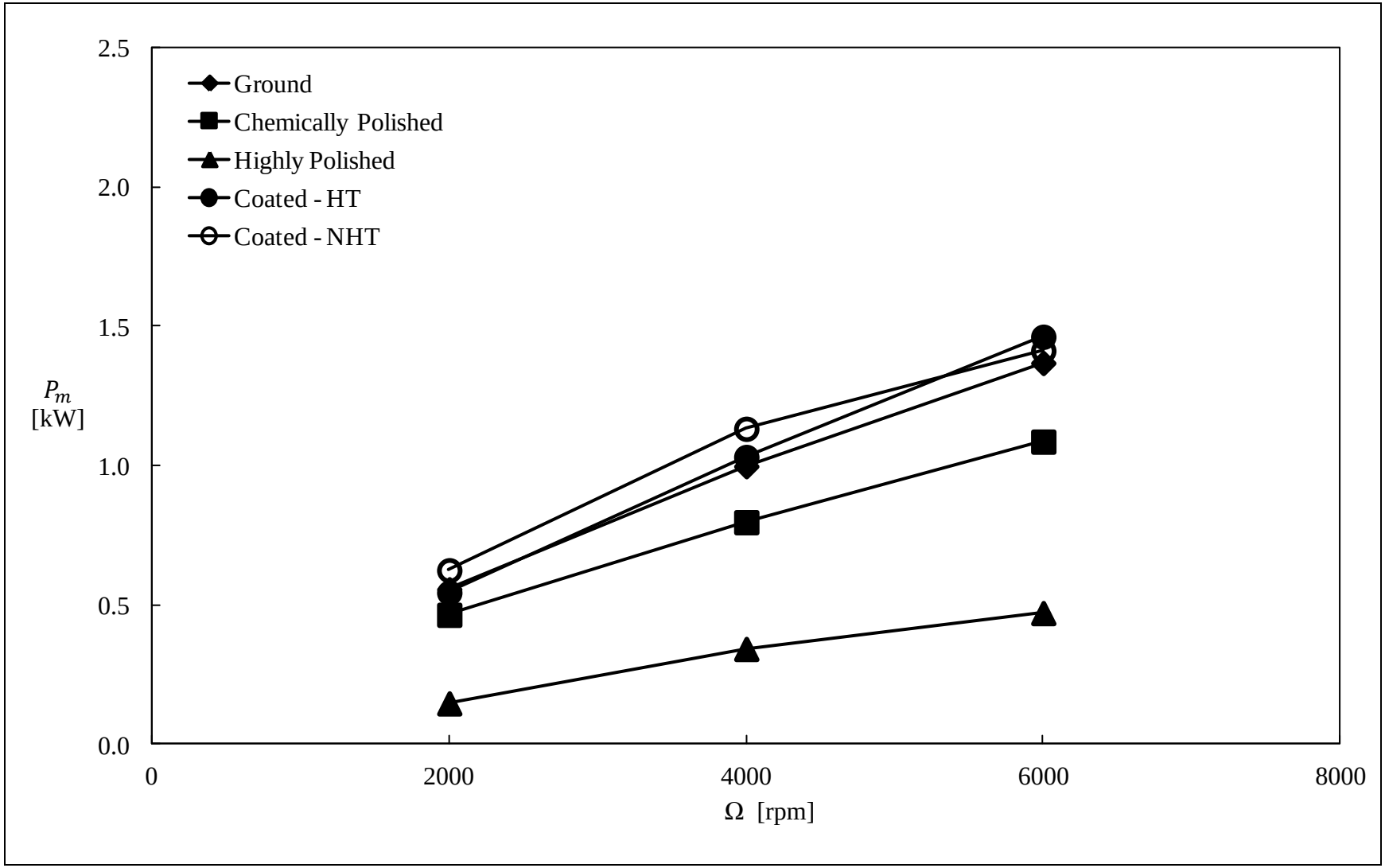

Figure 43. Comparison of measured mechanical power losses of gear pairs having different surface treatments at T_c = 306 Nm.

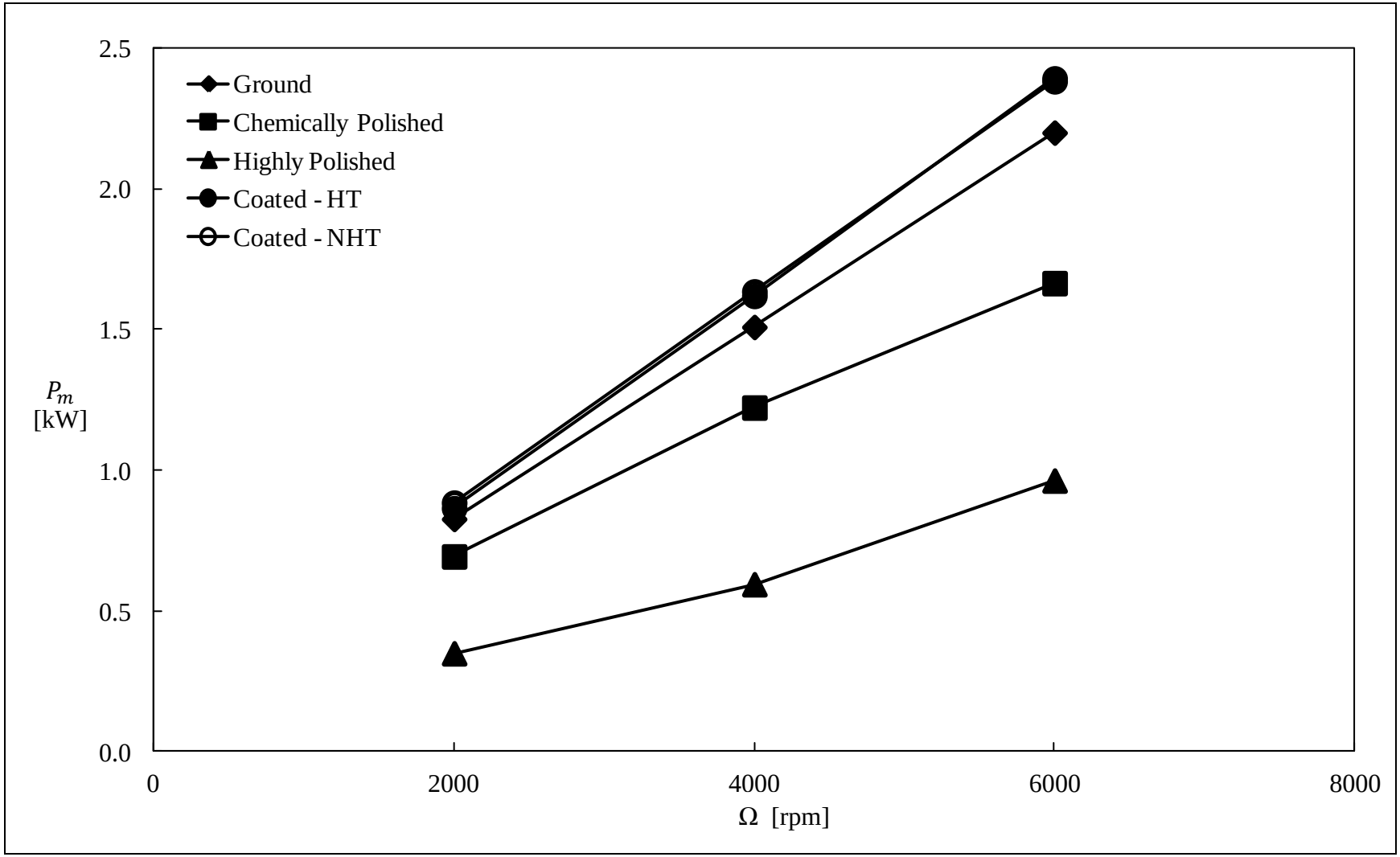

Figure 44. Comparison of measured mechanical power losses of gear pairs having different surface treatments at T_c = 459 Nm.

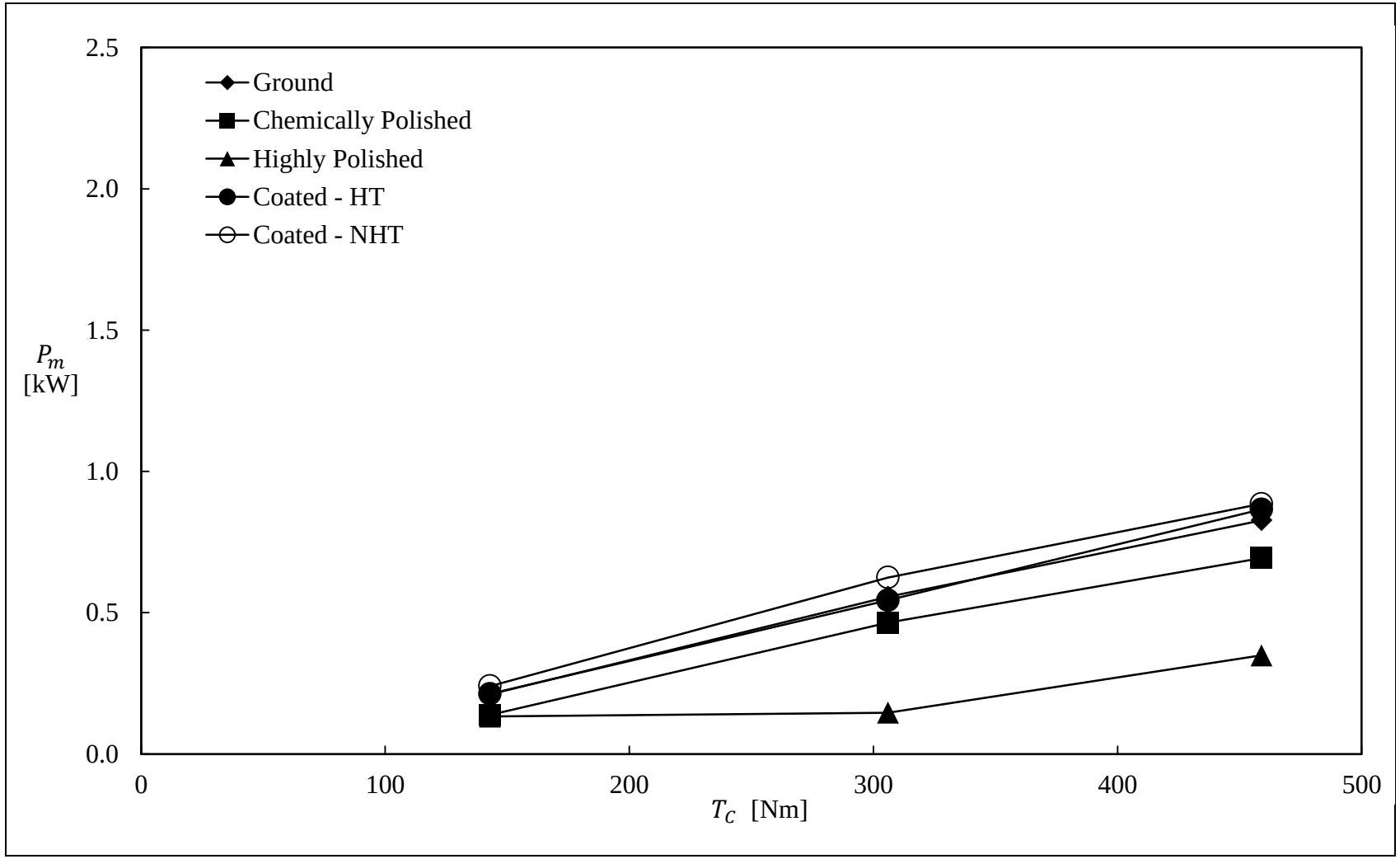

Figure 45. Comparison of measured mechanical power losses of gear pairs having different surface treatments at Ω = 2000 rpm.

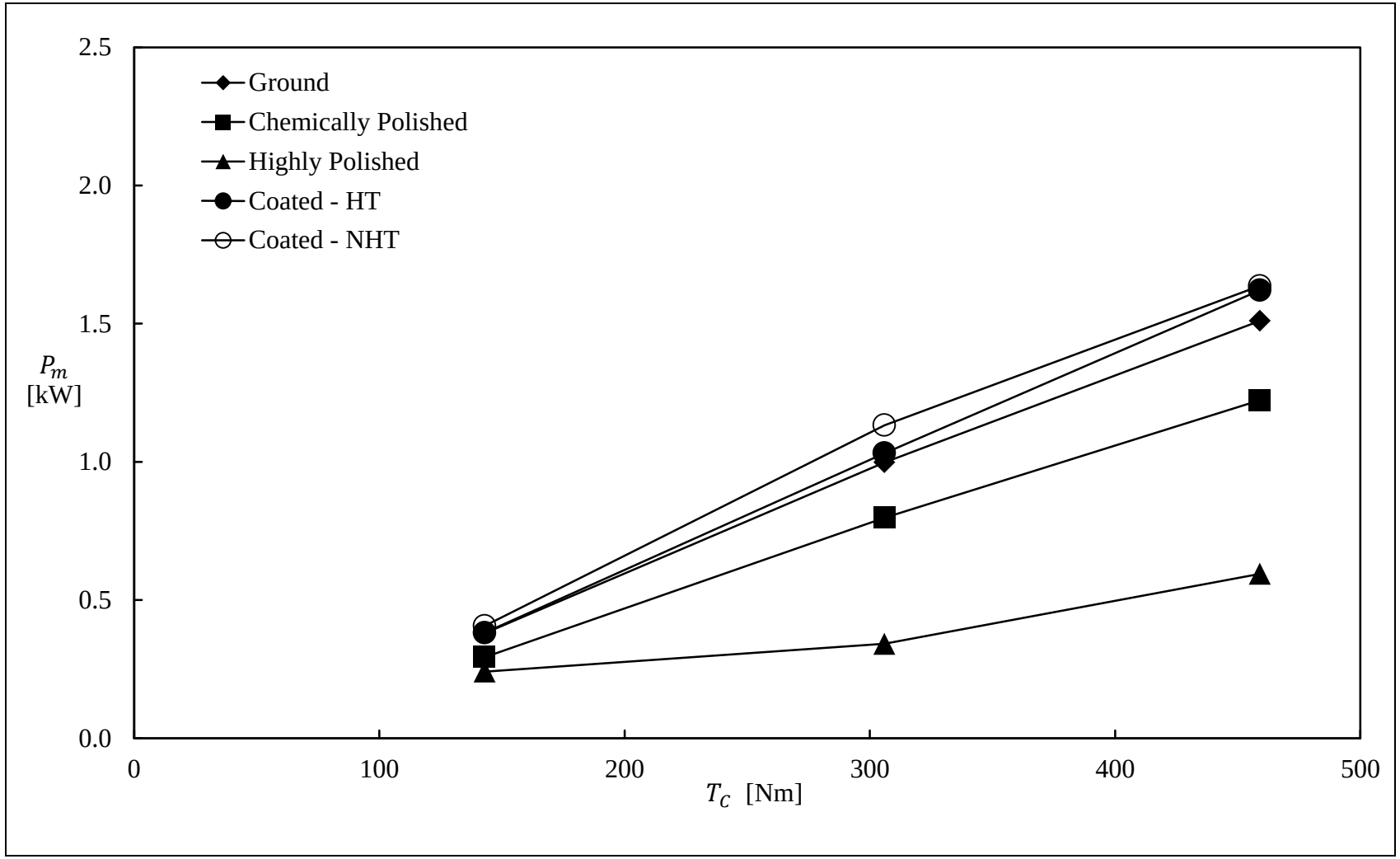

Figure 46. Comparison of measured mechanical power losses of gear pairs having different surface treatments at Ω = 4000 rpm.

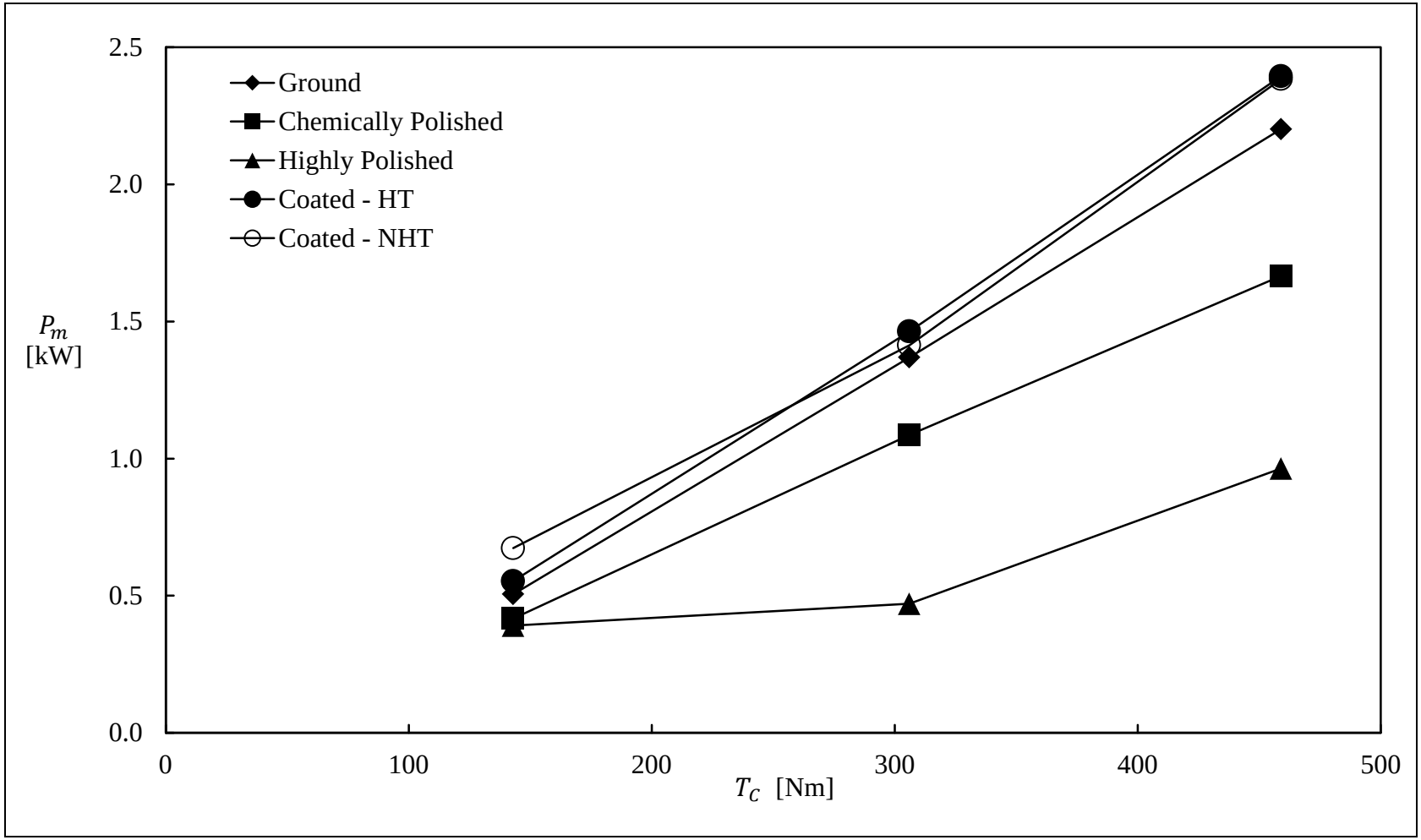

Figure 47. Comparison of measured mechanical power losses of gear pairs having different surface treatments at Ω = 6000 rpm.

5. Conclusion

5.1 Summary

In this experimental study, performance attributes of various surface treatments were investigated. The surfaces considered were (1) hard-ground (G) surfaces at RMS roughness amplitudes of about 0.4 μm, (2) chemically polished (CP) surfaces with an isotropic texture at a roughness of 0.1 μm, (3) highly polished (HP) surfaces representing extremely smooth conditions at 0.02 μm, and (4) chemically applied NiB-coated surfaces. These surface treatments were applied to two types of case-hardened base materials: AISI 5120 alloy steel, representative of automotive gear steels, and AISI 9310 steel, representing the most common aerospace gear steel. A two-disk test methodology was developed to test these specimens with two types of oils: 80W90, a typical ground vehicle fluid, and DOD-PRF-85734, representative of aerospace gear oils. With operating conditions defined by normal load (contact pressure), rolling (entraining) speed, slide-to-roll-ratio, oil inlet temperature, and oil flow rate, three types of two-disk experiments were performed to evaluate the performance of these surface treatments. These included traction (friction coefficient) tests at various rolling speeds and normal loads, long-cycle wear tests at extreme sliding conditions, and scuffing tests under constant speed and incrementally increasing load conditions with normal and starved oil flow rates. The two-disk experiments showed clearly that a reduction in surface roughness amplitudes results in significant reductions in the friction and wear coefficients, while enhancing the scuffing performance of the contacts even under starved lubrication conditions.

The same surface treatments were applied to unity-ratio spur gear pairs to quantify their impact on the power losses of gear pairs. In line with the their respective friction coefficients, the smoother surfaces were shown to result in lower mechanical power losses, while the spin losses remained unchanged regardless of the surface treatment.

Throughout both two-disk and spur gear experiments, NiB-coated test surfaces were observed to lack the durability to provide any tangible improvements over baseline G surfaces. Traction and wear tests with NiB-coated rollers exhibited peeling and accelerated wear of the coating layer. The same level of deterioration was evident in the gear efficiency tests.

5.2 Major Conclusions

Major conclusions from the two-disk and gear pair test results presented in sections 3 and 4, respectively, are listed as follows:

- The friction coefficient values of lubricated contacts and the resultant mechanical gear mesh power losses are both reduced by making the surfaces smoother. Specifically:

- Friction coefficients of CP surfaces were about 5%–38% lower than those for G surfaces at a representative slide-to-roll ratio value of $R = 0.5$.
- Friction coefficients of HP surfaces were 35%–87% lower than those for G surfaces at $R = 0.5$.
- Mechanical power losses of CP spur gear pairs were 6% to 35% lower than those for G spur gears. This corresponded to a 0.09% to 0.23% improvement over G gear total efficiency. Under all load and speed conditions, G gears were 99.11% to 99.46% efficient, while CP gears had efficiency in the 99.26% to 99.56% range.
- Mechanical power losses of HP spur gear pairs were 23% to 74% lower than those for G spur gears, corresponding to a 0.12% to 0.65% improvement over G gear efficiency. Under all load and speed conditions, G gears were 99.11% to 99.46% efficient while HP gears had efficiency in the 99.58% to 99.77% range.
- Surface treatments were observed to have no impact on the spin power losses of the gear pairs, and their impact was solely on the mechanical power losses.

- Both CP and HP surfaces exhibited superior wear characteristic with no tangible wear depths after long-cycle wear tests.
- Due to their low surface traction, both CP and HP surfaces exhibited scuffing performance that was superior to that of G surfaces. Scuffing tests under both normal and starved lubrication conditions exhibited lower surface bulk temperature for polished surfaces with no scuffing failures within the contact pressure range of the tests. Contrarily, G surfaces under starved conditions failed due to scuffing.
- Based on traction, efficiency, wear, and scuffing test results from the two-disk and gear setups, it can be concluded that smoothening of the contacting surfaces to remove the amplitudes and directionality of the machining marks improves the durability of the contact significantly. This was true for both the 9310/DOD-PRF-85734 and 5120/80W90 combinations.
- The NiB coating considered in this study was shown to be unsuitable for high-pressure and high-sliding conditions that exist in gear contacts. Even after limited traction wear of scuffing test cycles, the coating layer was observed to deteriorate significantly. While the efficiency results for NiB-coated surfaces were presented together with the others, they should be interpreted in view of this endurance problem.

- Overall, it can be concluded that the two-disk test methodology and associated test and inspection procedures developed in this study provide a cost-effective, accelerated, and reliable means to screen and evaluate any surface treatment.

5.3 Recommendations for Future Work

The research conducted throughout this study can be expanded and augmented in many areas:

- The number of two-disk tests at each operating condition can be repeated several times to bring a certain level of statistical significance to the database.
- The two-disk test matrix can be expanded to incorporate wider ranges and additional increments of normal load F_n and rolling velocity u_r for the traction and wear tests.
- The NiB coating used in this study was an off-the-shelf coating recipe. Further development and refinement of this type of coating is needed so these performance tests can be repeated without the durability problems observed in this study. In addition, other types of coatings (including chemical vapor deposition and physical vapor deposition coatings) marketed commercially to enhance gear contact performance can be evaluated using the methodologies developed on this study.
- Gear scuffing tests should be performed to determine the effect of surface finish on gear scuffing.
- Gear contact fatigue tests should be performed to determine the effect of surface finish on gear spalling and micropitting performance.

6. References

1. Li, S.; Kahraman, A. A Method to Derive Friction and Rolling Power Loss Formulae for Mixed Elastohydrodynamic Lubrication. *Journal of Advanced Mechanical Design, Systems, and Manufacturing* **2011**, *5* (4), 252–263.

2. Li, S.; Kahraman, A. A Mixed EHL Model With Asymmetric Integrated Control Volume Discretization. *Tribology International* **2009**, *42*, 1163–1172.

3. Krantz, T.; Kahraman, A. An Experimental Investigation of the Influence of the Lubricant Viscosity and Additives on Gear Wear. *Tribology Transactions* **2004**, January–March, 138–148.

4. Xu, H.; Kahraman, A.; Anderson, N. E.; Maddock, D. Prediction of Mechanical Efficiency of Parallel-Axis Gear Pairs. *Journal of Mechanical Design* **2007**, *129*, 58–68.

5. Petry-Johnson, T.; Kahraman, A.; Anderson, N. E.; Chase, D. An Experimental and Theoretical Investigation of Power Losses of High-Speed Spur Gears. *Journal of Mechanical Design* **2008**, *130* (6), 062601.

6. Moorhead, M. Experimental Investigation of Spur Gear Efficiency and the Development of a Helical Gear Efficiency Test Machine. Master's Thesis, The Ohio State University, Columbus, OH, 2007.

7. Vaidyanathan, A. An Experimental Investigation of Helical Gear Efficiency. Master's Thesis, The Ohio State University, Columbus, OH, 2009.

8. Li, S.; Kahraman, A. Prediction of Spur Gear Mechanical Power Losses Using a Transient Elastohydrodynamic Lubrication Model. *Tribology Transactions* **2010**, *53*, 554–563.

9. Li, S.; Vaidyanathan, A.; Harianto, J.; Kahraman, A. Influence of Design Parameters on Mechanical Power Losses of Helical Gear Pairs. *Journal of Advanced Mechanical Design, Systems, and Manufacturing* **2008**, *3* (2), 146–158.

10. Britton, R. D.; Elcoate, C. D.; Alanou, M. P.; Evans, H. P.; Snidle, R. W. Effect of Surface Finish on Gear Tooth Friction. *Transactions of the ASME* **2000**, *122*, 354–360.

11. Talbot, D.; Kahraman, A.; Singh, A. An Experimental Investigation of the Efficiency of Planetary Gear Sets. *Journal of Mechanical Design* **2012**, *134* (2), 021003.

12. Seetharaman, S.; Kahraman, A. Load-Independent Power Losses of a Spur Gear Pair: Model Formulation. *ASME Journal of Tribology* **2009**, *131*, 022201-1–022201.

13. Seetharaman, S.; Kahraman, A.; Moorhead, M.; Petry-Johnson, T. Load-Independent Power Losses of a Spur Gear Pair: Experiments and Model Validation. *ASME Journal of Tribology* **2009**, *131*, 022202-1–022202.

14. Talbot, D. An Experimental and Theoretical Investigation of the Efficiency of Planetary Gear Sets. Doctoral Dissertation, The Ohio State University, Columbus, OH, 2012.

15. Hilty, D. An Experimental Investigation of Spin Power Losses of Planetary Gear Sets. Master's Thesis, The Ohio State University, Columbus, OH, 2010.

16. Diab, Y.; Ville, F.; Velex, P. Prediction of Power Losses Due to Tooth Friction in Gears. *Tribology Transactions* **2006**, *49*, 260–270.

17. Liou, J. A Theroretical and Experimental Investigation of Roller and Gear Scuffing. Doctoral Dissertation, The Ohio State University, Columbus, OH, 2010.

18. Xu, H.; Kahraman, A. Prediction of Friction Power Losses of Hypoid Gear Pairs. *Proceedings of the IMechE, Part K: Journal of Multi-Body Dynamics* **2007**, *221* (3), 387–400.

19. Bluestein, J. An Experimental Study of the Impact of Various Tooth Surface Treatments on Spur Gear Pitting Life. Master's Thesis, The Ohio State University, Columbus, OH, 2007.

20. Klein, M. An Experimental Investigation of Materials and Surface Treatments on Gear Contact Fatigue Life. Master's Thesis, The Ohio State University, Columbus, OH, 2009.

21. Li, S.; Kahraman, A.; Klein, M. A Fatigue Model for Spur Gear Contacts Operating Under Mixed Elastohydrodynamic Lubrication Conditions. *Journal of Mechanical Design* **2012**, 041007.1–041007.11.

22. Li, S. Lubrication and Contact Fatigue Models for Roller and Gear Contacts, Doctoral Dissertation, The Ohio State University, Columbus, OH, 2009.

23. Li, S.; Kahraman, A. A Fatigue Model for Contacts Under Mixed Elastohydrodynamic Lubrication Conditions. *International Journal of Fatigue* **2010**, *33*, 427–436.

24. Krantz, T.; Alanou, M.; Evans, H.; Snidle, R. Surface Fatigue Lives of Case-Carburized Gears With an Improved Surface Finish. *Proceedings of ASME 2000 Design Engineering Technical Conferences and Computers and Information in Engineering Conference*, DETC2000/PTG-14373, Baltimore, MD, 10–13 September 2000.

25. Natarajan, R.; Krishnamurthy, R. Surface Durability of Power Transmission Gears. *Proceedings of Sixth World Congress on Theory of Machines and Mechanisms*, New Delhi, India, 15–20 December 1983; pp 902–905.

26. Blake, G.; Reynolds, J. Case Study Involving Surface Durability and Improved Surface Finish. *AGMA Fall Technical Meeting*, Cincinnati, OH, 30 October–1 November 2011.

27. Tanaka, S.; Ishibashi, A.; Ezoe, S. Appreciable Increases in Surface Durability of Gear Pairs With Mirror-Like Finish. *Transactions of the ASME* **1984**, *84*.

28. Popgoshev, D.; Valori, R. Scuffing Resistance of Advanced Gear Material/Lubricant Combinations. *Journal of Lubrication Technology* **1980**, *102*, 253–256.

29. Lee, S.; Cheng, H. Scuffing Theory Modeling and Experimental Correlations. *Journal of Tribology* **1991**, *113*, 327–334.

30. Alanou, M.; Evans, H.; Snidle, R. Effect of Different Surface Treatments and Coatings on the Scuffing Performance of Hardened Steel Discs at Very High Sliding Speeds. *Tribology International* **2004**, *37*, 93–102.

31. Li, S.; Kahraman, A.; Anderson, N.; Wedeven, V. A Model to Predict Scuffing Failures of a Ball-on-Disk Contact. *Tribology International*, accepted for publication.

32. Young, W.; Budynas, R. *Roark's Formulas for Stress and Strain*; McGraw-Hill: New York, 2002.

33. Chase, D. The Development of an Efficiency Test Methodology for High Speed Gearboxes. Master's Thesis, The Ohio State University, Columbus, OH, 2005.

INTENTIONALLY LEFT BLANK.

Appendix. A Sample Gear Coordinate Measurement Machine Inspection Report for a Highly Polished Test Gear

This appendix appears in its original form, without editorial change.

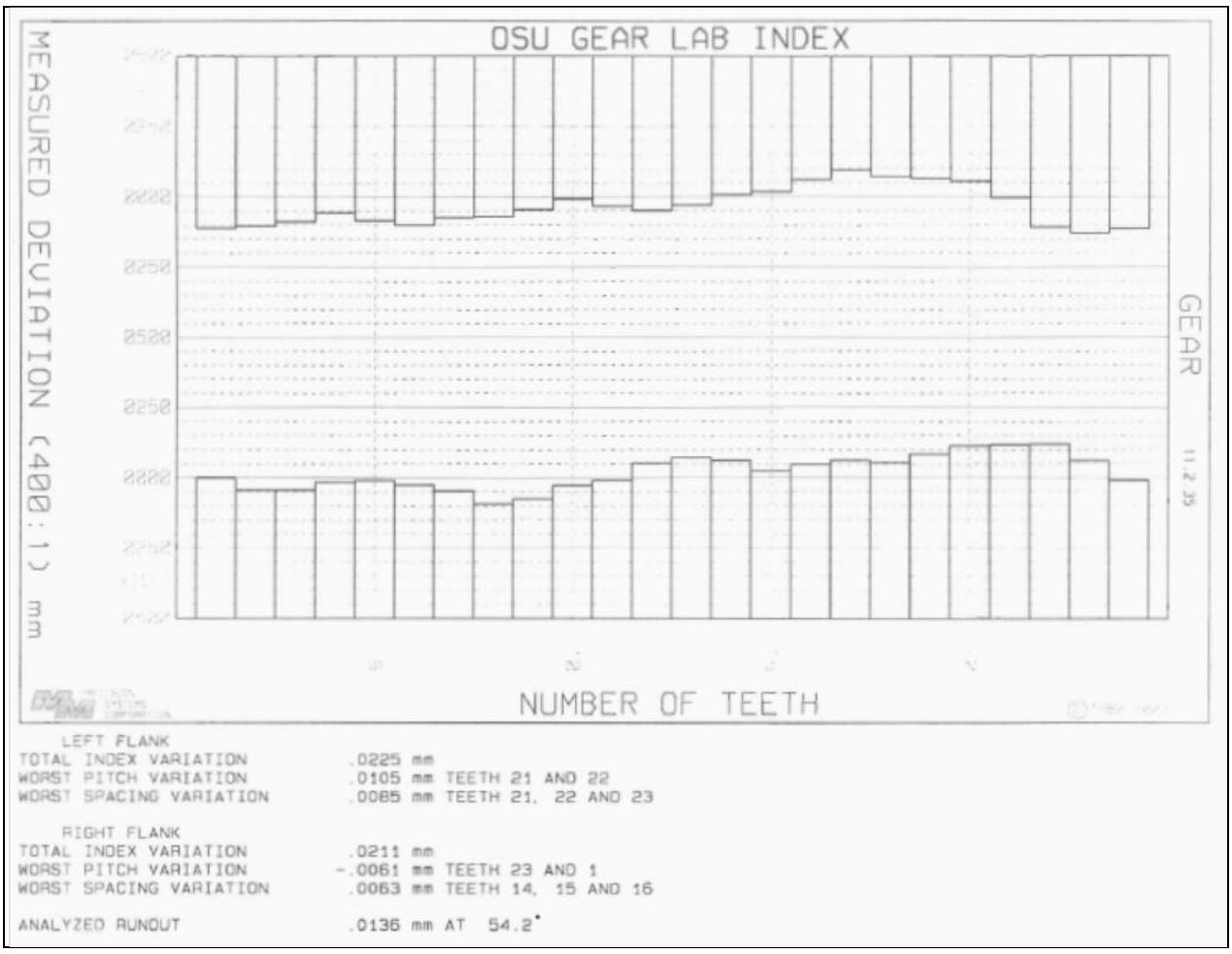

Figure A-1. Index error measurement.

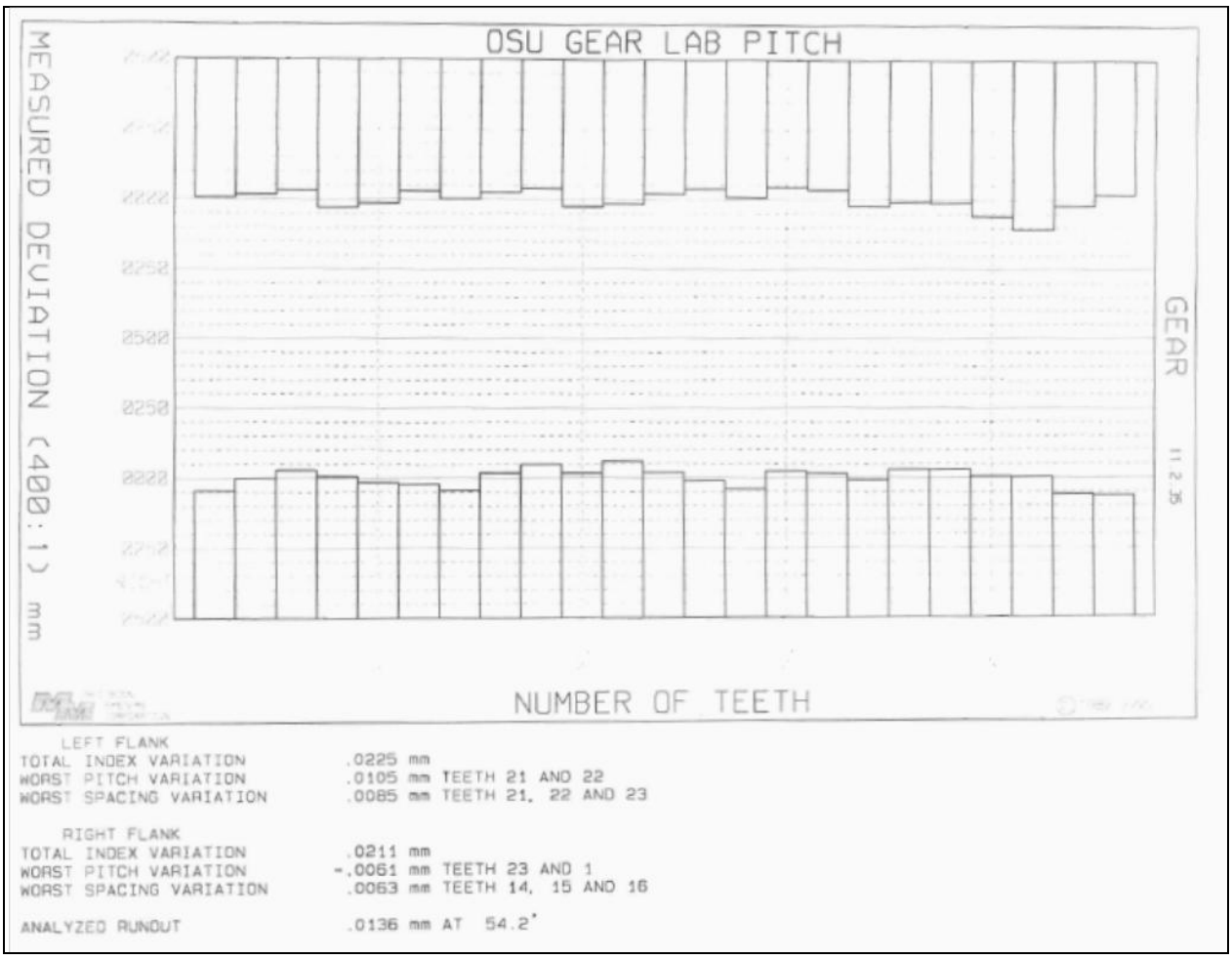

Figure A-2. Pitch error measurement.

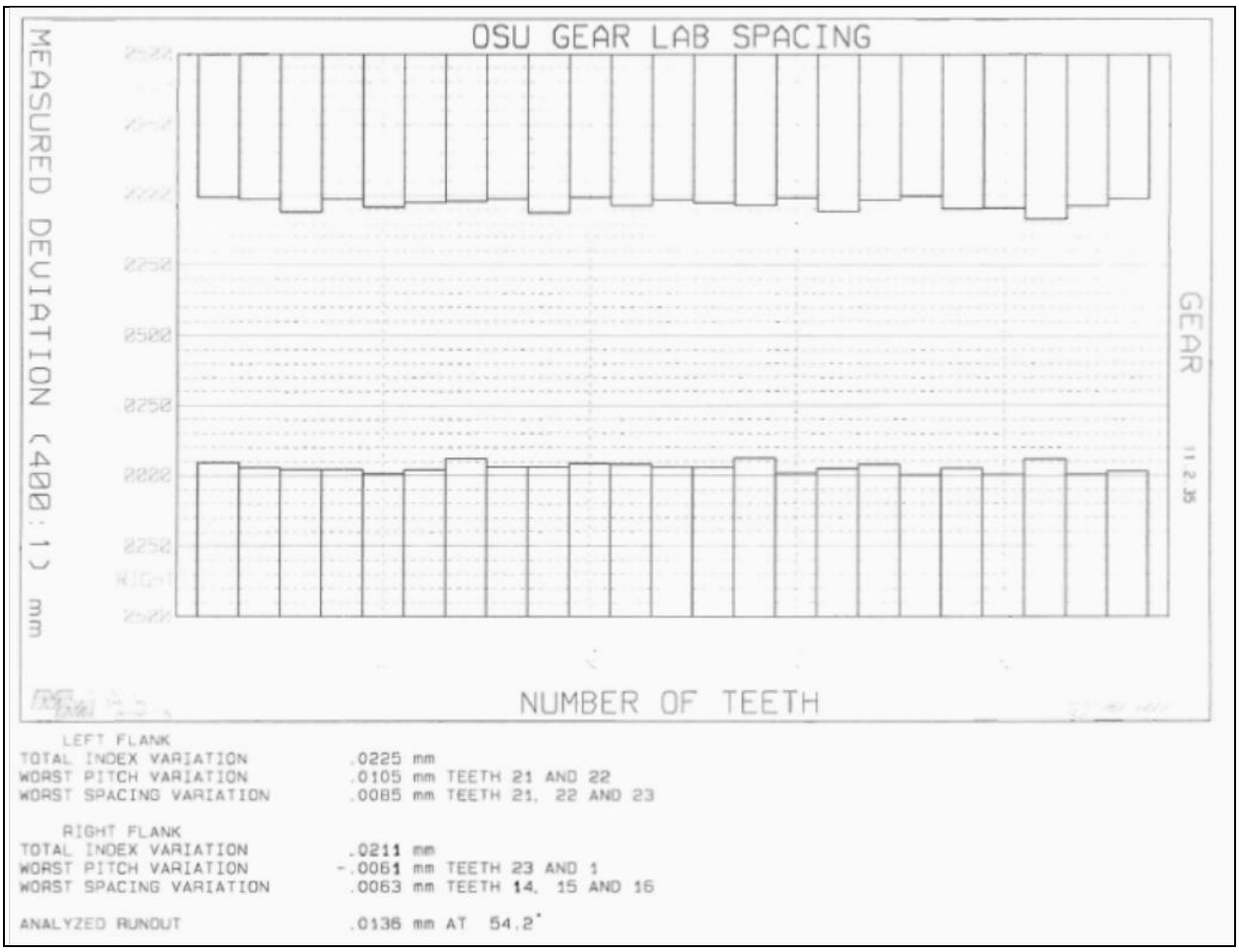

Figure A-3. Tooth spacing error measurement.

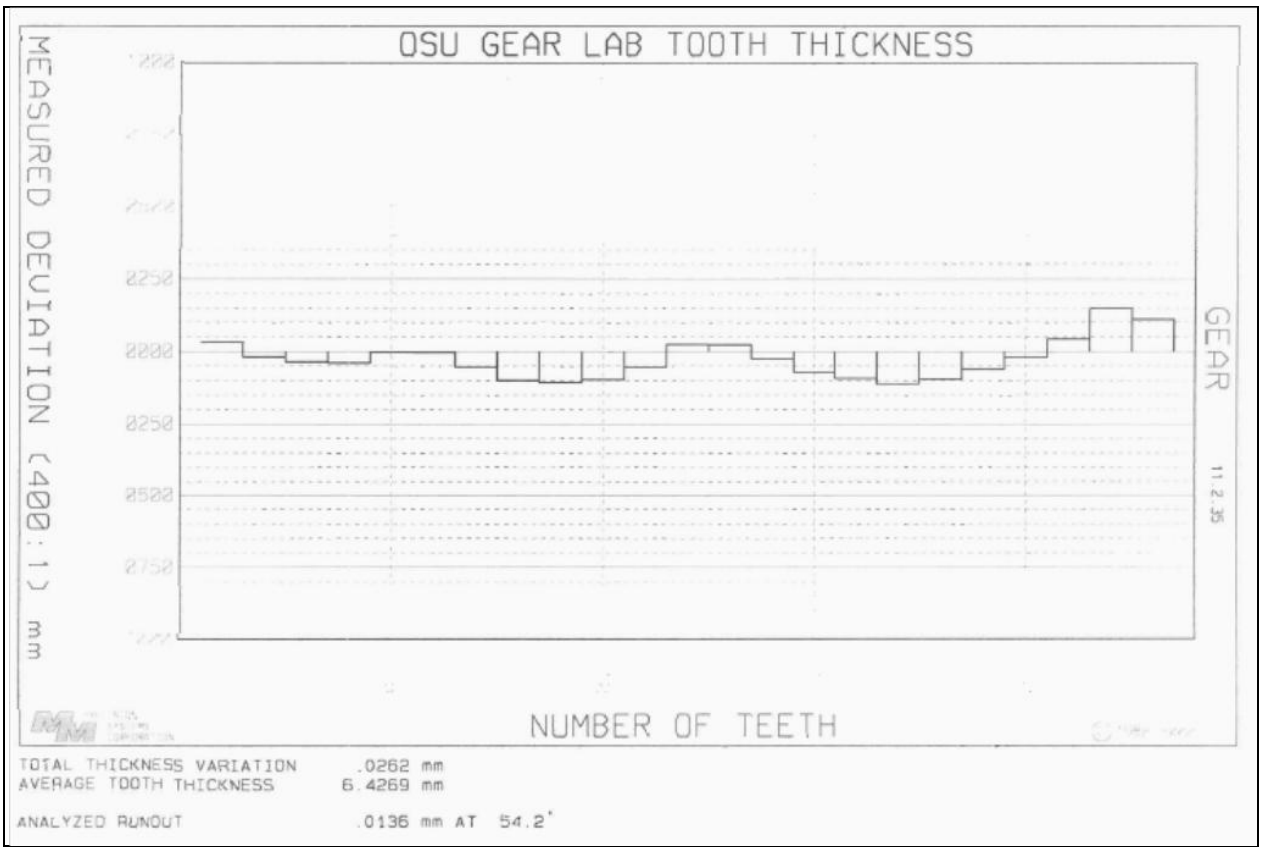

Figure A-4. Tooth thickness measurement.

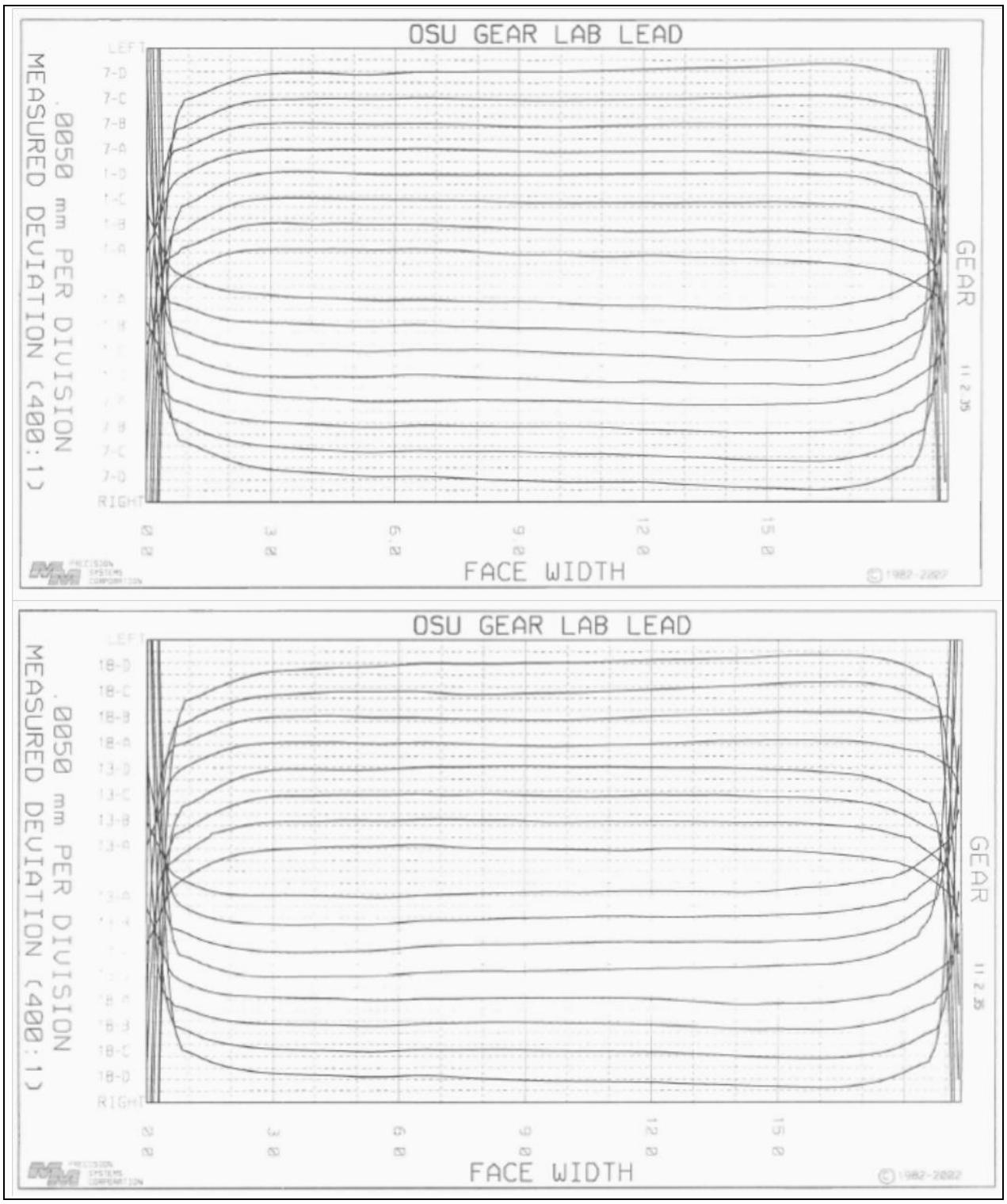

Figure A-5. Measured tooth lead traces.

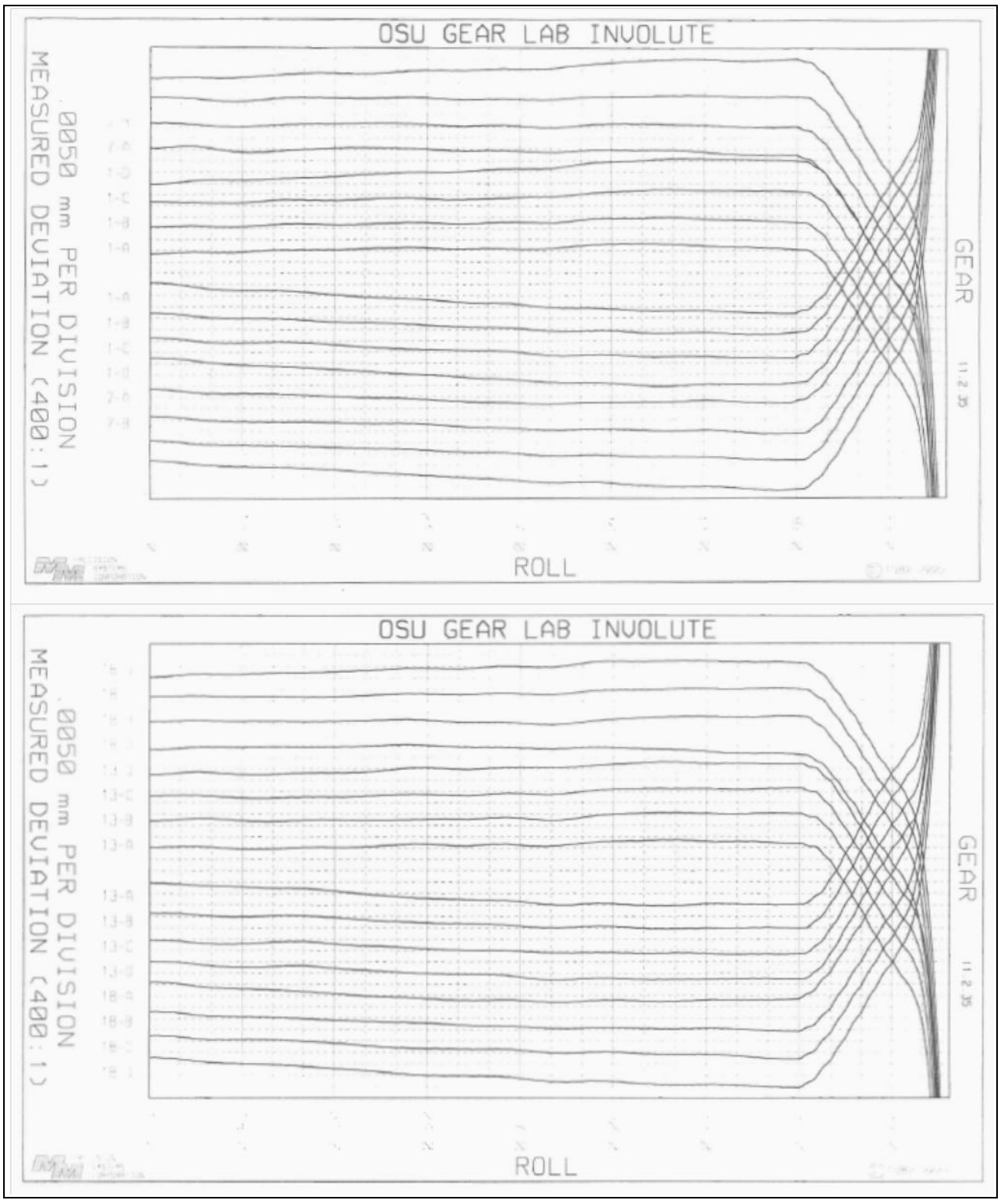

Figure A-6. Measured tooth profile traces.

NO. OF
COPIES ORGANIZATION

1 (PDF) DEFENSE TECHNICAL INFORMATION CTR DTIC OCA

1 (PDF) DIRECTOR US ARMY RESEARCH LAB RDRL CIO LL

1 (PDF) GOVT PRINTG OFC A MALHOTRA

ABERDEEN PROVING GROUND

1 (PDF) DIR USARL RDRL VTP K LABERGE